Bacterial Chemotaxis in a Noisy Environment

A Thesis

Submitted for the degree of
Doctor of Philosophy (Science) in Physics

by
Shobhan Dev Mandal

Department of Physics
Univerity of Calcutta

2023

"So much of life, it seems to me, is determined by pure randomness"

- Sidney Poitier

Acknowledgements

At first I would like to acknowledge my supervisor Prof. Sakuntala Catterjee for guiding me throughout this whole journey of my Ph.D with proper guidance and support. I have enjoyed the freedom she has always given me while working on the research problem. From providing research idea to help in code-development, at each and every aspect I have received valuable supervision from her, which builds the foundation of this thesis.

I would like to acknowledge Prof. Punyabrata Pradhan, Prof. Jaydeb chakrabarty and Dr. Suman Chakraborty for their valuable questions and comments during seminars and meetings.

I would also like to acknowledge my M.Sc project supervisor Dr. Amitabha Nandi who has paved the way for me to enter the world of scientific research. The primitive training I obtained from him has been very helpfull during my Ph.D days. I also want to acknowledge my classmates and friends I spent with during my M.Sc study in IIT Bombay. In the hostel life I interacted with them all the times, I played a lot of games, went for vacation, trekking. Barua, Sarkar, Seth, Raju, Sudipta, Adhip, Srijit, Amit, Puja, Pritha, Debadrita, Aritra, Sucharita all are brilliant reserachers and great companions also. Interactions with them helped me a lot to choose a research career.

I would like to thank my classmates and teachers I met during my B.Sc study in Maulana Azad College. Spending three years in the atmosphere of Physics department of the college has made me thinking of taking science as a career. Interactions with Anupam, Saptarshi, Illius, Parichay, Avisek, Shubhankar, Soubhik, Basu, Kalam have been always very helpful for me.

I would like to acknowledge my senior group members Subrata Da, Sadhu Da and Shauri Di from whom I always obtained necessary help, support and knowledge whenever I required it. Apart from my group members I also want to thank other seniors I met in SNB, like Sumanta Da, Sankar Da, Arghya Da, Pratik Da, Lalu Da, Suvasis Da, Souvonik Da, Rakesh Da, Deba Da, Goba Da, Supriyo Da, Monalisa Di, Sutapa Di, Dhiraj Da, Anirban Da, Santanu Da, Koushik Da, Paru Da, Kaustav Da, Vishal bhayia, Amrit Da with whom I have spent many good times and shared many memorable events and experiences. I have a lot of friends in SNB, without whom my life would not be easy in SNB. Among them I want to mention the name of Rahul, Tanmoy, Premasis, Prasun, Debayan, Anish, Panda, Susmita, Sayan, Abhik, Anwesha, Deepshikha, Monalisa, Jyotirmay, Sumana, Saniur, Suvrasis, Pabi, Didhiti, Anupam, Swarnali. I would also like to thank my juniors like Samir, Riju, Kaka, Soham, Suvojit, Anirban, Soma, Kankana, Suravi, Shinjini, Animesh, Soumen, Sourav, Rupayan, Chandradip, Ramesh, Jayarsi, Abhijit, Sudip, Pallabi with whom also I have many sweet memories in SNB.

I will never forget the life in SNB. It was so colorful throughout these five years for me. Cricket in every weekend was just like a new breath and with all seniors and juniors I have enjoyed it fully. I was not a great footballer when I came to SNB. But playing football in SNB ground throughout these years has made me better player. Similarly I was not a singer as well. But SNB has made me a singer. Those bose fest evenings will be ever live in my mind when a roaring audience is cheering for a song in my voice.

I would like to acknowledge my parents and my elder sisters who have given care and

support and love from early stages of my life. I would like to acknowledge my uncle and teacher, Dev Dulal Mandal who have taught and groomed me from my childhood. I give my gratitude to my grand mother, my uncles, aunts and other family members also who are so important in my life.

I can't forget to mention about SNB mess cooking-team members (Ganesh, Kajal, Ramu, Rajib Da, Sanjay Da, Monaranjan Da) who are also close to my heart. I want to thank all the cleaners, all security members, gardeners, workers who keep the atmosphere in SNB so nice and healthy.

At last I would like to acknowledge all my teachers from my school days who have helped me to reach at this stage. I also thank all my friends in school life, with whom I have spent a large span of my early life. Finally, I would like to acknowledge all those good people I have met in life, who have enriched me by any way.

Publication list

1. **Effect of receptor clustering on chemotactic performance of E. coli: Sensing versus adaptation** by Shobhan Dev Mandal and Sakuntala Chatterjee, Phys. Rev. E Letters 103, L030401, 2021.

2. **Effect of receptor cooperativity on methylation dynamics in bacterial chemotaxis with weak and strong gradient** by Shobhan Dev Mandal and Sakuntala Chatterjee, Phys. Rev. E 105, 014411, 2022.

3. **Effect of switching time scale of receptor activity on chemotactic performance of escherichia coli** by Shobhan Dev Mandal and Sakuntala Chatterjee, Invited article in Indian Journal of Physics, Special Issue: Physical Views of Cellular Processes, Volume 96, Issue 9, pages 2619–2627, 2022.

4. **Bacterial chemotaxis in spatio-temporally varying attractant profile** by Shobhan Dev Mandal and Sakuntala Chatterjee (Manuscript in preparation).

Contents

List of Figures

List of Tables

Dedicated to those who follow their dreams .

Chapter 1

Introduction

Chemotaxis is a phenomenon in which a cell or organism shows motion in response to a chemical environment. With the help of this motion the organism swims to the region where attractant chemical (for example, nutrient) concentration is high or moves away from some toxic or poisonous substance. Numerous biological phenomena are controlled by chemotaxis in both unicellular and multicellular organisms. Some examples are bacteria searching for food, sperm moving towards an egg for fertilization, wound healing, process of tissue development, axon growth and guidance, immune reaction, neuronal migration, lymphocyte migration during final stage of its maturation in bone marrow etc.

A large number of microorganisms perform chemotaxis. Some examples are Escherichia Coli, Salmonella typhimurium, Bacillus subtillis etc. E. coli is the most well-studied organism among them. E. coli cells are rod-shaped, about 2.5 μm long and a large number of thick, long helical filaments called "flagella" have come out of the cell body. In the junction of each flagellum and cell body there is a motor. When motors rotate in counter clockwise (CCW) direction, due to their spatial structure flagella form a bundle which acts as a propeller and help the cell to swim smoothly. This is called a run. But when motor rotation takes place in clockwise (CW) direction the bundle gets dispersed and the cell undergoes an erratic motion with no net displacement (Fig. 1.1). This is called a tumble. Typical run duration is 1 sec and typical tumble duration is 0.1 sec for a wild type E.coli. In presence of a attractant gradient bacteria accumulate in the region of higher concentrations and it is achieved by modulation of run duration. Towards increasing concentration of attractant runs get elongated and along the decreasing concentration of attractant runs get shortened. [1] (Fig. 1.2). Therefore, cell experiences a net chemotactic drift along increasing concentration. Modulation of run duration is controlled by an intracellular signalling network which senses the stimuli coming from environment and responds accordingly.

1.1 Key features of signalling pathway

The signalling pathway governing chemotaxis of an E.coli has two main modules: sensing module and adaptation module [2]. These two modules are coupled by activity of the chemoreceptors. Chemoreceptors present in cell membrane are the primary agents to sense the ligand concentration in the environment. In active state receptors cause phosphorylation to the kinase protein associated to the receptors. Activity of the receptors gets suppressed when ligand molecules get attached to the receptors. Conversely when ligand molecules get detached from the receptor the activity is pushed up. This effect of ligand binding and unbinding is conveyed through sensing module and run-tumble motility of the cell is controlled.

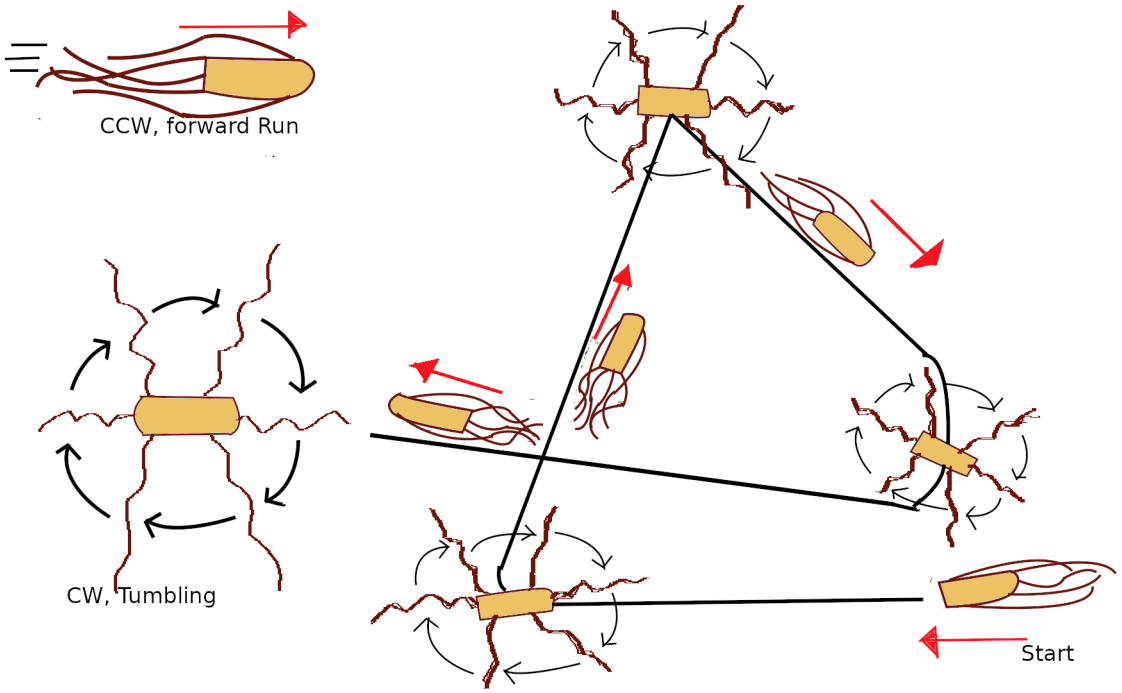

Figure 1.1: Run-tumble motion of E.coli bacteria

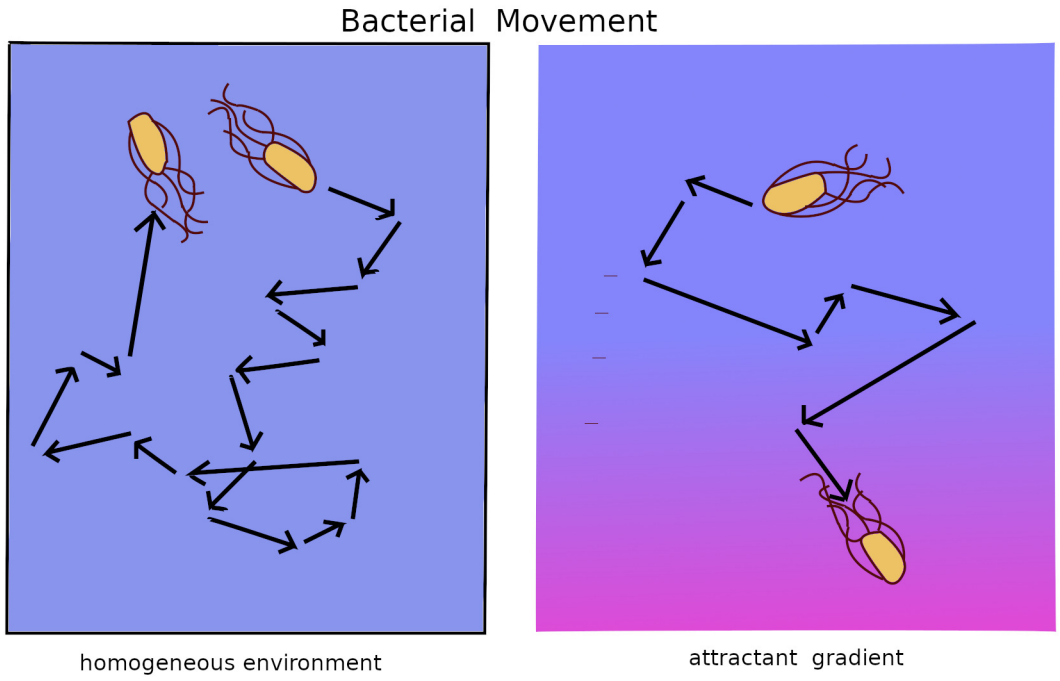

Figure 1.2: Net drift along increasing concentration

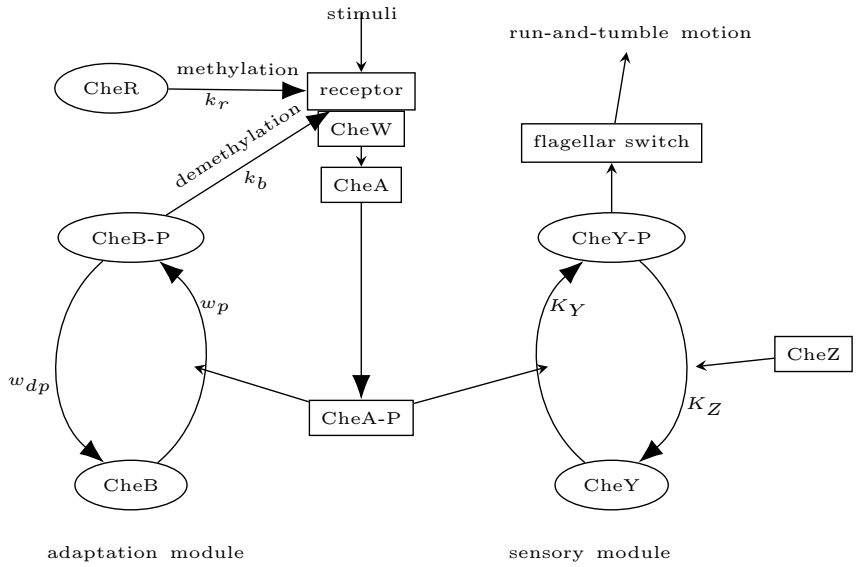

Figure 1.3: Schematic diagram of E.coli signalling pathway.

In the region of high attractant concentration receptors easily bind to attractant molecules and this reduces the total activity of the cell. Low activity in turn reduces the tumbling bias of the cell causing elongation of run duration. On the other hand in the region of low attractant concentration probability of ligand binding decreases resulting an increase in total activity of the cell. High activity induces frequent tumbling of the cell. Hence run duration is shortened. Therefore, along increasing (decreasing) concentration run durations are extended (shortened) causing a net drift towards the region of higher attractant concentration [3, 4].

Adaptation module provides a negative feedback in the network such that total activity of the cell never becomes very high or very low [5, 6]. It always maintains a mean level of activity and it is achieved by changing the methylation level of receptors. When activity of a receptor gets too low (high) it gets methylated (demethylated) by particular enzyme molecule and as a result activity is increased (decreased). Therefore, activity is restored to the adapted value.

Another important feature of the signaling pathway is cooperativity among receptors. This leads to close organization of receptors in a neighbourhood to form clusters or "signalling teams" [7]. Due to the cooperativity among receptors in a cluster they remain in same state of activity and if switching in activity takes place then it is simultaneous switching of all the receptors in the cluster. This coupling of activity of neighbouring receptors in a cluster amplifies the ligand sensitivity of the cell several times and cell is able to sense even very weak gradient of attractant in the extracellular environment [8, 9].

1.2 Noise in signalling pathway

Due to stochastic gene expression, protein-protein interaction etc the population level of protein molecules in the network undergoes constant fluctuation. Out of all these fluctuations, methylation noise has been found to be most important. In the signaling network methylation-demethylation step is the slowest one and any fluctuation present at this level appears as a slow noise. This slow noise in the pathway cannot be integrated out easily and hence is considered as most significant source of fluctuation. Earlier it was believed that switching of motor

rotational states of flagella is a Poisson process and CCW and CW intervals should follow exponential distribution. However, an experiment by Korobkova et al. showed that in a wild type E.coli cell low concentration of methylating enzyme molecule CheR gives rise to large temporal variations in CCW intervals which causes the distribution of CCW intervals to show power law behaviour [10]. This means very long CCW intervals, or equivalently, very long runs can occur with a significant probability. To explain this experimental observation Tu and Grinstein had considered a simple two level system (representing CW and CCW modes) and analytically shown that when the transition rate between the modes fluctuate with time, CCW interval distribution indeed follows a power law [11]. Matthus et al also derived the power law in run length (CCW) distribution from superposition of many exponential distributions at different CheR concentrations caused due to concentration shift during stochastic fluctuations [12].

Despite the incessant fluctuation in the signalling network chemotactic ability of a single cell E.coli is preserved [5]. Both behavioural variability and chemotactic performance have been observed to get amplified simultaneously in ultra-sensitive non-linear kinase activation region, which implies that the cell with larger magnitude of noise show better chemotactic response [13]. Sneddon et al had reported that noise does benefit to E.coli cell by lengthening CCW bias states of individual motors in shallow gradient and hence making coordinated switching of multiple flagellar motors which generally does not happen in absence of noise [14]. In a theoretical work Flores et al. found noise originating from the receptor methylation is beneficial for chemotaxis above a critical value in presence of an exponential gradient whereas below this critical value noise cannot enhance the chemotactic drift in sinusoidal ligand profile [15]. By performing simulation Dev et al. was able to find the existence of a threshold value of CheY-P concentration below which cell moves opposite to the nutrient gradient and this threshold value decreases with methylation noise causing chemotactic efficiency to get enhanced. But at very large methylation noise performance drops because high stochastic fluctuation in methylation level control the dynamics and cell cannot follow the gradient at all. So at an intermediate value of methylation noise chemotactic performance is at its best [16]. In an experimental work by Frankel et al. stochastic gene expression giving rise to variability in protein levels of individual cells in a population is actually found to be advantageous for adaptation because cells with different protein levels are able to survive in different environmental conditions [17]. By comparing the motor response output of a wild type E.coli cell and a mutant strain lacking the source of noise He et al. inferred that noise plays key role in a coordinated motor movement and thereby enhancing the bacterial drift [18].

1.3 Motivation of the Thesis

Recently in experiments Colin et al. [19] and Keegstra et al [20] have independently observed that dense organization of receptor dimers to form "signalling teams" or cluster gives rise to significant amount of fluctuation in the network. In a mutant strain lacking the adaptation enzymes CheR and CheB they found long-term fluctuation in the pathway activity by single FRET (Fluorescence resonance energy transfer) measurement. When they have disrupted this clustering arrangement of chemoreceptors, they haven't observed any low frequency noise which appears in presence of receptor clustering. From here they have concluded that apart from methylation noise receptor clustering is another equally important source of noise in E.coli chemotaxis.

In this thesis we ask the important question: how does this newly found noise source affect the chemotactic behavior of the cell? We address this question by performing extensive

numerical simulations on a detailed theoretical model.

1.4 Main results

1.4.1 Sensing versus adaptation competition for best chemotactic performance

To investigate how receptor clustering affects the chemotactic performance of the cell, we quantify performance by several different measurements. We find each of these quantities reaches a peak value for a particular size of the receptor cluster. This means there is an optimum size of the receptor cluster, or equivalently, an optimum strength of cooperative interaction for which the chemotactic performance is at its best [21]. We explain this surprising effect from a competition between the sensing and adaptation modules of the signaling network. We show that while larger cooperativity amplifies the environmental signal and enhances performance, it also causes large pathway noise which in turn adversely affects the ability of the cell to sense its chemical environment. As a result of this interplay a performance peak is obtained.

1.4.2 Sensing-adaptation interplay resulting in rich methylation dynamics

Although E.coli chemotaxis is a well-studied system, so far there has been no study correlating the dynamics of receptor activity or methylation level to the change in extra-cellular ligand concentration, as the cell navigates through different chemical environments. We have studied this complex dynamics in a systematic way and also observed how this dynamics gets affected by sensing-adaptation interplay mentioned in Section 1.4.1. We study the temporal variation of average methylation level of a receptor cluster while the cell swims up and down the gradient in a linearly varying attractant profile. We find that interplay between sensing and adaptation modules of the signalling network expresses itself in different ways depending on the gradient strength of attractant profile and size of the receptor cluster [22].

1.4.3 Time-scale of activity switching affects chemotactic drift

In E.coli chemotaxis motion the transition of activity of chemoreceptors between active and inactive modes is one of the crucial steps. We have studied how the time-scale of this transition affects the chemotactic performance. Drift velocity is a measure of chemotactic performance, which quantifies how fast the cell climbs up the gradient. We observe that as switching rate of activity increases drift velocity also increases and finally reaches a saturation value for very fast switching. We explain this interesting behavior by studying how sensing adaptation interplay affects the activity variation in qualitatively different way during an uphill run and a downhill run of the cell [23].

1.4.4 Chemotaxis in a time-varying ligand environment

The environment outside the cell is often found to be time-varying in nature. For E.coli chemotaxis also time-varying attractant environment has been considered in many earlier studies. In an experimental work Li et al. [24] measured the chemotactic drift velocity in a travelling sin wave of attractant profile. Motivated by this, we have studied the chemotactic performance

of a single E.coli cell in presence of an attractant profile that has a traveling wave form. For simplicity, we have considered a traveling sine wave. As a function of the propagation speed of the traveling wave we monitor the spatially averaged chemotactic drift velocity of the cell and find highly non-trivial behavior. As expected, for very high propagation speed the cell is not able to sense the variation and experiences only an average attractant concentration and its drift velocity vanishes. Similarly, for zero propagation speed, the cell experiences a static sine wave profile of the attractant, and from symmetry the drift velocity vanishes in this limit too. However, for finite traveling wave speed, drift velocity shows highly interesting behavior consisting of a negative minimum for small wave speed and positive maximum for large speed. In probing further we see that near the minima of drift velocity rightward and leftward run duration show a minima and maxima respectively. We explain this non-trivial behavior from the difference in effective gradient faced by the cell during a run in the same direction and in the opposite direction of the traveling wave. The relative velocity between the running cell and the moving wave takes different values depending on the direction of the run. In particular when the run speed matches with the speed of the traveling wave, the cell is able to 'ride' the wave when it is moving in the same direction, but experiences a fast oscillating profile while moving in the opposite direction. The variation in drift velocity can be explained from this effect.

1.5 Plan of the Thesis

In chapter 2 we discuss about our model and simulation details. In chapter 3 effect of clustering noise on the chemotactic responses has been studied . We present our results on methylation dynamics of chemoreceptors for weak and stong attractant gradient in chapter 4 and 5 respectively. Chapter 6 contains the study of chemotactic performance as a function of activity switching time-scale of receptor cluster. In chapter 7 we present our work on chemotactic response of an E.coli cell in a spatiotemporally varying ligand profile.

Bibliography

[1] Douglas A Brown and Howard C Berg. Temporal stimulation of chemotaxis in escherichia coli. *Proceedings of the National Academy of Sciences*, 71(4):1388–1392, 1974.

[2] Yuhai Tu. Quantitative modeling of bacterial chemotaxis: signal amplification and accurate adaptation. *Annual review of biophysics*, 42:337–359, 2013.

[3] Julius Adler. A method for measuring chemotaxis and use of the method to determine optimum conditions for chemotaxis by *Escherichia coli*. *Microbiology*, 74(1):77–91, 1973.

[4] Steven M Block, Jeffrey E Segall, and Howard C Berg. Impulse responses in bacterial chemotaxis. *Cell*, 31(1):215–226, 1982.

[5] Naama Barkai and Stan Leibler. Robustness in simple biochemical networks. *Nature*, 387(6636):913–917, 1997.

[6] Clinton H Hansen, Robert G Endres, and Ned S Wingreen. Chemotaxis in *Escherichia coli*: a molecular model for robust precise adaptation. *PLoS Comput Biol*, 4(1):e1, 2008.

[7] John S Parkinson, Gerald L Hazelbauer, and Joseph J Falke. Signaling and sensory adaptation in escherichia coli chemoreceptors: 2015 update. *Trends in microbiology*, 23(5):257–266, 2015.

[8] TAJ Duke and Dennis Bray. Heightened sensitivity of a lattice of membrane receptors. *Proceedings of the National Academy of Sciences*, 96(18):10104–10108, 1999.

[9] Victor Sourjik and Howard C Berg. Functional interactions between receptors in bacterial chemotaxis. *Nature*, 428(6981):437–441, 2004.

[10] Ekaterina Korobkova, Thierry Emonet, Jose MG Vilar, Thomas S Shimizu, and Philippe Cluzel. From molecular noise to behavioural variability in a single bacterium. *Nature*, 428(6982):574–578, 2004.

[11] Yuhai Tu and G Grinstein. How white noise generates power-law switching in bacterial flagellar motors. *Physical review letters*, 94(20):208101, 2005.

[12] Franziska Matthäus, Mario S Mommer, Tine Curk, and Jure Dobnikar. On the origin and characteristics of noise-induced lévy walks of e. coli. *PloS one*, 6(4), 2011.

[13] Thierry Emonet and Philippe Cluzel. Relationship between cellular response and behavioral variability in bacterial chemotaxis. *Proceedings of the National Academy of Sciences*, 105(9):3304–3309, 2008.

[14] Michael W Sneddon, William Pontius, and Thierry Emonet. Stochastic coordination of multiple actuators reduces latency and improves chemotactic response in bacteria. *Proceedings of the National Academy of Sciences*, 109(3):805–810, 2012.

[15] Marlo Flores, Thomas S Shimizu, Pieter Rein ten Wolde, and Filipe Tostevin. Signaling noise enhances chemotactic drift of *E. coli*. *Physical review letters*, 109(14):148101, 2012.

[16] Subrata Dev and Sakuntala Chatterjee. Optimal methylation noise for best chemotactic performance of *E. coli*. *Physical Review E*, 97(3):032420, 2018.

[17] Nicholas W Frankel, William Pontius, Yann S Dufour, Junjiajia Long, Luis Hernandez-Nunez, and Thierry Emonet. Adaptability of non-genetic diversity in bacterial chemotaxis. *Elife*, 3:e03526, 2014.

[18] Rui He, Rongjing Zhang, and Junhua Yuan. Noise-induced increase of sensitivity in bacterial chemotaxis. *Biophysical journal*, 111(2):430–437, 2016.

[19] Remy Colin, Christelle Rosazza, Ady Vaknin, and Victor Sourjik. Multiple sources of slow activity fluctuations in a bacterial chemosensory network. *Elife*, 6:e26796, 2017.

[20] Johannes M Keegstra, Keita Kamino, François Anquez, Milena D Lazova, Thierry Emonet, and Thomas S Shimizu. Phenotypic diversity and temporal variability in a bacterial signaling network revealed by single-cell fret. *Elife*, 6:e27455, 2017.

[21] Shobhan Dev Mandal and Sakuntala Chatterjee. Effect of receptor clustering on chemotactic performance of *E. coli*: Sensing versus adaptation. *Phys. Rev. E Letter*, 103:L030401, Mar 2021.

[22] Shobhan Dev Mandal and Sakuntala Chatterjee. Effect of receptor cooperativity on methylation dynamics in bacterial chemotaxis with weak and strong gradient. *Physical Review E*, 105(1):014411, 2022.

[23] Shobhan Dev Mandal and Sakuntala Chatterjee. Effect of switching time scale of receptor activity on chemotactic performance of escherichia coli. *Indian Journal of Physics, Special Issue: Physical Views of Cellular processes*, 96:2619–2627, 2022.

[24] Zhaojun Li, Qiuxian Cai, Xuanqi Zhang, Guangwei Si, Qi Ouyang, Chunxiong Luo, and Yuhai Tu. Barrier crossing in escherichia coli chemotaxis. *Physical review letters*, 118(9):098101, 2017.

Chapter 2

Model description and simulation details

Internal biochemical network that governs the run-and-tumble motion of E. coli consists of two modules: sensing module and adaptation module. Sensing module senses the input signal coming from environment and controls the run-tumble motion. Adaptation module uses a negative feedback mechanism to make sure receptor activity does not get too high or too low. This two modules are coupled via receptor activity. We describe the reaction network using a detailed model, which consists of three main parts: (i) activity switching of receptor clusters, (ii) binding-unbinding dynamics between the receptors and the enzyme molecules which control the receptor methylation level, (iii) run-tumble motility of the cell. Below we discuss each part in details.

2.1 Activity switching of receptor clusters

In an E.coli cell, few thousand chemoreceptors are present, which exist in the form of dimers [1, 2]. Three receptor dimers form a trimer of dimer (TD). Each dimer remains either in active state or in inactive state. According to MWC model [3, 4] free energy difference between active and inactive state of a receptor dimer (in units of K_BT) can be written as

$$\epsilon[c(x), m] = \log \frac{1 + c(x)/K_{min}}{1 + c(x)/K_{max}} + \epsilon_0 - \epsilon_1 m \tag{2.1}$$

where $c(x)$ is ligand concentration at position x of the cell and m is methylation level of the dimer which can take any integer value from 0 to 8 [5, 6]. K_{min} and K_{max} set the range of sensitivity for the cell, i.e., if $K_{min} < c(x) < K_{max}$ then cell can sense the concentration. ϵ_0 and ϵ_1 are two constants. Receptor cooperativity means that neighboring receptors prefer to be in the same activity state. We describe this using "all-or-nothing" model [4] where clusters or 'signaling teams' consisting of n TDs are formed. All receptors within the same cluster switch their activity in unison. Size of the cluster is denoted by n and for simplicity, we assume all clusters have the same size. So each cluster contains $3n$ number of dimers and the total free energy of a cluster is the sum of individual free energies of all $3n$ dimers in the cluster

$$F = 3n \log \frac{1 + c(x)/K_{min}}{1 + c(x)/K_{max}} + 3n\epsilon_0 - \sum_{j}^{3n} \epsilon_1 m(j) \tag{2.2}$$

where $m(j)$ stands for the methylation level of j-th dimer in the cluster. Adapted value of activity of a cluster is defined as the probability to find the cluster in active state and its

long time-average is given by $[1 + \exp(F)]^{-1}$. The transition probability between active and inactive states of a cluster depends on F. From the principle of local detailed balance activity of a cluster can flip from inactive to active state with a rate $\frac{w_a}{1+\exp(F)}$ and reverse transition from active to inactive state happens with a rate $\frac{w_a \exp(F)}{1+\exp(F)}$). Here ω_a denotes the characteristic time scale of activity transition.

2.2 Binding-unbinding dynamics of enzymes to receptors for (de)methylation

Each receptor dimer inside the clusters has methylation level between 0 and 8 and takes only integer values. Enzyme CheR and phosphorylated CheB or CheB-P control the methylation level (m) of the dimers. A CheB-P molecule binds to an active dimer and demethylates it to reduce its m value by 1, provided that $m > 0$. Similarly a CheR molecule binds to an inactive dimer and methylates it to increase its m value by 1, provide $m < 8$. From Eq. 2.2 it follows that methylation decreases the free energy and therefore increases the activity. Similarly demethylation increases the free energy and decreases the activity.

An enzyme molecule can bind to one dimer at a time and number of CheR and CheB molecules in the cell are very low [7] compared to the total number of dimers in the cell [7]. Because of this methylation level of a dimer changes very slowly. However, this doesn't impair the adaptation capability of the cell and an E.coli is known to show near-perfect adaptation [8, 9]. To explain this a number of mechanisms, like "assistance neighbourhood" and "enzyme brachiation" have been proposed and experimentally verified [10, 11]. In an assistance neighbourhood model, an enzyme molecule bound to a dimer modifies not only the methylation level of that dimer, but also of neighbouring dimers in the cluster as well. In brachiation mechanism an enzyme molecule can perform random walk on the receptor array and move from one dimer to another to modify its methylation level. We have used the flavour of these mechanisms in our model by allowing unbinding of a bound enzyme from a dimer and then rebinding of same enzyme molecule to another dimer in the cluster. Since binding between a free enzyme in the cytoplasm and dimer is a slow process, one binding event causing only one (de)methylation won't be enough for perfect adaptation. Hence we use this distributive methylation strategy which has been described below in more details.

Number of CheR and CheB molecules in the cell are denoted by N_R and N_B respectively. An enzyme molecule from cytoplasmic bulk binds to a free dimer in its tether site or modification site [12, 5, 13]. Binding rates to both of these sites are slow, yet binding to tether site is relatively faster [12, 5, 13, 14]. So we consider only tether binding in our model. CheR binds to tether site of a dimer with a rate w_r, provided it is not bound to any other enzyme already and methylates it with rate k_r provided the dimer belongs to an inactive cluster and its methylation level is less than 8. A bound CheR can unbind from the dimer with rate w_u. After unbinding, the enzyme randomly chooses another dimer in the same cluster. If this new dimer is unoccupied, then the enzyme molecule binds to it and modifies its methylation level in the same way. If the new dimer is already occupied, then the enzyme molecule returns to the cytoplasmic bulk. A CheB molecule in the cytoplasm can undergo phosphorylation by an active receptor with a rate w_p to form CheB-P. Similarly a bulk CheB-P molecule can undergo dephosphorylation in the cytoplasm with rate w_{dp} to form CheB. From cytoplasmic bulk a CheB-P can bind to a free dimer. The binding-unbinding dynamics of a CheB-P is very similar to the dynamics of CheR described above, with tether binding rate w_b. A CheB-P molecule bound to a dimer belonging to an active cluster, can demethylate the dimer with a rate k_b provided its methylation level is

Table 2.1

Symbol	Description	Value	References
N_{dim}	Total number of receptor dimers	7200	[5, 7]
N_R	Total number of CheR protein molecules	140	[5, 7]
N_B	Total number of CheB protein molecules	240	[5, 7]
ϵ_0	Basal energy of receptor dimer	$1\ k_BT$	[5, 18, 6, 19]
ϵ_1	Receptor energy change per methyl group addition	$1\ k_BT$	[5, 18, 6, 19]
K_{min}	Minimum concentration receptor can sense	$18\ \mu M$	[20], [15]
K_{max}	Maximum concentration receptor can sense	$3000\ \mu M$	[15, 20]
w_a	Flipping rate of activity	$0.75\ s^{-1}$	Present study
ω	Switching frequency of motor	$1.3\ s^{-1}$	[16, 21]
Δ_1	Non-dimensional constant regulating motor switching	10	[16, 21]
Δ_2	Non dimensional constant regulating motor switching	20	[16, 21]
Y_0	Adopted value of the fraction of CheY-P protein	0.34	[16, 21]
K_Y	Phosphorylation rate of CheY molecule	$1.7\ s^{-1}$	[15, 22]
K_Z	Dephosphorylation rate of CheY molecule	$2\ s^{-1}$	[15, 22]
w_r	Binding rate of bulk CheR to an unoccupied dimer	$0.068\ s^{-1}$	[5, 14]
w_b	Binding rate of bulk CheB-P to an unoccupied dimer	$0.061\ s^{-1}$	[5, 14]
w_u	Unbinding rate of bound CheR and CheB-P	$5\ s^{-1}$	[5, 14]
k_r	Methylation rate of bound CheR	$2.7\ s^{-1}$	[5, 14]
k_b	Demethylation rate of bound CheB-P	$3\ s^{-1}$	[5, 14]
w_p	CheB phosphorylation rate	$3\ s^{-1}$	[5, 23]
w_{dp}	CheB-P dephosphorylation rate	$0.37\ s^{-1}$	[5]

non-zero.

2.3 Run-tumble motility

Total activity a is defined as the fraction of active clusters in the cell and it decides the CheY-P protein level in flagellar motor. High activity means high level of CheY-P protein and hence high tumbling bias. The rate equation which governs the amount of fraction of CheY-P is [15]

$$\frac{dY_P}{dt} = K_Y a(1 - Y_P) - K_Z Y_P \tag{2.3}$$

where $Y_P = \frac{[CheY-P]}{[CheY]}$, K_Y and K_Z are constants of phosphorylation and dephosphorylation respectively. The transition between run and tumble mode is decided by Y_P. A cell in CCW rotational state or in run mode can switch to CW rotational state or tumble mode with rate $\omega exp(-G)$ where $G = \Delta_1 - \frac{\Delta_2}{1+Y_0/Y_P}$ and the opposite switch from tumble to run happens with a rate $\omega exp(G)$[16, 6, 17]. Y_0 is the adapted value of Y_P in our system, Δ_1 and Δ_2 are two constants.

We present the values of all model parameters in Table 2.1.

2.4 Simulation Details

We consider run-and-tumble motion of the chemotactic cell both in one dimensional and two dimensional box. For simulation in $1D$ we take a lattice of length L along x-axis with two reflecting walls at two ends of it. Cell moves with a speed v, in dt time step it travels a distance vdt. So vdt serves as a natural lattice spacing here. Unless explicitly stated otherwise, we work with a linear attractant profile in this thesis, whose form is $c(x) = c_0(1 + x/x_0)$. For a one dimensional box, the trajectories are straight line and there are two possible directions: either rightward or leftward. During rightward (leftward) run cell experiences a linear increase (decrease) in concentration. If a new run starts the new run can be a rightward run or a leftward run with equal chance. We have used $L = 2000\ \mu m$, $v = 20\ \mu/s$, $dt = 0.01\ s$, $c_0 = 200\ \mu M$, $x_0 = 40\ mm$, $4\ mm$.

For simulation in $2D$, we take a $L_x \times L_y$ box with reflecting boundaries at four walls. We apply nutrient concentration gradient along x-direction only with similar form of $c(x)$ used in $1D$ case. Cell moves in xy plane with velocity v and during a run cell bends its trajectory by rotational diffusion with diffusivity D_θ. We allow this bending to make our model more realistic because E.coli does not move in perfect straight lines during runs. Its trajectory shows slight bending [24, 25]. When new run starts cell randomly chooses any angle θ between zero and 2π and starts a new run along that direction. We have used $L_x = 2000\ \mu m$, $L_y = 800\ \mu m$, $D_\theta = 0.062\ \mu m^2/s$. All other parameters are same as in $1D$ case.

Bibliography

[1] Jun Liu, Bo Hu, Dustin R Morado, Sneha Jani, Michael D Manson, and William Margolin. Molecular architecture of chemoreceptor arrays revealed by cryoelectron tomography of *Escherichia coli* minicells. *Proceedings of National Academy of Sciences*, 109(23):E1481–E1488, 2012.

[2] Ariane Briegel, Xiaoxiao Li, Alexandrine M Bilwes, Kelly T Hughes, Grant J Jensen, and Brian R Crane. Bacterial chemoreceptor arrays are hexagonally packed trimers of receptor dimers networked by rings of kinase and coupling proteins. *Proceedings of the National Academy of Sciences*, 109(10):3766–3771, 2012.

[3] Bernardo A Mello and Yuhai Tu. An allosteric model for heterogeneous receptor complexes: understanding bacterial chemotaxis responses to multiple stimuli. *Proceedings of the National Academy of Sciences*, 102(48):17354–17359, 2005.

[4] Jacque Monod, Jeffries Wyman, and Jean-Pierre Changeux. On the nature of allosteric transitions: a plausible model. *J Mol Biol*, 12(1):88–118, 1965.

[5] William Pontius, Michael W Sneddon, and Thierry Emonet. Adaptation dynamics in densely clustered chemoreceptors. *PLoS computational biology*, 9(9), 2013.

[6] Yann S Dufour, Xiongfei Fu, Luis Hernandez-Nunez, and Thierry Emonet. Limits of feedback control in bacterial chemotaxis. *PLoS Comput Biol*, 10(6):e1003694, 2014.

[7] Mingshan Li and Gerald L Hazelbauer. Cellular stoichiometry of the components of the chemotaxis signaling complex. *Journal of bacteriology*, 186(12):3687–3694, 2004.

[8] Howard C Berg and PM Tedesco. Transient response to chemotactic stimuli in *Escherichia coli*. *Proceedings of the National Academy of Sciences*, 72(8):3235–3239, 1975.

[9] Michael F Goy, Martin S Springer, and Julius Adler. Sensory transduction in *Escherichia coli*: role of a protein methylation reaction in sensory adaptation. *Proceedings of the National Academy of Sciences*, 74(11):4964–4968, 1977.

[10] Juan E Keymer, Robert G Endres, Monica Skoge, Yigal Meir, and Ned S Wingreen. Chemosensing in *Escherichia coli*: two regimes of two-state receptors. *Proceedings of the National Academy of Sciences*, 103(6):1786–1791, 2006.

[11] Robert G Endres and Ned S Wingreen. Precise adaptation in bacterial chemotaxis through "assistance neighborhoods". *Proceedings of the National Academy of Sciences*, 103(35):13040–13044, 2006.

[12] Jiongru Wu, Jiayin Li, Guoyong Li, David G Long, and Robert M Weis. The receptor binding site for the methyltransferase of bacterial chemotaxis is distinct from the sites of methylation. *Biochemistry*, 35(15):4984–4993, 1996.

[13] Xiuhong Feng, Angela A Lilly, and Gerald L Hazelbauer. Enhanced function conferred on low-abundance chemoreceptor trg by a methyltransferase-docking site. *Journal of bacteriology*, 181(10):3164–3171, 1999.

[14] Sonja Schulmeister, Michaela Ruttorf, Sebastian Thiem, David Kentner, Dirk Lebiedz, and Victor Sourjik. Protein exchange dynamics at chemoreceptor clusters in *Escherichia coli*. *Proceedings of the National Academy of Sciences*, 105(17):6403–6408, 2008.

[15] Marlo Flores, Thomas S Shimizu, Pieter Rein ten Wolde, and Filipe Tostevin. Signaling noise enhances chemotactic drift of *E. coli*. *Physical review letters*, 109(14):148101, 2012.

[16] Michael W Sneddon, William Pontius, and Thierry Emonet. Stochastic coordination of multiple actuators reduces latency and improves chemotactic response in bacteria. *Proceedings of the National Academy of Sciences*, 109(3):805–810, 2012.

[17] Gabriele Micali, Rémy Colin, Victor Sourjik, and Robert G Endres. Drift and behavior of *E. coli* cells. *Biophysical journal*, 113(11):2321–2325, 2017.

[18] Nicholas W Frankel, William Pontius, Yann S Dufour, Junjiajia Long, Luis Hernandez-Nunez, and Thierry Emonet. Adaptability of non-genetic diversity in bacterial chemotaxis. *Elife*, 3:e03526, 2014.

[19] Junjiajia Long, Steven W Zucker, and Thierry Emonet. Feedback between motion and sensation provides nonlinear boost in run-and-tumble navigation. *PLoS computational biology*, 13(3):e1005429, 2017.

[20] Lili Jiang, Qi Ouyang, and Yuhai Tu. Quantitative modeling of *Escherichia coli* chemotactic motion in environments varying in space and time. *PLoS Comput Biol*, 6(4):e1000735, 2010.

[21] Michael W Sneddon, James R Faeder, and Thierry Emonet. Efficient modeling, simulation and coarse-graining of biological complexity with nfsim. *Nature methods*, 8(2):177–183, 2011.

[22] Yuhai Tu, Thomas S Shimizu, and Howard C Berg. Modeling the chemotactic response of *Escherichia coli* to time-varying stimuli. *Proceedings of the National Academy of Sciences*, 105(39):14855–14860, 2008.

[23] Richard C Stewart, Knut Jahreis, and John S Parkinson. Rapid phosphotransfer to CheY from a CheA protein lacking the CheY-binding domain. *Biochemistry*, 39(43):13157–13165, 2000.

[24] Howard C Berg and Douglas A Brown. Chemotaxis in *Escherichia coli* analysed by three-dimensional tracking. *Nature*, 239(5374):500–504, 1972.

[25] Richa Karmakar, RVS Uday Bhaskar, Rajesh E Jesudasan, Mahesh S Tirumkudulu, and KV Venkatesh. Enhancement of swimming speed leads to a more-efficient chemotactic response to repellent. *Applied and environmental microbiology*, 82(4):1205–1214, 2016.

Chapter 3

Effect of receptor clustering on chemotactic performance of E.coli

In this chapter we ask how chemotactic performance is affected by the noise arising from clustering arrangement of chemoreceptors. To address this question we perform numerical simulation in a detailed theoretical model and what we observe is that an optimum size of receptor clusters or "signalling teams" exists, at which chemotatic efficiency is at its best.

As size of the receptor clusters increases, more dimers are involved to sense the input signal. So cooperative interaction among receptors increases and input signal gets amplified. Therefore, runs up the gradient get more extended and runs down the gradient get more shortened. This enhances the chemotactic drift. But as size of the receptor clusters increases number of clusters decreases and total activity is calculated over fewer number of teams. That's why fluctuation in the activity increases and adaptation module starts responding strongly to this large fluctuation for maintaining perfect adaptation. So receptor dimers now experience large change in their methylation levels. Therefore, variation in methylation free energy becomes much higher than the variation in ligand free energy and overall dynamics is controlled by the methylation part of the free energy. Cell becomes less responsive to what is happening to its ligand environment. Hence chemotactic performance deteriorates at very large cluster size. So at an intermediate cluster size best performance is obtained. Therefore, Our study reveals a crucial point that sensing versus adaptation competition can give rise to a performance peak.

In chapter 2 we have described about our model in details. In this chapter we present our simulation results. We have performed simulation both in one and two spatial dimensions. We first observe how fluctuation in the activity depends on receptor cluster size. Then we see how various quantities like localization, drift velocity etc depend on cluster size. We investigate further to reveal the mechanism that gives rise to such dependence of chemotactic responses on clustering noise. These results have been published in [1].

3.1 Clustering as a source of noise

Total activity of the cell is $a = \sum_{k=1}^{N_c} a_k/N_c$. Here a_k is the activity of k-th cluster. So a_k can take discrete values either 1 for active state or 0 for inactive state. N_c is the total number of clusters. If we consider the flipping of activity (a_k) of each cluster between 1 and 0 happens independent of each other then from central limit theorem it is expected that the total activity (a) should follow a Gaussian distribution and width of the distribution should be inversely proportional with N_c. Again $N_c = N_{dim}/3n$. So width of the distribution should linearly scale

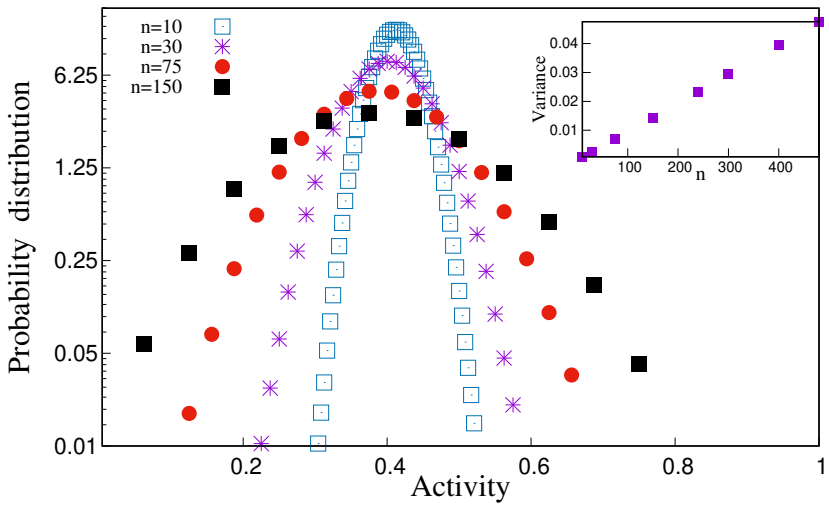

Figure 3.1: Probability distribution of average activity a at different cluster-size(n). The Distribution gets wider and variance increases linearly with n, which implies that as n increases fluctuation in the system. We can tune the noise in the pathway by varying this cluster size n of the system.

with n. Although in our model a_k of different k are not completely uncorrelated, we still see that the distribution of total activity is Gaussian in nature and variance linearly scales with n (Fig 3.1).

3.2 Data for Two Dimensions

3.2.1 Localization as a function of cluster size

Let $P(x)$ be the probability of finding the cell at position x. For efficient chemotaxis $P(x)$ should be large where $c(x)$ is high and $P(x)$ is small where $c(x)$ is low. Here, we have used a linear form of $c(x)$. When the gradient of $c(x)$ is not very large, $P(x)$ also shows a linear form. The slope of $P(x)$ is a measure of chemotactic performance. Quantitatively localization can be defined as average nutrient concentration experienced by the cell at steady state. Mathematically it can be written as $\langle C\rangle = \int_0^L c(x)P(x)dx$. It is clear from the expression that $\langle C\rangle$ takes large value only when both $c(x)$ and $P(x)$ are large. So when slope of $P(x)$ is large, localization $\langle C\rangle$ also takes large value. The main plot of Fig 3.2A shows that the slope of $P(x)$ has a peak with cluster size n. It increases initially when n increases from a very small value, attains a maximum value at intermediate value of n and then it decreases slowly when n is very large. So there exists an optimum value of n, at which slope of $P(x)$ as well as localization $\langle C\rangle$ is maximum.

3.2.2 Drift Velocity as a function of cluster size

Drift velocity is another important chemotactic response for a moving cell in non-uniform concentration profile. In uniform or flat concentration profile the inherent stochasticity of the system helps the cell to diffuse equally in every direction, which results a homogeneous population in long time limit. But in non-uniform profile runs in the direction of increasing attractant concentration get extended and runs in the direction of decreasing attractant concentration get shortened. Therefore, a net drift velocity is resulted in the direction of increasing concentration[2]. Drift velocity of chemotactic cell is responsible for spatial variation in the steady state position distribution $P(x)$ of the cell[3, 4], without which it would be a purely diffusive motion of the cell homogenizing the population all over the surface.

To measure drift velocity quantitatively we define it as net displacement of the cell in a run divided by average duration of a run. A net displacement is resulted only when average displacement of the cell due to rightward (up the gradient) and leftward (down the gradient) runs are not equal. To measure this difference we define two quantities $d_R(x)$ and $d_L(x)$ which denotes the total duration of rightward and leftward runs respectively starting from an arbitrary position x. Let $N_R(x)$ and $N_L(x)$ be total number of these rightward and leftward runs, within an observation time window t_{obs}. So average run duration (in either direction) starting from position x will be $\tau(x) = \frac{d_R(x)+d_L(x)}{N_R(x)+N_L(x)}$. Now let the probability that a run starts from position x is $Q_{tum}(x) = N^{-1}[N_R(x) + N_L(x)]$, where N is normalization constant $N = \int_0^L dx' N_R(x') + N_L(x')$. Then average displacement will be given by $\Delta = \int dx Q_{tum}(x) v \frac{d_R(x)-d_L(x)}{N_R(x)+N_L(x)}$. So drift velocity ($V$) can be calculated as average displacement in a run Δ divided by average duration of a run τ, where $\tau = \int \tau(x) Q_{tum}(x)$. So final expression for chemotactic drift velocity is given by

$$V = \frac{\Delta}{\tau} = \frac{v \int dx [d_R(x) - d_L(x)}{\int dx' d_R(x') + d_L(x')} \tag{3.1}$$

Another way of measuring Drift Velocity is to note the net displacement (Δ) of the cell in a finite time interval T and then divide Δ by T. We denote this Drift velocity as U. So by definition $U = \Delta/T$. We have measured both U and V as a function n and observed an optimum value of n where U and V takes maximum values. in Fig 3.2B we have shown the data for U (main plot) and V (inset) as a function of n.

3.2.3 Mean first passage time till next tumble

At the core of chemotactic sensing lies the differential behavior of the cell when the nutrient level in its environment goes up or down. This difference should be large for a good performance. When a cell is running in the direction of increasing nutrient concentration, its tumbling rate decreases and the run is extended. Similarly, for a run towards a lower nutrient level, the tumbling rate increases and the run is shortened. We measure the time till the first tumble during an uphill run and a downhill run and plot their difference in Fig. 3.3A. This difference shows a peak at a specific size of the receptor cluster.

For a tethered cell also a similar quantity can be defined. In this case a tethered cell in CCW motor rotational state is exposed to a nutrient profile increasing linearly with time and the time till the first switching of motor rotational state from CCW to CW is noted. Similarly a tethered cell in CCW motor rotational state is exposed to a nutrient profile decreasing linearly with time and the time till the first switching of motor rotational state from CCW to CW is noted. The difference of the noted time between the increasing and decreasing case is analogous to the

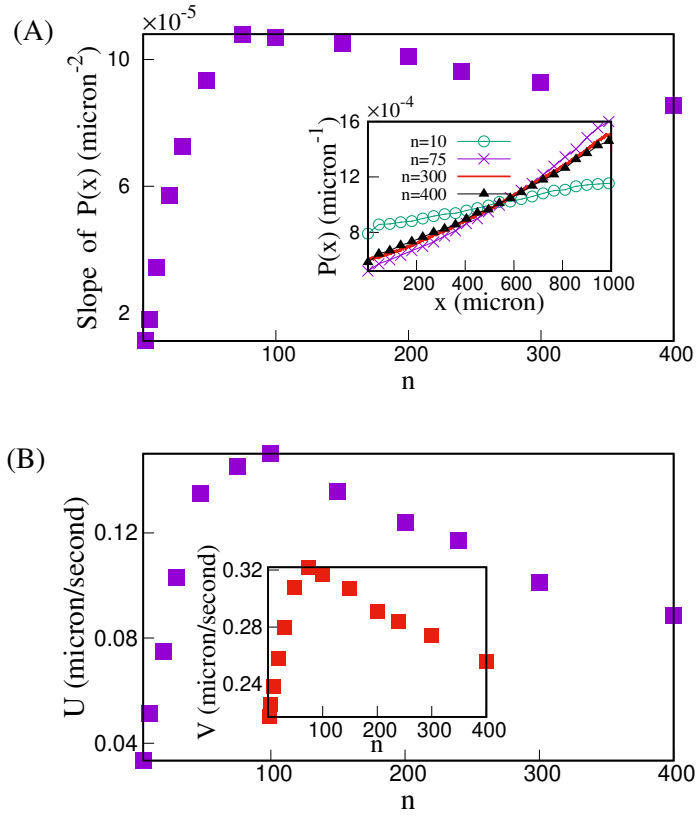

Figure 3.2: Peak in localization and drift velocity as a function of receptor cluster size. (A) The x-position distribution of the cell shows steepest variation at an optimum n. Inset shows form of $P(x)$ for few different n values. (B) Chemotactic drift velocity measured from net displacement in a run(Inset) and net displacement in a fixed time-interval T (main plot) both show peak for a specific n. We have used a linearly varying nutrient profile here. Each data point have been averaged over at least 10^7 configurations. The simulation parameters are specified in Sec. 2.4.

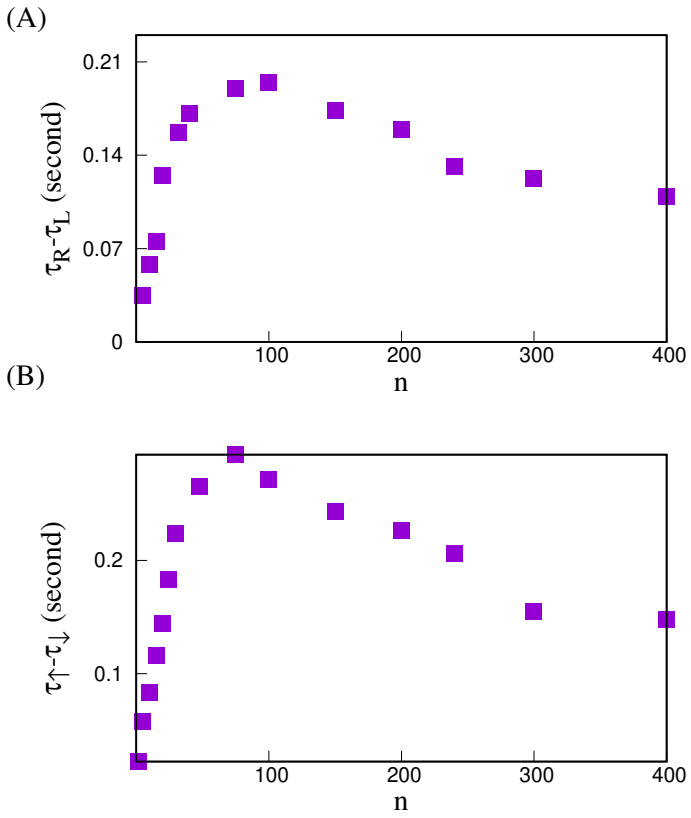

Figure 3.3: Motor response of the cell shows highest sensitivity at a specific size of receptor cluster. (A) For a swimming cell, the mean first passage time to the tumble mode for uphill run (τ_R) and downhill run (τ_L) shows largest difference at a particular n. (B) For a tethered cell in CCW mode, the mean first passage time to CW mode when the nutrient level is ramped up $(\tau_\uparrow)$ and ramped down $(\tau_\downarrow)$ shows largest difference at a specific n. All data have been averaged over at least 10^6 configurations. The other simulation parameters are as in Fig. 3.2

difference of first tumble time for a running cell. We see in Fig 3.3B that for a tethered cell also this quantity shows a peak as a function of n.

3.2.4 Competition between sensing and adaptation

Free energy (F) of a receptor cluster has two parts: one is sum of ligand binding energy of all dimers in the cluster (F_L) and another is sum of methylation level of all dimers in the cluster (F_m). In our model we assume that all dimers in the cluster experience same ligand concentration $c(x)$ which is function of cell position. As n increases more dimers are involved in sensing the nutrient and hence F_L is proportional to n. We already have noticed that width of activity distribution is narrow at small n (Fig. 3.1), which implies that activity never goes far away from the adapted value in this case. Therefore, role of adaptation is very weak and change in F_m is negligible. So motion is mainly controlled by F_L. Contribution of F_L increases linearly with n. That means as n increases free energy reaches to higher (lower) value during runs up (down) the gradient. Probability to find a cluster in active state is given by $[1 + \ exp(F)]^{-1}$. So activity gets more suppressed (elevated) in uphill (downhill) runs. It causes more elongation (shortening) of runs up (down) the gradient. Therefore net drift along the gradient increases

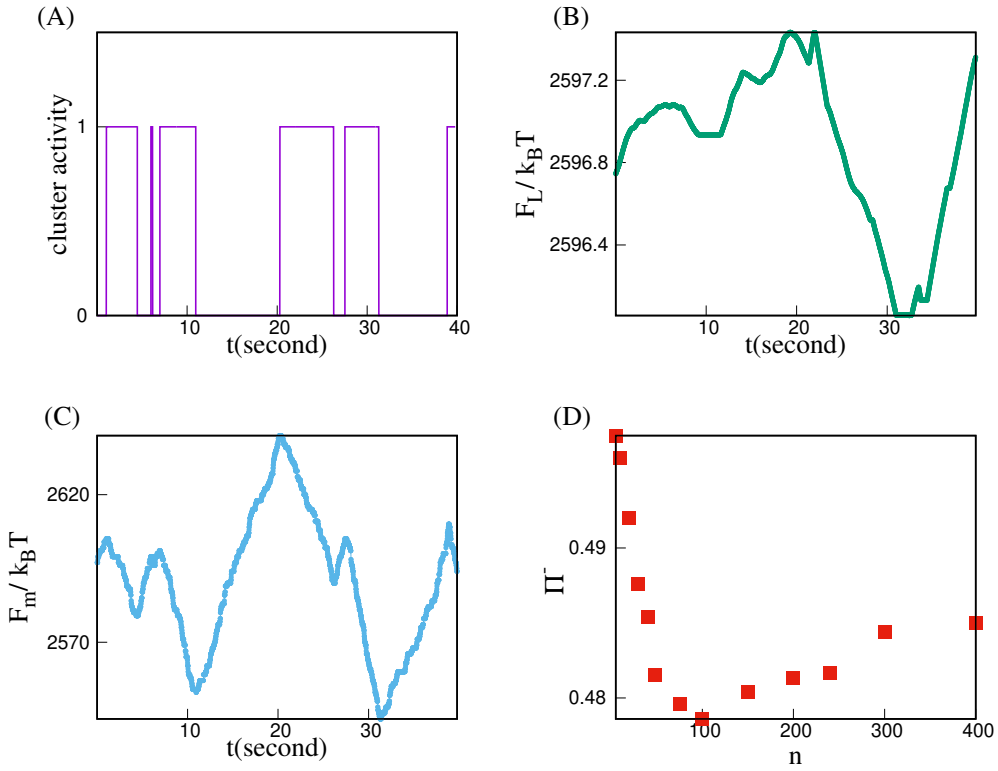

Figure 3.4: Typical time-series of activity along with methylation component and ligand component of free energy of a receptor cluster of size $n = 200$. The time-series has been recorded in steady state over a time-window of $40s$. (A) shows few transitions of activity state of the cluster. (B) shows simultaneous variation of free energy (in unit of k_BT) due to ligand binding which directly captures the run-tumble trajectory of the cell. (C) records variation of methylation free energy (in unit of k_BT) of the cluster which is seen to roughly follow the activity transitions. The scale of variation of ligand binding energy is negligible compared to that of methylation for the present value of n. (D) Probability Π^- that in a time interval $T = 40s$ the net displacement of the cell is negative, shows a minimum and then increases for large n. The simulation parameters used are same as those in Fig. 3.2.

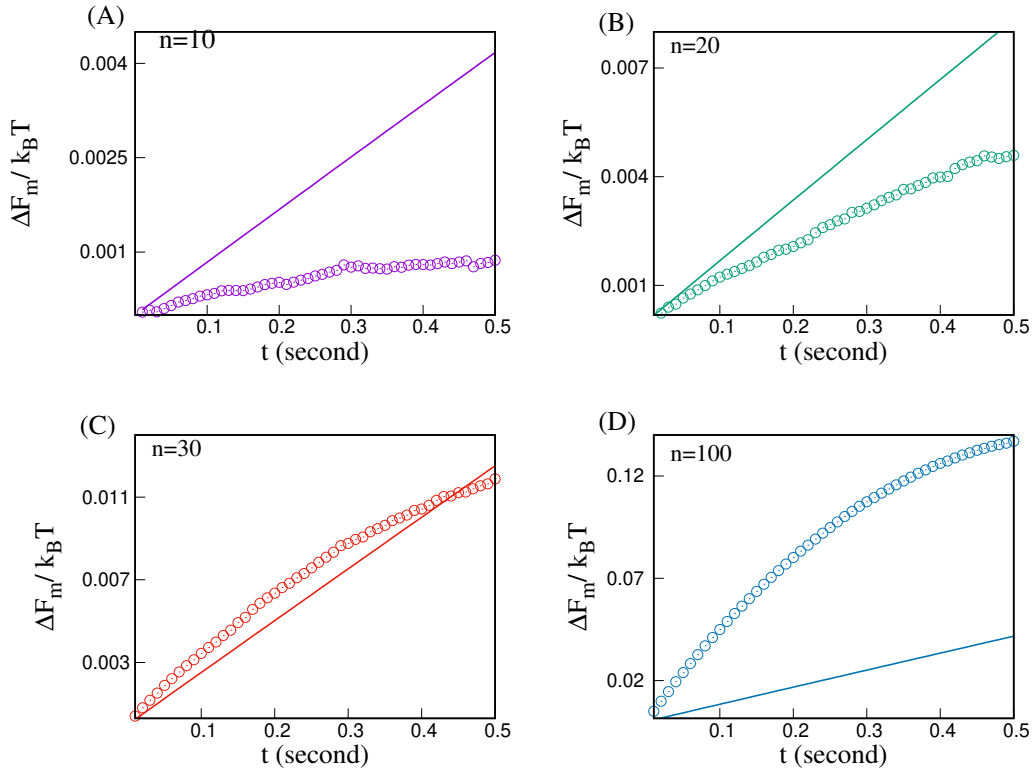

Figure 3.5: Average change ΔF_m in methylation free energy (discrete points) of a cluster for first $0.5s$ during an uphill run for 4 different n values. The continuous lines show the change in ligand free energy of the cluster. For small n the change in ligand free energy dominates but as n increases, ΔF_m takes over. These data have been averaged over at least 2×10^6 samples.

with n and chemotactic performance gets enhanced. But at large n huge fluctuation in activity is observed (Fig. 3.1) and hence adaptation comes to play major role by causing rapid methylation and demethylation to receptors. This increases F_m significantly and a competition develops between sensing and adaptation. At very large n fluctuation is so high that adaptation wins in the competition. Therefore, adaptation controls the motion and cell is less sensitive to the ligand concentration profile. It cannot follow the gradient efficiently and even probability of showing a net negative drift increases (Fig. 3.4D). So performance deteriorates at very large n and a peak is observed in chemotactic performance as function of n.

In support of our arguments we measure the change in F_L and change in F_m as a function of time from the beginning of uphill runs. In linear concentration profile during uphill runs F_L increases linearly with time. We see F_m also increases with time. But at small n the increase in F_m is much smaller than increase in F_L (Fig 3.5A,B). This clearly reveals that when n is small cluster free energy (F) is mainly dominated by F_L and sensitivity controls the motion. But as n increases ΔF_m starts to grow faster with time and a competition develops between ΔF_L and ΔF_m. As n increases further ΔF_m completely dominates over ΔF_L (Fig 3.5D). Temporal variation in F_m becomes very large compared to the temporal variation of F_L. We have shown this for $n = 200$ in Fig. 3.4 where in a time series of activity corresponding change in F_L and F_m have been shown. Clearly F_m varies over much wider range than the range of variation F_L. So variation in cluster free energy (F) is mainly controlled by ΔF_m now. Therefore, F_m wins the competition and control the overall dynamics at very large n. That means sensitivity to ligand becomes very less and performance gets deteriorated.

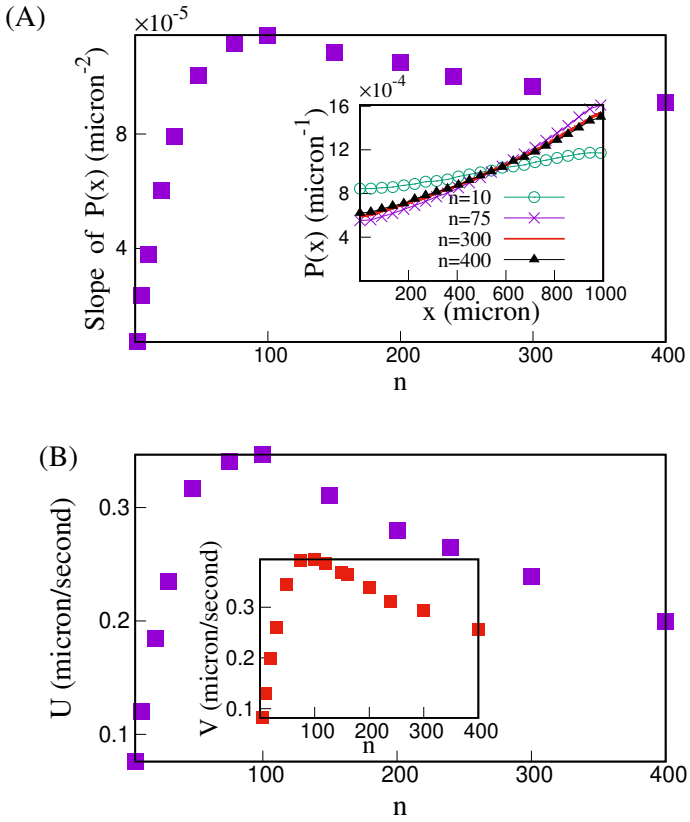

Figure 3.6: (A) In presence of a linear nutrient concentration profile with weak gradient, the steady state position distribution $P(x)$ of the cell is almost linear. The steepness shows a peak with n. Inset shows some representative $P(x)$ plots for few chosen n values. (B) Chemotactic drift velocity measured from net displacement in a run (main plot) and from net displacement in a fixed time-interval $T = 10s$ (inset) show peak with n. The data points are averaged over at least 10^7 histories. The simulation parameters are same as Fig. 3.2

3.3 Data for one dimension

We have also performed the simulations for one spatial dimension. We see some quantitative difference from the $2D$ data here, although qualitative nature is same and our conclusions are remain valid here as well. Data for localization and drift velocity as a function of cluster size have been presented in Fig. 3.6A and 3.6B respectively. Data for difference in first tumble time as a function of n are shown in Fig. 3.7. Competition between F_L and F_m has been shown in Fig. 3.8.

3.4 Discussion

In this work we have studied how the receptor clustering noise affects chemotactic response of a single cell E.coli. We see chemotactic responses showing a performance peak as function of receptor cluster size. Cooperativity among receptors increases with cluster size and input signal gets multiplied several times. So ligand sensitivity increases and better chemotaxis is observed. But when size of the clusters reaches a very high value then number of clusters becomes very low and fluctuation in receptor activity becomes very high. In this case to main-

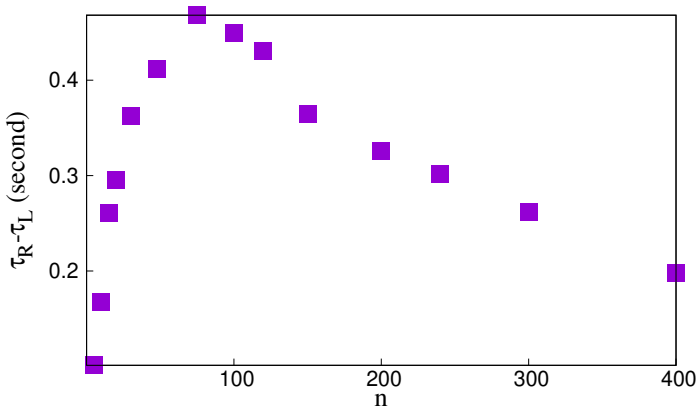

Figure 3.7: During a rightward (leftward) run of the cell when it is headed towards regions with more (less) nutrient, τ_R (τ_L) denote the average time till the next tumble. The difference $(\tau_R - \tau_L)$ shows a peak as a function of n. Each data point is averaged over at least 10^6 histories. All simulation parameters are same as Fig. 3.2

.

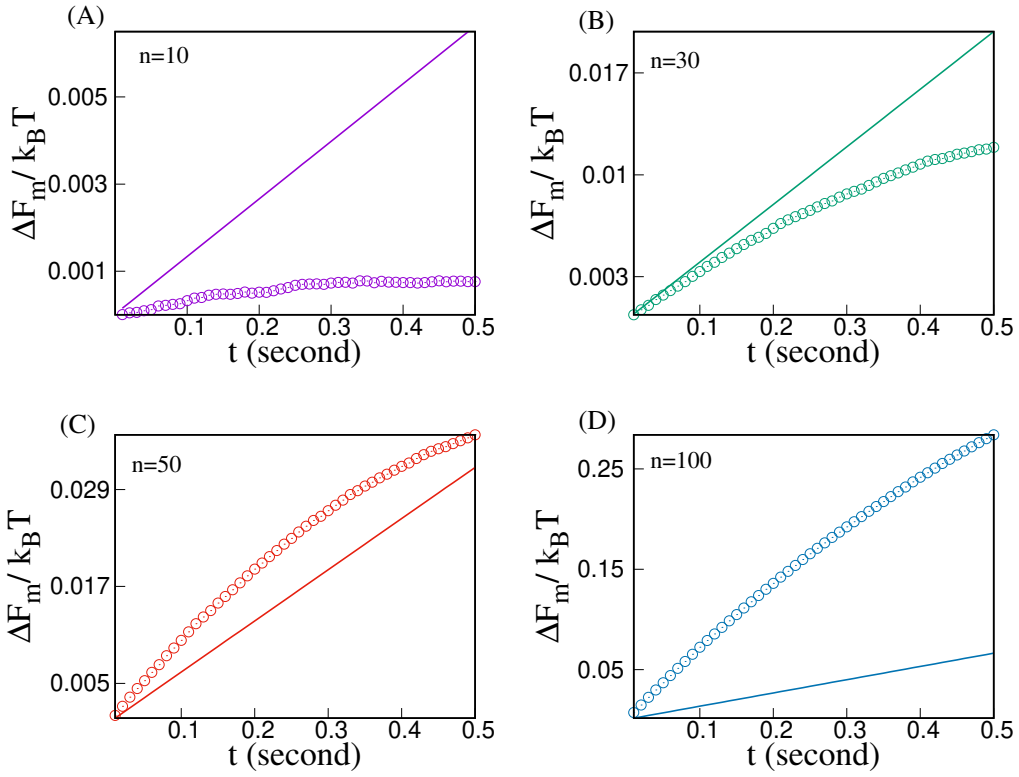

Figure 3.8: Average change ΔF_m (in unit of $k_B T$) in methylation free energy (discrete points) of a cluster for first $0.5s$ during an uphill run for 4 different cluster sizes. For comparison, the corresponding change in ligand free energy (in unit of $k_B T$) has been shown by continuous lines. For small n the change in ligand free energy dominates but as n increases, ΔF_m takes over. These data have been averaged over at least 2×10^6 histories.

tain the adapted activity, methylation and demethylation processes happen rapidly. This causes huge variation in methylation level of receptors, which actually starts controlling overall dynamics by dominating over the ligand part of the free energy. This reduces the performance. Thus at an intermediate cluster size the chemotactic performance of the cell is at its best.

Optimal size of receptor cluster have been reported earlier for fluctuating ligand signal. It was argued that receptor cooperativity not only amplifies the ligand signal but also the noise present in it. Therefore, a trade-off is needed where cluster size should be large enough to amplify even very weak input signal and simultaneously small enough so that amplified noise in the input signal does not hamper the sensitivity [5]. In another study where both ligand noise and intracellular biochemical noise were considered, it was found that receptor clustering is beneficial until amplified noise does not exceed the biochemical noise [6]. But the optimal signalling team size we have reported here is for the ligand concentration profile which is not fluctuating with time. To the best of our knowledge such optimality is completely new in this field and was not known so far.

Our result of the optimum cluster size for best chemotactic performance can be experimentally verified. One can track the trajectory of the cell, get information about each run and tumble by monitoring the switching events of one rotational sate (CCW) to another (CW) of flagellar motor. Using this data it can be directly verified whether the localisation, drift velocity etc shows a performance peak or not. For a tethered cell in CCW rotational mode it is easy to note the average time taken when switching to CW rotational mode takes place in a ramped up and ramped down ligand environment and verify whether the quantity $(\tau_\uparrow - \tau_\downarrow)$ shows a performance peak or not. In our study best performance is observed for clusters which contain ~ 70 TDs for both swimming and tethered cell. But in experiment exact quantitative agreement with our result may not be found. To make our model simpler we haven't considered the hexagonal geometry of the spatial arrangement of the receptor array [7, 8] or more importantly, the energy cost due to curvature of the cell membrane induced by the receptor clusters [9, 10, 11]. But in future to understand more complex model incorporating those above mentioned things our simple analysis might be helpful. Inclusion of those complex things in the model won't alter our key finding of interplay between ligand free energy and methylation energy, which can be experimentally investigated as the cooperative interaction among the receptors is varied [12, 13]. It has been already observed in experiment that stronger interaction among receptors is responsible for the formation of large clusters and also gives rise to larger activity fluctuation in tethered cell [13, 12]. Finally, our study will surely raise the important issue of competition between sensing and adaptation in a broad area of biological system. In those wide class of systems it would be interesting to see the similar performance peak as we obtained is also observed or not.

Bibliography

[1] Shobhan Dev Mandal and Sakuntala Chatterjee. Effect of receptor clustering on chemotactic performance of *E. coli*: Sensing versus adaptation. *Phys. Rev. E Letter*, 103:L030401, Mar 2021.

[2] P-G De Gennes. Chemotaxis: the role of internal delays. *European Biophysics Journal*, 33(8):691–693, 2004.

[3] Sakuntala Chatterjee, Rava Azeredo da Silveira, and Yariv Kafri. Chemotaxis when bacteria remember: drift versus diffusion. *PLoS computational biology*, 7(12), 2011.

[4] Yariv Kafri and Rava Azeredo da Silveira. Steady-state chemotaxis in *Escherichia coli*. *Physical review letters*, 100(23):238101, 2008.

[5] Robert G Endres, Olga Oleksiuk, Clinton H Hansen, Yigal Meir, Victor Sourjik, and Ned S Wingreen. Variable sizes of *Escherichia coli* chemoreceptor signaling teams. *Molecular systems biology*, 4(1):211, 2008.

[6] Gerardo Aquino, Diana Clausznitzer, Sylvain Tollis, and Robert G Endres. Optimal receptor-cluster size determined by intrinsic and extrinsic noise. *Physical Review E*, 83(2):021914, 2011.

[7] Ariane Briegel, Xiaoxiao Li, Alexandrine M Bilwes, Kelly T Hughes, Grant J Jensen, and Brian R Crane. Bacterial chemoreceptor arrays are hexagonally packed trimers of receptor dimers networked by rings of kinase and coupling proteins. *Proceedings of the National Academy of Sciences*, 109(10):3766–3771, 2012.

[8] Jun Liu, Bo Hu, Dustin R Morado, Sneha Jani, Michael D Manson, and William Margolin. Molecular architecture of chemoreceptor arrays revealed by cryoelectron tomography of *Escherichia coli* minicells. *Proceedings of National Academy of Sciences*, 109(23):E1481–E1488, 2012.

[9] Robert G Endres. Polar chemoreceptor clustering by coupled trimers of dimers. *Biophysical journal*, 96(2):453–463, 2009.

[10] Christoph A Haselwandter and Ned S Wingreen. The role of membrane-mediated interactions in the assembly and architecture of chemoreceptor lattices. *PLoS computational biology*, 10(12):e1003932, 2014.

[11] Will Draper and Jan Liphardt. Origins of chemoreceptor curvature sorting in *Escherichia coli*. *Nature communications*, 8(1):1–9, 2017.

[12] Johannes M Keegstra, Keita Kamino, François Anquez, Milena D Lazova, Thierry Emonet, and Thomas S Shimizu. Phenotypic diversity and temporal variability in a bacterial signaling network revealed by single-cell fret. *Elife*, 6:e27455, 2017.

[13] Remy Colin, Christelle Rosazza, Ady Vaknin, and Victor Sourjik. Multiple sources of slow activity fluctuations in a bacterial chemosensory network. *Elife*, 6:e26796, 2017.

Chapter 4

Effect of receptor clustering on methylation dynamics in weak attractant gradient

In this chapter we study the temporal variation of methylation level of a receptor cluster while the cell moves in a linear concentration profile. Here we have considered a weak gradient of the profile, for which position distribution of the cell takes almost a linear form.

Due to complex nature of the chemotaxis network it is not trivial to predict the temporal variation of methylation level. Binding of attractant to the receptors suppresses the activity and unbinding causes rise in the activity. Again due to feedback present in the network active clusters get demethylated and inactive clusters get methylated. So this coupled dynamics makes the methylation dynamics quite complicated. Our study unravels this complex dynamics and provides useful insights into the interdependence of different dynamical variables in the signaling network.

We explicitly consider two different types (directions) of runs: uphill and downhill. As the names suggest, during an uphill run the local attractant concentration increases along the cell trajectory and during a downhill run it decreases. We show that methylation dynamics of uphill and downhill runs are qualitatively similar for weak gradient. Although some quantitative differences appear depending upon the run direction and strength of receptor cooperativity. We observe here average change of methylation level during those runs as a function of time right from the beginning of the runs.

In chapter 2 we have described our model in details. In this chapter we present our simulation results on methylation dynamics of chemoreceptors. Here we consider a linear attractant profile of the form $c(x) = c_0(1 + x/x_0)$, as described in chapter 2. For weak gradient we use $x_0 = 40\ mm$. We have studied in both one and two spatial dimensions. Most of the results discussed here are for $1d$, while $2d$ results which are qualitatively similar to $1d$ results, have been presented towards the end of this chapter. The results we have presented here have been published in [1]

4.1 Temporal variation of methylation levels

We consider a large enough number of uphill and downhill runs of variable durations and average over them to measure the methylation variation. Let $N^+(t)$ and $N^-(t)$ be the numbers of uphill and downhill runs initiating at time $t = 0$ and continuing upto time t. But as time goes on some of the runs gets terminated. So $N^{\pm}(t)$ decreases with time. Let consider $m_i^+(t)$ as

the methylation level of a particular cluster in i-th uphill run at time t. Similarly we can define $m_i^-(t)$ for i-th downhill run. Now we define here two quantities

$$\Delta m^{\pm}(t) = \sum_{i=1}^{N^{\pm}(t)} \frac{m_i^{\pm}(t) - m_i^{\pm}(0)}{N^{\pm}(t)}$$

and

$$\delta m^{\pm}(t) = \frac{\sum_{i=1}^{N^{\pm}(t)} m_i^{\pm}(t)}{N^{\pm}(t)} - \frac{\sum_{i=1}^{N^{\pm}(0)} m_i^{\pm}(0)}{N^{\pm}(0)}$$

Here $\Delta m^+(t)$ $[\Delta m^-(t)]$ considers those uphill (downhill) runs which persist at least till time t and measures the average change in methylation in those runs. However, $\delta m^+(t)$ $[\delta m^-(t)]$ considers average methylation level of all uphill (downhill) runs persistent till time t and subtracts from it the average methylation level of all uphill (downhill) runs which started at time $t = 0$, irrespective of their durations. The main difference between two quantities $\Delta m^{\pm}(t)$ and $\delta m^{\pm}(t)$ is the choice of ensemble over which initial average methylation level (at $t = 0$) is calculated. This initial ensemble for $\Delta m^{\pm}(t)$ is those runs which continues upto time t and for $\delta m \pm (t)$ it is all runs started at $t = 0$ no matter they continue upto time t or tumble before time t. We have shown that this initial choice of ensemble is very crucial for the methylation dynamics and can result in completely different outcome. We are interested in the effect of receptor cooperativity on the temporal variation of these quantities. We find the effect is very different for weak gradient case and strong gradient case. We separately present these two cases in this chapter and the following chapter. For comparison, we also show results for the homogeneous attractant environment for which $\Delta m^+(t)$ and $\Delta m^-(t)$ become identical. Similarly, $\delta m^+(t)$ and $\delta m^-(t)$ also become same in this limit. One might expect that the methylation variation for the homogeneous environment lies in between the uphill and downhill variation. But we show below that it is not always true.

4.2 Role of initial activity

We first study in Fig. 4.1 the distribution of activity a_0 values at the beginning of a run . The distribution is unimodal and gets wider with increasing n or gradient strength [2, 3, 4, 5, 6, 7, 8]. The distribution is also roughly symmetric about the peak. The mean value of a_0, as well as the adapted level of activity, lie close to the peak position. Therefore, the activity values near the peak can be considered to be in the medium range, the ones near the left (right) tail belong to low (high) range. In Fig. 4.2 we show the distribution of run durations which start with low, medium or high activity values. As expected, the long runs are least probable for high a_0 and most probable for low a_0. The integrated quantity is the number of runs persisting at least till time t, starting with a_0 values belonging to these three different ranges. We denote this quantity by $N^{\pm}(t|a_0)$. In Fig. 4.3 we plot $N^+(t|a_0)$, number of uphill runs starting with a_0 values and surviving upto t. As expected, for all gradient strength and all cooperativity, $N^+(t|a_0)$ is largest for runs starting with medium range of a_0 (green cross points) because that is where the most probable value of a_0 lies (shown by red dot in each panel of Fig. 4.1). Fig. 4.3 also shows that $N^+(t|a_0)$ has sharpest drop for high a_0 (blue star points), specially at small t since these are the runs associated with high tumbling bias. We find very similar behavior for $N^-(t|a_0)$ also (data not shown here). Number of runs persisting till time t and starting with any a_0 values can be denoted by $N^{\pm}(t)$. Fig 4.4 shows exponential decay of $N^{\pm}(t)$ in both weak and strong gradient. As we show below, these variations plays a crucial role in $\Delta m^{\pm}(t)$ behavior.

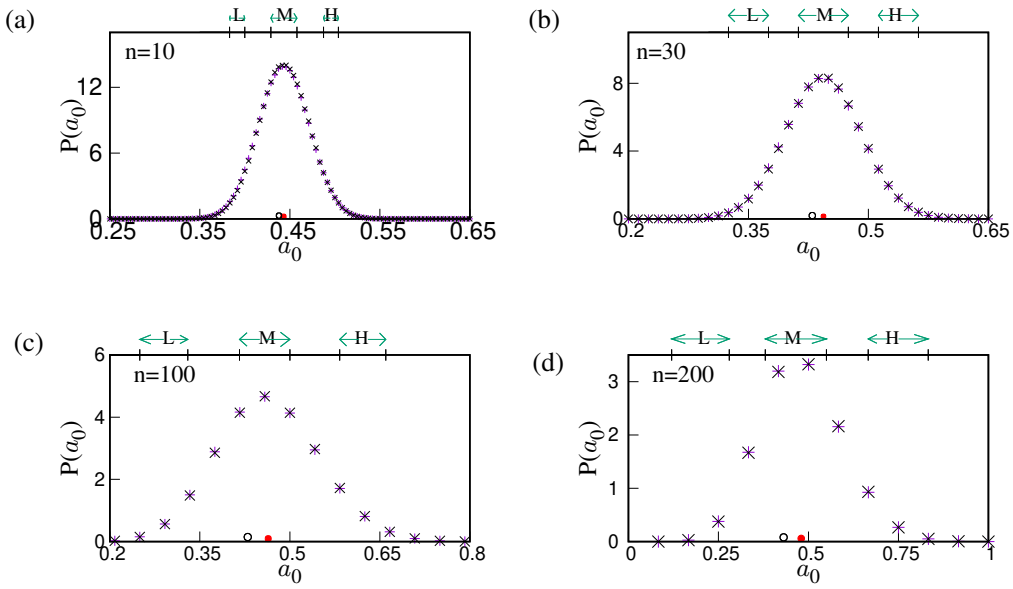

Figure 4.1: Distribution of activity a_0 at the start of a run in weak gradient. The low (L), medium (M) and high (H) ranges of values of a_0 have been shown. These ranges are defined with reference to the mean a_0 value shown by the red point. The empty circle on the x-axis shows the adapted activity value which also belongs to the medium range. Each data point has been averaged over at least 10^6 histories. All simulation parameters are specified in Sec. 2.4.

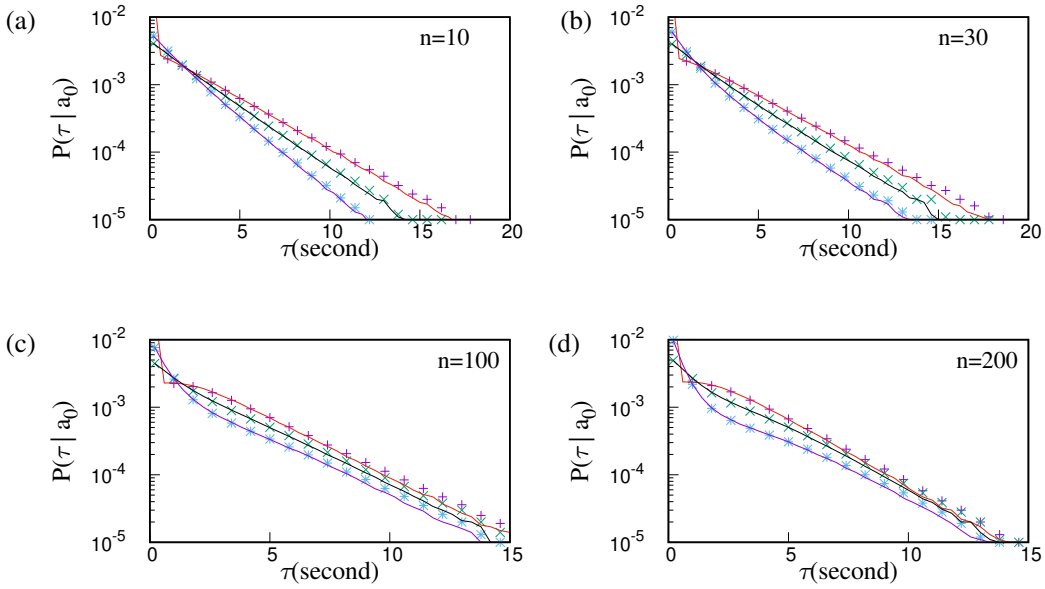

Figure 4.2: Distribution of run durations starting with low (purple empty square), medium (green filled circle) and high (blue empty circle) values of initial activity. Curves with discrete points stand for weak gradient case and solid line curves that pass through discrete points stand for gradient-free profile. As expected, runs starting with lower activity values survive the longest. Each data point has been averaged over at least 2×10^6 times. All simulation parameters are specified in Sec. 2.4.

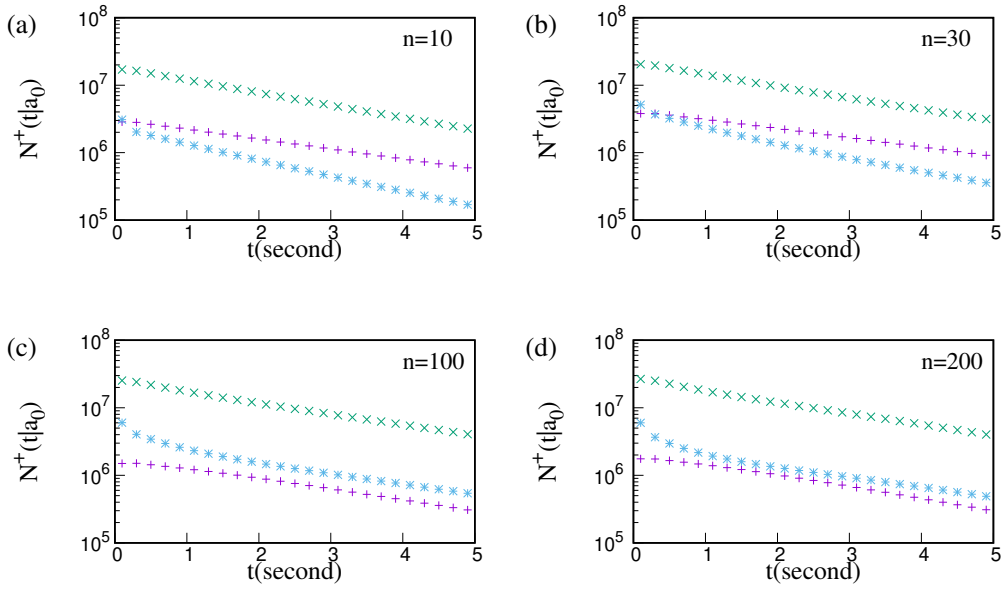

Figure 4.3: Number of surviving runs as a function of time for runs starting with three activity zones, which are high activity (blue stars), medium activity (green cross) and low activity (purple plus). Each data point has been averaged over at least 10^5 histories. All simulation parameters are specified in Sec. 2.4.

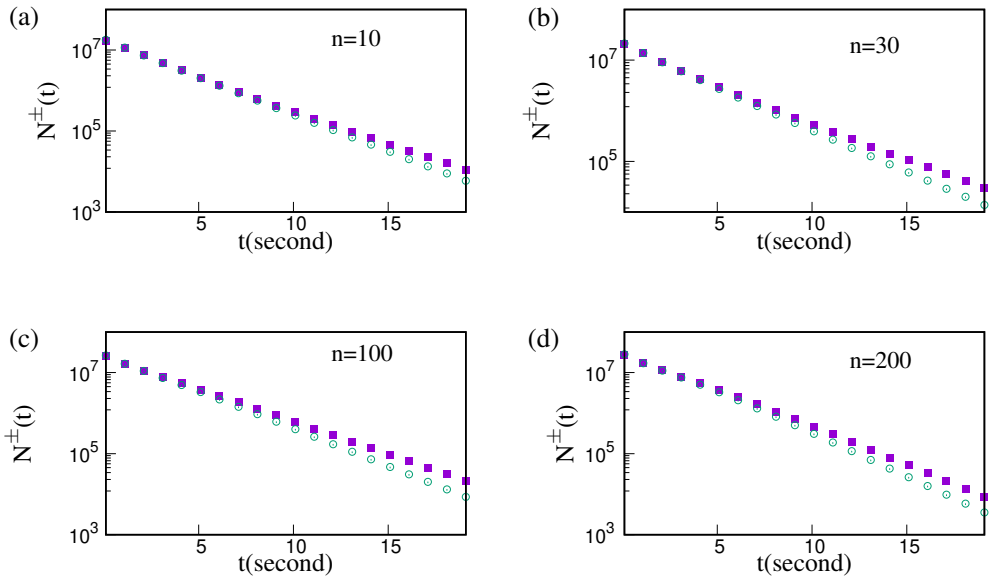

Figure 4.4: Number of surviving runs as a function of time for both uphill(purple solid square) and downhill(green empty circles) runs. It shows that number of downhill runs drops faster than number of uphill ones. Each data has been averaged over at least 10^5 histories. All simulation parameters are specified in Sec. 2.4.

In Fig. 4.5 we plot $\Delta m^{\pm}(t|a_0)$, defined as the methylation variation during a run starting with low, medium or high a_0 . We expect that for small a_0 we should have methylation, for large a_0 we should have demethylation and for medium a_0 change in methylation should have small magnitude. This is exactly what we find for small n, as shown in Fig. 4.5a. For large n the behavior is same as above for small t but for large t our data in Figs. 4.5(c) and 4.5(d) of Fig. 4.5 show positive values of $\Delta m^{\pm}(t|a_0)$ which indicates methylation. This is consistent with our data in Fig. 4.6(e)–4.6(h). It may appear counter-intuitive why for large a_0 even downhill runs show methylation at large times. Actually, the initial strong demethylation lowers the activity significantly since for large n flipping of activity states of even few signaling teams can cause the activity value to fall below its adapted level. This triggers methylation for large t. In Fig. 4.5 we also show the data for flat attractant profile. As expected, it lies between the uphill and downhill curves.

4.3 Variation of $\Delta m^{\pm}(t)$ in weak gradient

We present our data for $\Delta m^{\pm}(t)$ in Fig. 4.6 for different values of the receptor cluster size n. Using the insights obtained from looking at the methylation variation for different activity range, we can now explain the data for $\Delta m^{+}(t)$ in Fig. 4.6. For $n = 10$ Fig.4.6(a) shows that $\Delta m^{+}(t)$ starts from 0, decreases slightly to become negative for small t and then increases steadily with t. This means for small t the uphill runs show demethylation and then they switch

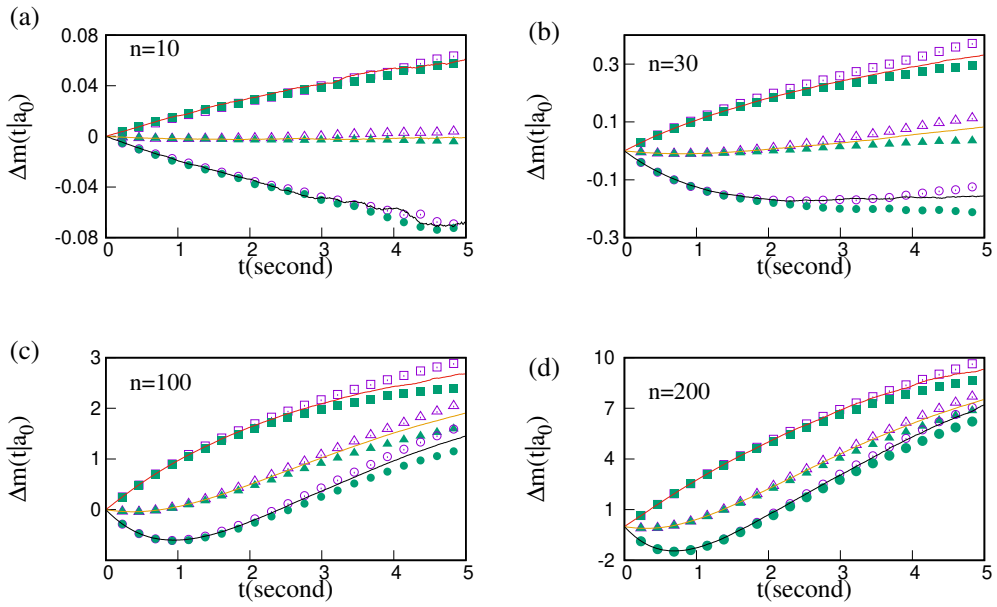

Figure 4.5: $\Delta m^{\pm}(t|a_0))$ for runs starting with three different activity ranges. The square, triangular and circular symbols correspond to low, medium and high a_0 values while the empty (filled) symbols are for uphill (downhill) runs. Among the solid lines, the top (red), middle (yellow) and the bottom (black) ones correspond to low, medium and high a_0 runs for the flat profile. Each data point has been averaged at least 10^5 histories. All simulation parameters are specified in Sec. 2.4.

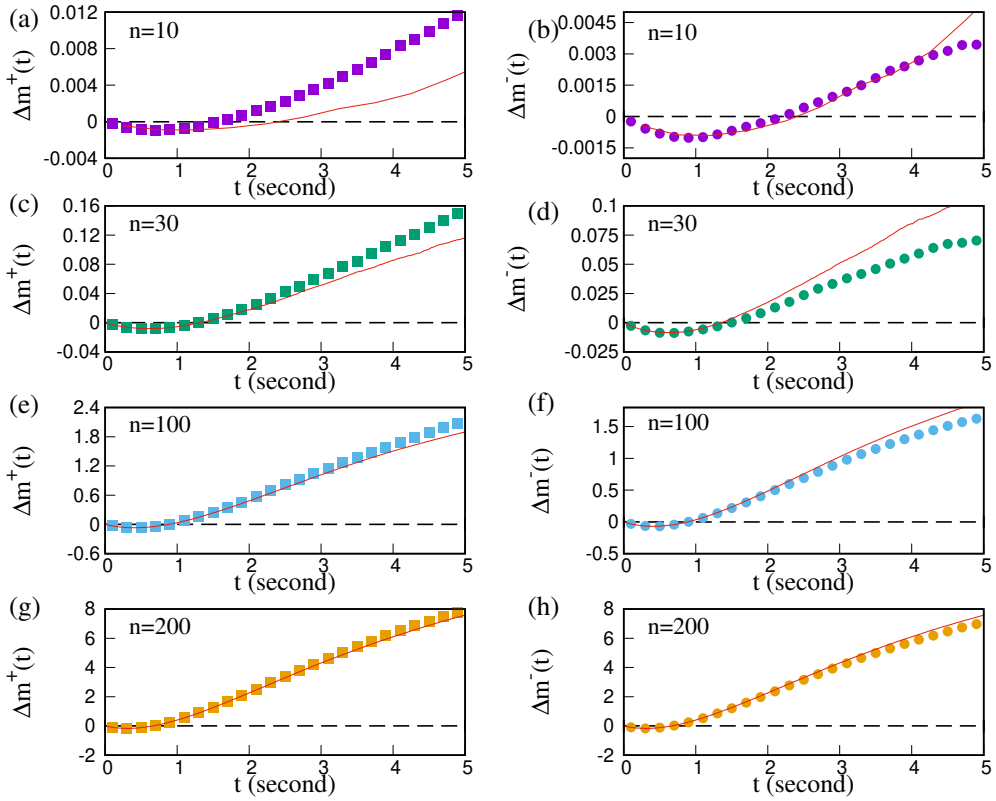

Figure 4.6: Temporal variation of $\Delta m^{\pm}(t)$ for different n: left panel shows plots for $\Delta m^{+}(t)$ for the uphill runs and the right panel shows $\Delta m^{-}(t)$ for the downhill runs. Initial demethylation is due to short high activity runs and later methylation is due to long runs with low activity. These data are for a one dimensional motion of the cell in a box of size L across which a linear concentration profile $c(x)$ of the nutrient is set up with weak gradient. All simulation parameters are specified in Sec. 2.4. These data are averaged over at least 3×10^6 histories.

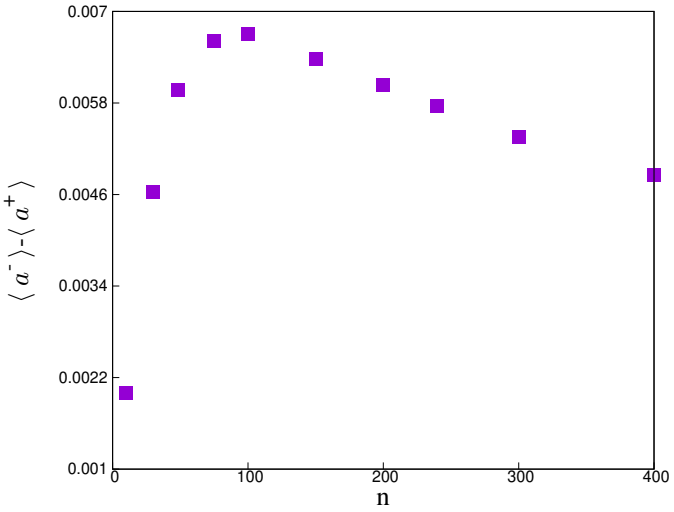

Figure 4.7: Difference of average activity during uphill and downhill runs. The difference decreases with n for large n which reflects dominance of adaptation module over sensing module. These data are for $1d$ motion of the cell with weak gradient of $c(x)$. Each data point has been averaged over at least 10^7 histories. All simulation parameters are same as Fig. 4.6.

over to methylation. Note that our data in Fig. 4.5(a) show that the demethylation trend for high a_0 runs are stronger than the methylation trend for low a_0 runs. This is also consistent with our observation that mean value of a_0 is higher than the adapted activity [see Fig. 4.1(a)]. In other words, the short-time behavior of $\Delta m^+(t)$ is dominated by high a_0 runs which undergo demethylation. However, these runs are short and as time goes on, these short runs end and drop out of $N^+(t)$ population and only the longer runs remain, as seen in Fig. 4.3(a). These runs are associated with low activity and hence receptor methylation. Moreover, due to increasing $c(x)$ along the cell trajectory in this case, activity is lowered further. Thus methylation takes over and $\Delta m^+(t)$ shows positive growth. In Fig. 4.6(b) we show the data for $\Delta m^-(t)$ for the same cluster size. The qualitative behavior remains same here also. However, the late time growth due to methylation is much weaker in this case. This is expected since even for those runs with low activity which persist till late times, $c(x)$ keeps decreasing with t which tends to raise the activity. Because of this opposing effect coming from the ligand free energy, activity remains higher than the uphill runs, and average methylation shows a slower growth. To filter out the effect of the ligand concentration gradient, in Fig. 4.6 we also plot the methylation variation in absence of a gradient (red lines). As expected, we find the curve in this case lies in between $\Delta m^+(t)$ and $\Delta m^-(t)$.

For larger values of n, qualitative behavior remains the same, although the quantitative variation of $\Delta m^{\pm}(t)$ happens over a larger range now. This is expected since the number of receptors per cluster increases, the total change in methylation level of a cluster also increases. The negative values observed at small t also show similar trend, the minimum in $\Delta m^{\pm}(t)$ at small t becomes deeper as n increases. We also notice that for $n = 10, 30$ the range of variation of $\Delta m^+(t)$ and $\Delta m^-(t)$ are significantly different, but for $n = 100, 200$ the ranges are not as different for the uphill and downhill runs. Methylation is still slower for the downhill curve, but the values are much closer to the uphill curve. This is because for large n the activity fluctuations increase and then adaptation plays a bigger role in the signaling network and ligand free energy becomes less important [8, 6]. The difference in the cell behavior during an uphill and downhill run therefore decreases for large n. Fig. 4.7 we show this explicitly

by plotting the difference between average activity during an uphill and downhill run, and as expected, this difference decreases with n for large n. This explains why the temporal variation of methylation follows a similar course for large n, irrespective of whether the cell is running uphill or downhill.

4.4 Variation of $\delta m^{\pm}(t)$ in weak gradient

Surprisingly, the temporal variation of $\delta m^{\pm}(t)$ shows a completely different behavior. Our data for $n = 10$ in Fig. 4.8 show that $\delta m^{\pm}(t)$ starts from 0 and then it decreases with time for both uphill and downhill runs. This indicates uphill and downhill runs show demethylation on an average, which is opposite to what we had seen in Fig. 4.6 for the same cluster size. The reason behind this apparently contradicting observation is explained below. Since more and more runs terminate with time, $N^{\pm}(t)$ decreases with t. Since the tumbling bias increases with activity, it follows that majority of those terminated runs correspond to high activity and this can be directly verified from Fig 4.3a,c,e,g which shows that $N^{\pm}(t|a_0)$ of high a_0 drops out at much faster rate than the rate at which $N^{\pm}(t|a_0)$ of low a_0 and medium a_0 drops out. A high activity state is in turn associated with high methylation level. Therefore, those runs which drop out of $N^{\pm}(t)$ population, have high methylation level. Although positive values of $\Delta m^{\pm}(t)$ for moderate or large t ensure that runs which persist till such times undergo methylation, due to dropping out of high methylation states from the population, the average methylation level still decreases with time, making $\delta m^{\pm}(t)$ negative. Our data also show that $\delta m^{-}(t)$ takes a larger negative value at late times, compared to $\delta m^{+}(t)$. This is consistent with the fact that the positive growth of $\Delta m^{-}(t)$ is slower than that of $\Delta m^{+}(t)$ for large t (see Figs. 4.6a and 4.6b).

For $n = 30$ the trend remains similar, except $\delta m^{+}(t)$ after an initial decrease tends to saturate at larger t. This is because $\Delta m^{+}(t)$ for this n shows a strong growth for large t and although high methylation states continue to drop out of the population of $N^{+}(t)$, due to large rise in methylation level during the individual long runs, the decrease of average methylation level of all uphill runs gets arrested. This effect is even more prominent for $n = 100, 200$ where due to even stronger growth of $\Delta m^{\pm}(t)$, we find a trend reversal: $\delta m^{\pm}(t)$ after an initial decrease, show upward swing and start increasing with time. Here the decreasing tendency of population averaged methylation level due to tumbling is overcompensated by large growth in methylation in individual persistent runs. As expected, this effect is stronger for the uphill runs, and somewhat weaker for the downhill runs.

4.5 Data for two dimensions

We have also performed the simulations for two spatial dimensions. We see some quantitative difference from the $1D$ data here, although qualitative nature is same and our conclusions are remain valid here as well. Data for $\Delta m^{\pm}(t)$ and $\delta m^{\pm}(t)$ variation in weak gradient have been presented in Fig. 4.9 and 4.10 respectively.

4.6 Discussion

In this chapter we study the methylation dynamics of chemoreceptors of an E.coli cell while the cell navigates through a spatially varying ligand environment. We have performed this analysis

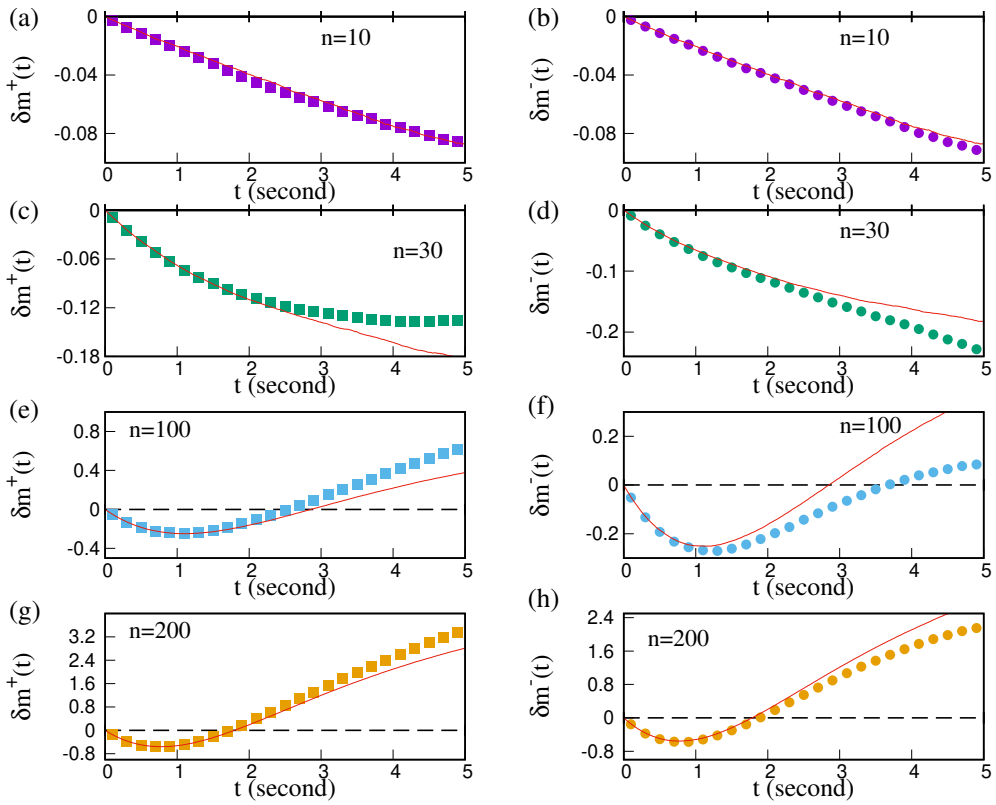

Figure 4.8: Temporal variation of $\delta m^{\pm}(t)$ for different n: left (right) panel with discrete square(circular) points corresponds to uphill (downhill) runs and red solid line in each panel shows $\delta m(t)$ for runs along either direction in homogeneous concentration profile to distinguish the effect of gradient-sensing. Increasing methylation level for long runs tends to increase average methylation, while dropping out of high methylation trajectories from $N^{\pm}(t)$ tends to decrease average methylation. In this competition the former wins for small n and the later wins for large n. These data are averaged over at least 5×10^5 histories. Other simulation details are same as in Fig. 4.6.

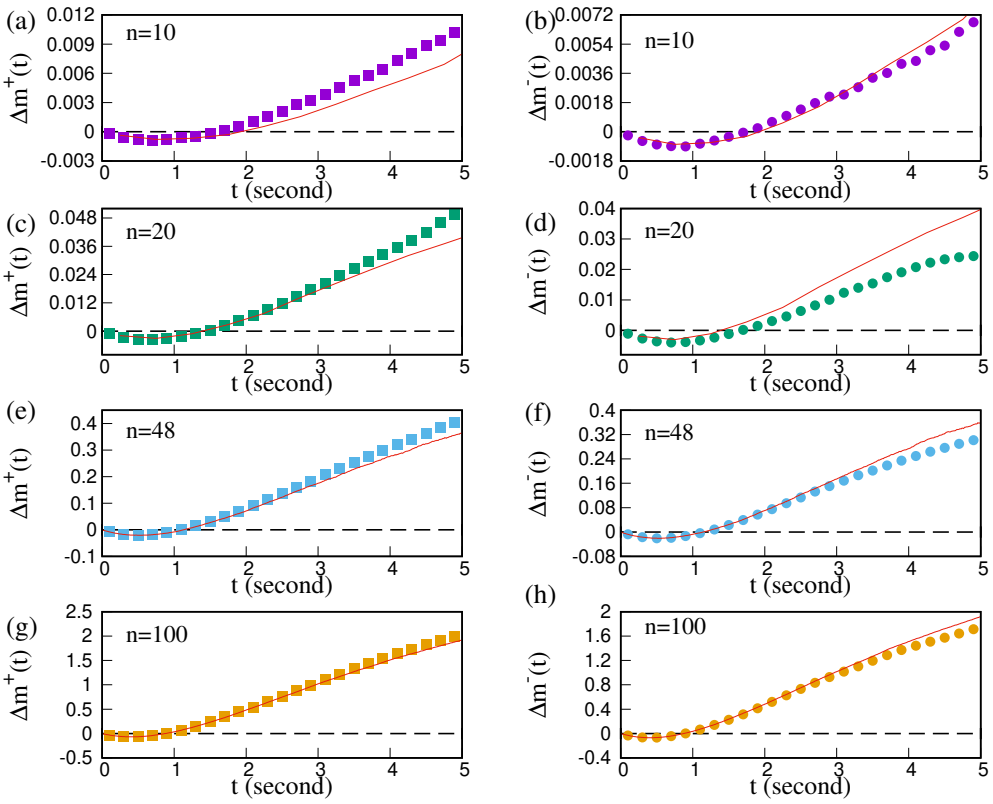

Figure 4.9: Temporal variation of $\Delta m^{\pm}(t)$ for different n in two dimensions: left panel shows plots for $\Delta m^{+}(t)$ for the uphill runs(with discrete square points) and the right panel shows $\Delta m^{-}(t)$ for the downhill runs(with discrete circular points). Red solid line in each panel shows $\Delta m(t)$ for runs along either direction in homogeneous concentration profile to distinguish the effect of gradient-sensing Here weak gradient of $c(x)$ is considered and the data look qualitatively similar to the one dimensional case, presented in Fig. 4.6. All simulation parameters are specified in Sec. 2.4. These data are averaged over at least 10^5 histories.

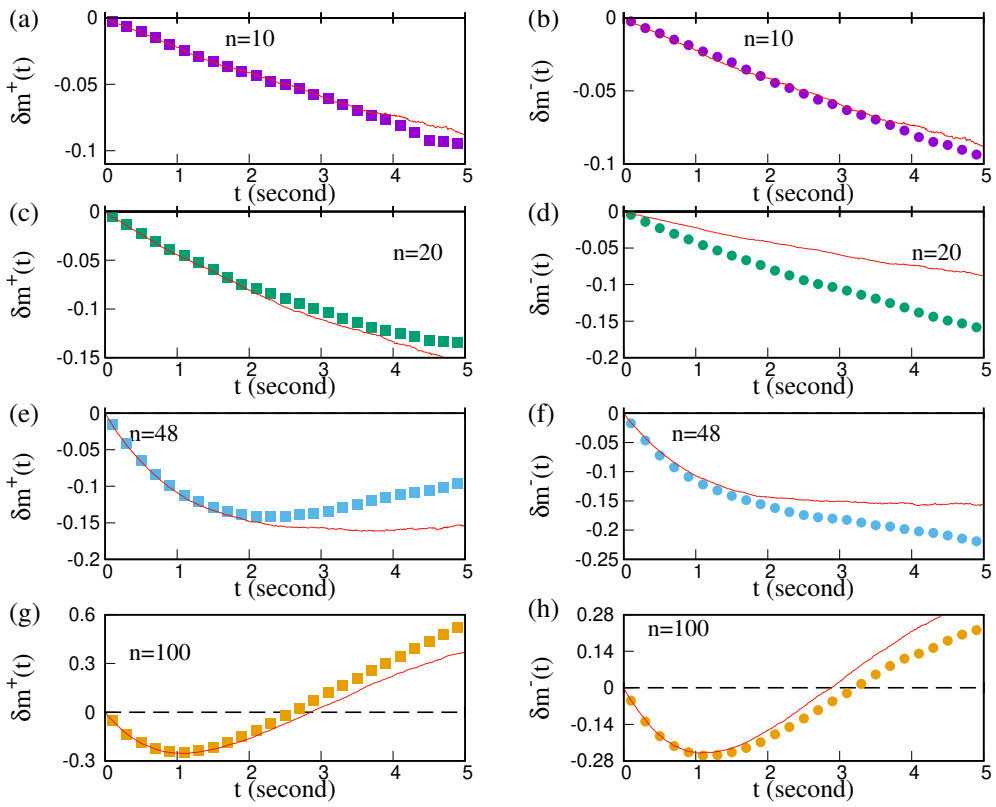

Figure 4.10: Temporal variation of $\delta m^{\pm}(t)$ for different n in two dimensions: left (right) column corresponds to uphill (downhill) runs by curves with discrete square(circular) points. Red solid line in each panel shows $\delta m(t)$ for runs along either direction in homogeneous concentration profile to distinguish the effect of gradient-sensing. As seen in the data for one dimension, $\delta m^{\pm}(t)$ and $\Delta m^{\pm}(t)$ show opposite trends for small n, while for large n their trends become similar. These data are averaged over at least 9×10^5 histories. Other simulation parameters are same as Fig. 4.9.

for weak gradient profile here. Our numerical simulations show that the receptor cooperativity strongly affects the methylation dynamics.

In all cases we find that initial variation of methylation level is controlled by a large number of short runs with high activity, which tumble quickly and drop out from the ensemble very first. That's why demethylation is observed just after initiation of the run. But in intermediate and large time only long runs survive with low initial activity and hence methylation is triggered. That's why for both uphill and downhill runs after initial demethylation we see methylation level increases continuously with time for the whole time range of our measurement. As size of the receptor clusters increases quantitative change is reflected in the behaviour of methylation level variation but the qualitative behaviour remains unaltered.

Bibliography

[1] Shobhan Dev Mandal and Sakuntala Chatterjee. Effect of receptor cooperativity on methylation dynamics in bacterial chemotaxis with weak and strong gradient. *Physical Review E*, 105(1):014411, 2022.

[2] Junjiajia Long, Steven W Zucker, and Thierry Emonet. Feedback between motion and sensation provides nonlinear boost in run-and-tumble navigation. *PLoS computational biology*, 13(3):e1005429, 2017.

[3] Chuan Xue and Xige Yang. Moment-flux models for bacterial chemotaxis in large signal gradients. *Journal of mathematical biology*, 73(4):977–1000, 2016.

[4] Weiran Sun and Min Tang. Macroscopic limits of pathway-based kinetic models for *E. coli* chemotaxis in large gradient environments. *Multiscale Modeling & Simulation*, 15(2):797–826, 2017.

[5] Gabriele Micali, Rémy Colin, Victor Sourjik, and Robert G Endres. Drift and behavior of *E. coli* cells. *Biophysical journal*, 113(11):2321–2325, 2017.

[6] Shobhan Dev Mandal and Sakuntala Chatterjee. Effect of receptor clustering on chemotactic performance of *E. coli*: Sensing versus adaptation. *Phys. Rev. E Letter*, 103:L030401, Mar 2021.

[7] Johannes M Keegstra, Keita Kamino, François Anquez, Milena D Lazova, Thierry Emonet, and Thomas S Shimizu. Phenotypic diversity and temporal variability in a bacterial signaling network revealed by single-cell fret. *Elife*, 6:e27455, 2017.

[8] Remy Colin, Christelle Rosazza, Ady Vaknin, and Victor Sourjik. Multiple sources of slow activity fluctuations in a bacterial chemosensory network. *Elife*, 6:e26796, 2017.

[9] Yann S Dufour, Xiongfei Fu, Luis Hernandez-Nunez, and Thierry Emonet. Limits of feedback control in bacterial chemotaxis. *PLoS Comput Biol*, 10(6):e1003694, 2014.

[10] Thomas S Shimizu, Yuhai Tu, and Howard C Berg. A modular gradient-sensing network for chemotaxis in *Escherichia coli* revealed by responses to time-varying stimuli. *Molecular systems biology*, 6(1):382, 2010.

[11] Ariane Briegel, Xiaoxiao Li, Alexandrine M Bilwes, Kelly T Hughes, Grant J Jensen, and Brian R Crane. Bacterial chemoreceptor arrays are hexagonally packed trimers of receptor dimers networked by rings of kinase and coupling proteins. *Proceedings of the National Academy of Sciences*, 109(10):3766–3771, 2012.

[12] Jun Liu, Bo Hu, Dustin R Morado, Sneha Jani, Michael D Manson, and William Margolin. Molecular architecture of chemoreceptor arrays revealed by cryoelectron tomography of *Escherichia coli* minicells. *Proceedings of National Academy of Sciences*, 109(23):E1481–E1488, 2012.

[13] Robert G Endres. Polar chemoreceptor clustering by coupled trimers of dimers. *Biophysical journal*, 96(2):453–463, 2009.

[14] Christoph A Haselwandter and Ned S Wingreen. The role of membrane-mediated interactions in the assembly and architecture of chemoreceptor lattices. *PLoS computational biology*, 10(12):e1003932, 2014.

[15] Will Draper and Jan Liphardt. Origins of chemoreceptor curvature sorting in *Escherichia coli*. *Nature communications*, 8(1):1–9, 2017.

Chapter 5

Effect of receptor clustering on methylation dynamics in strong attracctant gradient

In this chapter we study the temporal variation of methylation level of a receptor cluster while cell moves in a linear concentration profile with strong gradient. Here strong gradient corresponds to that strength of gradient for which linearizing approximation does not hold and position distribution of the cell takes a non-linear form.

In chapter 4 we have seen that for weak gradient methylation dynamics is quantitatively similar for uphill and downhill runs. But here nature of methylation variation for downhill runs are qualitatively very different from that of the uphill ones. Our data show the sensing versus adaptation interplay responding diversely to wide range of receptor cooperativity, which affects the temporal variation of methylation level significantly, specially for downhill mover. We explain our numerical observations from a detailed analysis of the coupled time evolution of receptor activity, methylation and ligand concentration within the signaling network. To our knowledge such a systematic study of methylation level variation has not been done so far.

In chapter 2 we have described our model in details. In this chapter we present our simulation results on methylation dynamics in strong gradient. We consider a linear attractant profile of the form $c(x) = c_0(1 + x/x_0)$, as described in chapter 2. For strong gradient we use $x_0 = 4$ mm. We have studied in both one and two spatial dimensions. Most of the results discussed here are for $1d$, while $2d$ results which are qualitatively similar to $1d$ case have been presented towards the end of the chapter. These results have been published in [1].

5.1 Role of initial activity

We first look into the activity distribution at the start of the run and define low, medium, and high ranges of activity as done in the previous subsection. In Fig. 5.1 we present the data for $P(a_0)$ which is wider than the weak gradient case [2, 3, 4, 5, 6] and identify the ranges of low, medium and high a_0. In Fig. 5.2 we show the distribution of run durations which start with low, medium or high activity values. As expected, the long runs are least probable for high a_0 and most probable for low a_0. The integrated quantity is the number of runs persisting at least till time t, starting with a_0 values belonging to these three different ranges. We denote this quantity by $N^{\pm}(t|a_0)$. In Fig. 5.3 we plot $N^{+}(t|a_0)$, number of uphill runs starting with a_0 values and surviving upto t. As expected, for all cooperativity, $N^{+}(t|a_0)$ is largest for runs starting with medium range of a_0 (green cross points) because that is where the most probable value of a_0

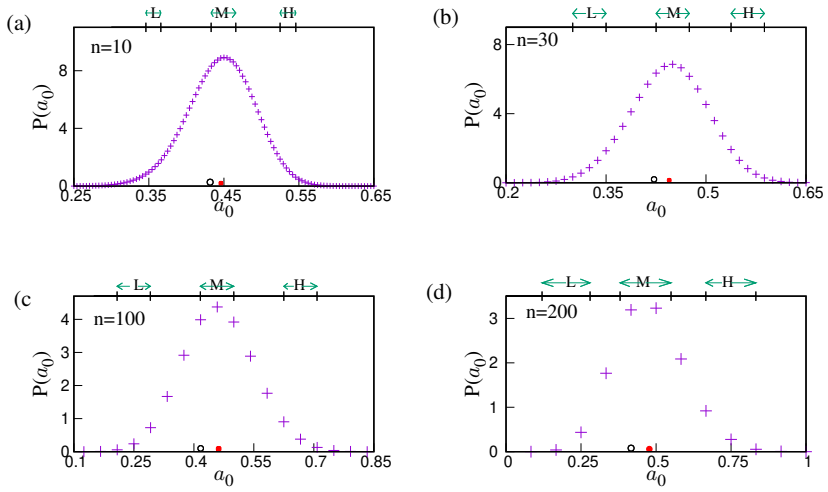

Figure 5.1: Distribution of activity a_0 at the start of a run in strong gradient. The low (L), medium (M) and high (H) ranges of values of a_0 have been shown. These ranges are defined with reference to the mean a_0 value shown by the red point. The empty circle on the x-axis shows the adapted activity value which also belongs to the medium range. Each data point has been averaged over at least 10^6 histories. All simulation parameters are specified in Sec. 2.4.

lies (shown by red dot in each panel of Fig. 5.1). Fig. 5.3 also shows that $N^+(t|a_0)$ has sharpest drop for high a_0 (blue star points), specially at small t since these are the runs associated with high tumbling bias. We find very similar behavior for $N^-(t|a_0)$ also (data not shown here). Number of runs persisting till time t and starting with any a_0 values can be denoted by $N^{\pm}(t)$. Fig 5.4 shows exponential decay of $N^{\pm}(t)$. As we show below, these variations plays a crucial role in $\Delta m^{\pm}(t)$ behavior.

In Fig. 5.5 we plot $\Delta m^{\pm}(t|a_0)$ with a_0 in one of these three ranges. The solid lines in these plots show the data for the zero gradient case where we have used same ranges of a_0 as in Fig. 5.1 which are significantly different from a_0 ranges for the flat attractant profile shown in Fig. 1.1 in chapter 4. Because of this difference we sometimes find in Fig. 5.5 the solid lines do not lie between the uphill and downhill curves.

For small n the behavior of $\Delta m^{\pm}(t|a_0)$ is qualitatively similar to the weak gradient case, i.e., methylation for low a_0 runs, demethylation for high a_0 runs and mild change in methylation for medium a_0 runs. For large n, we find all uphill runs, irrespective of their a_0 range, show methylation at large t. The uphill runs starting with large a_0 show initial demethylation which lower the activity. Moreover, increasing ligand concentration along the trajectory also tends to lower the activity. Due to these two effects activity falls below the adapted level and methylation takes over. For downhill runs our data in Fig. 5.5(b) show that low a_0 runs show weak methylation at large t and for medium and high a_0 we have demethylation. In this case, the already strong gradient, further amplified by receptor cooperativity controls the behavior at large times, initial activity plays a less significant role. The fast falling ligand concentration along the trajectory raises the activity resulting in demethylation. For $n = 100$ Fig. 5.5(c) shows that small a_0 runs show methylation for small times followed by a dip at larger times,

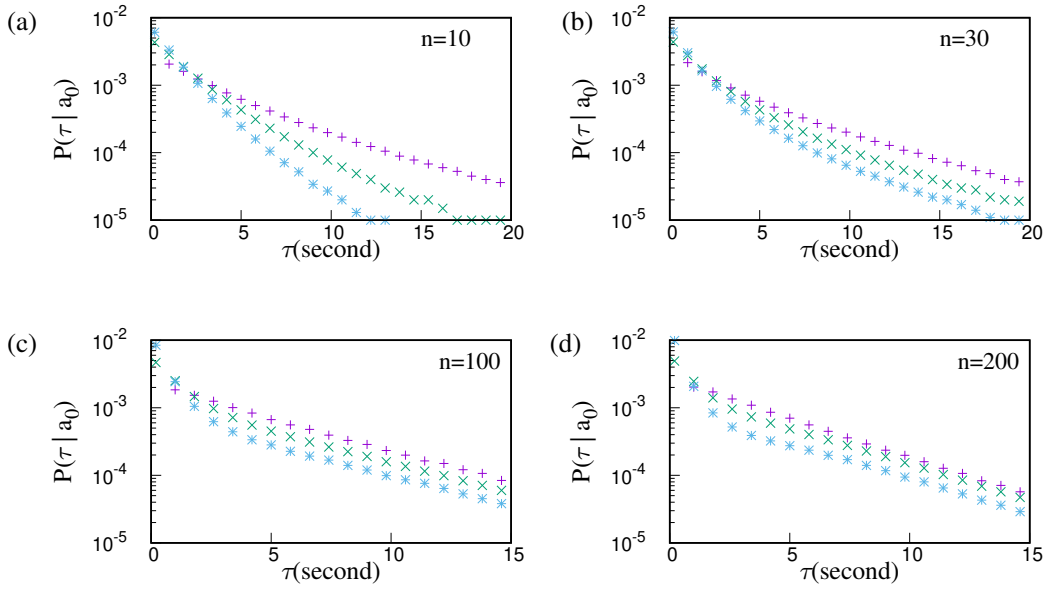

Figure 5.2: Distribution of run durations starting with low (purple empty square), medium (green filled circle) and high (blue empty circle) values of initial activity in strong gradient. As expected, runs starting with lower activity values survive the longest. Each data point has been averaged over at least 2×10^6 times. All simulation parameters are specified in Sec. 2.4.

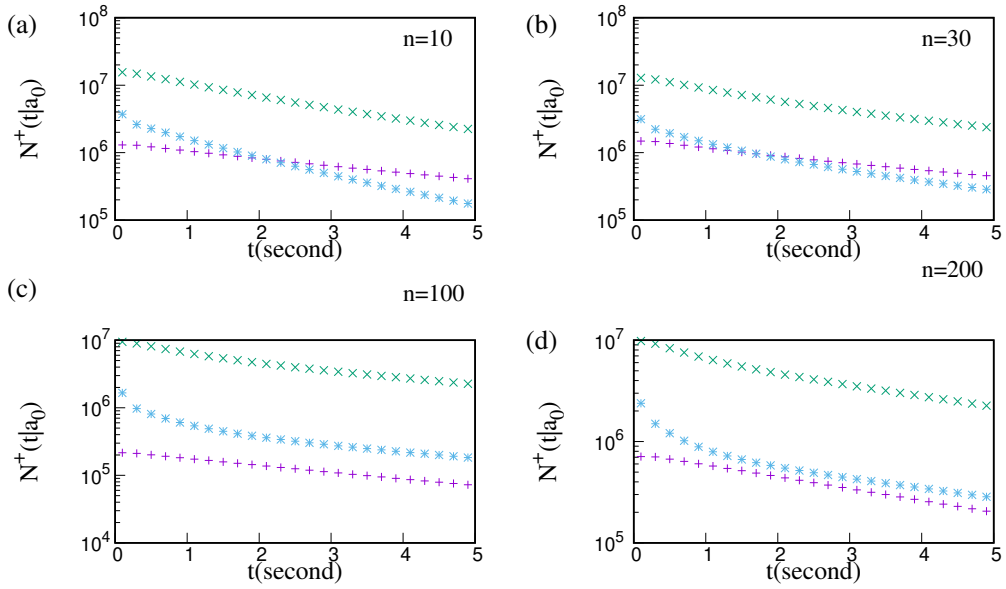

Figure 5.3: Number of surviving runs as a function of time for runs starting with three activity zones, which are high activity (blue stars), medium activity (green cross) and low activity (purple plus). Each data point has been averaged over at least 10^5 histories. All simulation parameters are specified in Sec. 2.4.

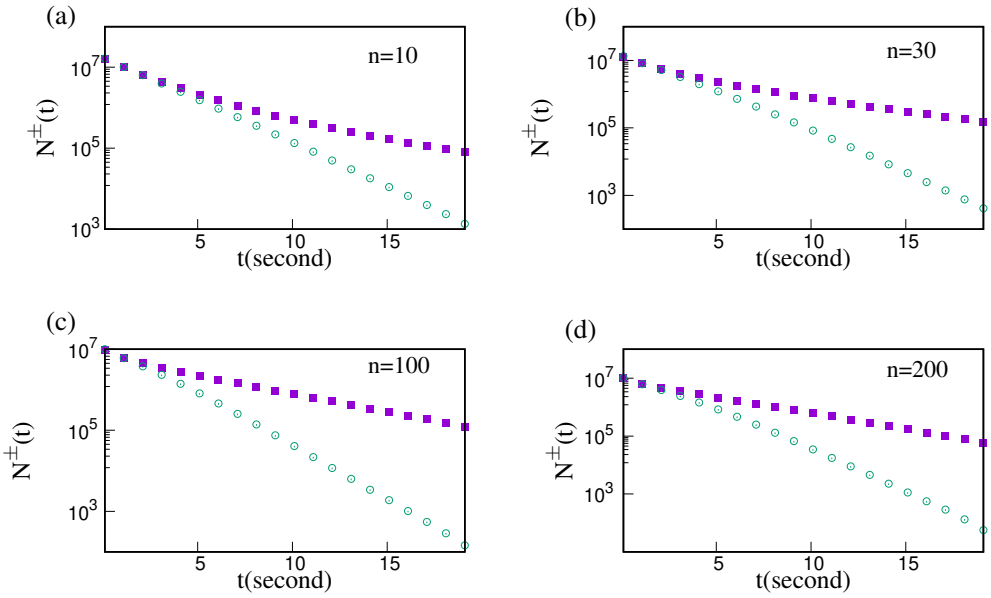

Figure 5.4: Number of surviving runs as a function of time for both uphill (purple solid square) and downhill (green empty circles) runs. It shows that number of downhill runs drops faster than number of uphill ones. Each data has been averaged over at least 10^5 histories. All simulation parameters are specified in Sec. 2.4.

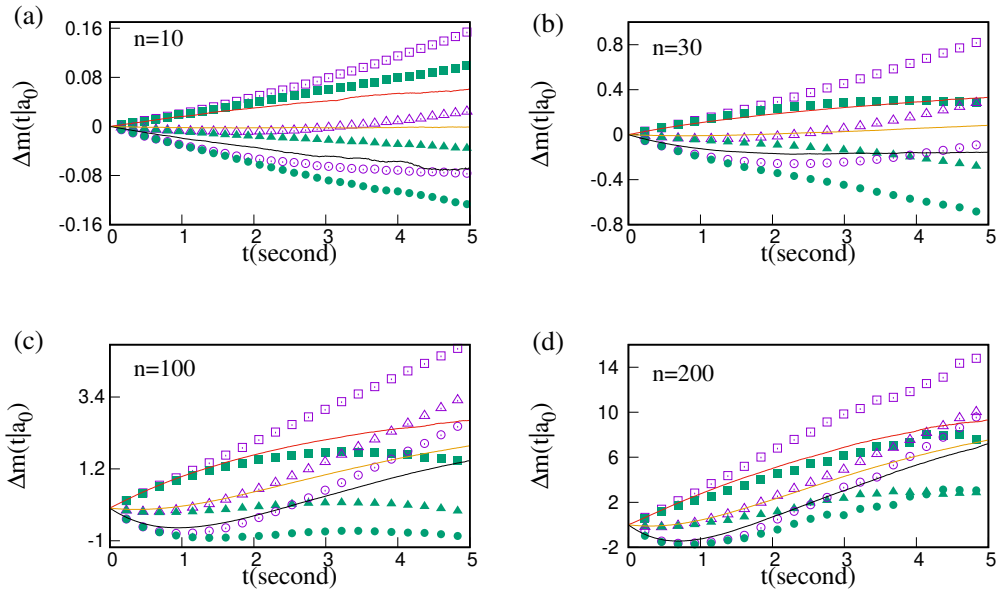

Figure 5.5: $\Delta m^{\pm}(t|a_0))$ for runs starting with three different activity ranges in strong gradient. The square, triangular and circular symbols correspond to low, medium and high a_0 values while the empty (filled) symbols are for uphill (downhill) runs. Among the solid lines, the top (red), middle (yellow) and the bottom (black) ones correspond to low, medium and high a_0 runs for the flat profile. Each data point has been averaged at least 10^5 histories. All simulation parameters are specified in Sec. 2.4.

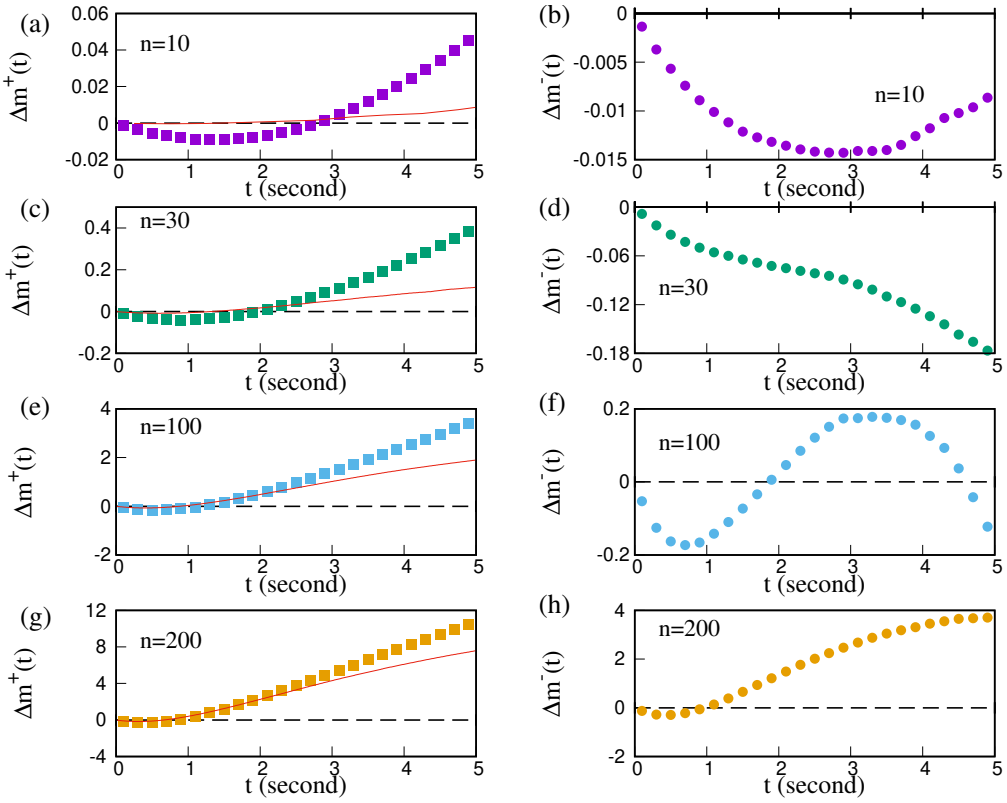

Figure 5.6: Temporal variation of $\Delta m^{\pm}(t)$ for different n and strong gradient case: left (right) panel with discrete square(circular) points corresponds to uphill (downhill) runs and red solid line in left panel(not shown in right panel since it is identical for both) shows $\Delta m(t)$ for runs along either direction in homogeneous concentration profile. While $\Delta m^{+}(t)$ shows qualitatively similar time-dependence as in the weak gradient case, the behavior of $\Delta m^{-}(t)$ is completely different. Unlike the weak gradient case, $\Delta m^{-}(t)$ shows significantly varying dynamics depending on the value of n. Such behavior is a result of interplay between the sensing module and adaptation module of the signaling network. Here, one dimensional motion of the cell is considered in presence of a strong gradient of $c(x)$. Other simulation parameters are specified in Sec. 2.4. These data have been averaged over at least 10^5 histories.

medium a_0 runs show negligible change in methylation and high a_0 runs show demethylation. For $n = 200$ we find medium and high a_0 runs show initial demethylation, followed by an upswing at late times.

5.2 Variation of $\Delta m^{\pm}(t)$ in strong gradient

Now we present our data for $\Delta m^{\pm}(t)$ in Fig. 5.6. Data presented in sec. 5.1 help us to understand the data in Fig. 5.6. Here an uphill (downhill) run experiences a steep increase (decrease) of attractant concentration with time because of the strong gradient present. For $n = 10$ both $\Delta m^{+}(t)$ and $\Delta m^{+}(t)$ decrease to become negative for small t. From exponential decay of $N^{\pm}(t)$ (see Fig. 5.4) it follows that the small time statistics are dominated by short runs which control the behavior of $\Delta m^{\pm}(t)$ for small t. These short runs are associated with high activity (or large tumbling bias) which is supported by our data in Fig. 5.2 where the high activity runs show highest probability for short durations. Such runs undergo demethylation. For moderate

or large t, due to fast increasing ligand free energy during uphill runs, the receptor clusters tend to switch to inactive states and hence methylation takes over, making $\Delta m^+(t)$ positive again. Interestingly, in Fig. 5.6(a), the red solid line that shows the methylation variation for zero gradient of the attractant, passes above the $\Delta m^+(t)$ curve at small t, unlike what we had seen for the weak gradient case. Although at larger t, the zero gradient data fall below the strong gradient data as seen in Fig. 4.6, the short-time behavior seems counter-intuitive. To explain this effect, we consider Fig. 4.1(a) and Fig. 5.1(a) where initial activity a_0 distribution at the start of a run is shown. The difference between mean a_0 and adapted a_0 is significantly larger for the strong gradient case and this makes the demethylation more pronounced. For downhill runs the short-time decrease of $\Delta m^-(t)$ is expectedly more pronounced because in addition to those runs which started off with high activity, there are runs which undergo a rise in activity due to rapidly decreasing $c(x)$. The demethylation is therefore stronger in this case. As time goes on, we see $\Delta m^-(t)$ reaches a minimum and then starts increasing again. This behavior can be explained as follows. The downhill runs which persist till large times even though a strong gradient is present in the system, need to have very low activity at the start of the run and as time goes on, the fraction of such runs in $N^-(t)$ population increases with time [see data in Fig. 5.3(a) where the number of low activity runs overtake that of high activity runs for moderate or large t]. These runs undergo methylation at short times and even if their activity increases with time, leading to demethylation at large times, the net change $\Delta m^-(t)$ has a smaller magnitude. This explains the negative minimum and subsequent rise of $\Delta m^-(t)$ (also see Section 5.3 for supporting data). However, in the time range we have observed, $\Delta m^-(t)$ does not change its sign and continue to remain negative. For the purpose of suitable choice of scales, we have not plotted the zero gradient data with $\Delta m^-(t)$ in Fig. 5.6. From the red lines in the left panels of Fig. 5.6 it is clear that $\Delta m^-(t)$ always lie below the zero gradient curve.

For higher values of n the qualitative behavior of $\Delta m^+(t)$ remains same, but $\Delta m^-(t)$ undergoes significant change in its dynamics. For $n = 30$ we find $\Delta m^-(t)$ monotonically decreases with time till the time range we have observed. In this case, the signal coming from the strong gradient gets even more amplified due to large value of n and the activity state of the receptors is mainly controlled by the ligand free energy. Along the downhill trajectory of the cell, the ligand free energy decreases rapidly and this raises the activity of the receptors. Even those runs which started with a low activity value, experience an increase in activity due to this effect. Our data in Fig. 5.5(b) are consistent with this where we see low activity downhill runs show a decrease in methylation rate at long times. The high activity results in demethylation and $\Delta m^-(t)$ becomes negative.

For $n = 100$ the behavior is even more interesting: $\Delta m^-(t)$ reaches a negative minimum at short times, then increases to become positive, reaches a positive maximum at large times and then starts decreasing strongly again to become negative. As we explain below, this rich behavior is a result of interplay between the sensing and adaptation modules of the network [7]. For large receptor clusters, the activity fluctuation in the cell is quite strong. When the activity becomes too high or too low, to restore it to its average level, adaptation needs to play an important role and can sometimes override the signal coming from ligand concentration variation in the cell's environment. For small t, the behavior of $\Delta m^-(t)$ is controlled by high activity runs. This can be clearly seen in Fig. 5.3(f) where number of high activity runs at short times is much higher than low activity ones. Note that Fig. 5.3 show data for uphill runs but we find very similar variation for the downhill runs as well. High activity runs cause strong demethylation. However, this demethylation process lowers the activity significantly and even though ligand concentration is dropping rapidly, it cannot keep up with the strong demethylation. The resulting low activity triggers methylation (see our data in Fig. 5.5(c)

where even for high activity downhill runs the initial demethylation slows down with time). Therefore, after reaching a minimum, $\Delta m^-(t)$ starts increasing again and even changes sign to become positive. At large times, when only very long runs survive in $N^-(t)$ population, the drop in ligand free energy along such long downhill trajectories becomes quite large which can now compete against the strong methylation variation experienced by the receptors. Therefore, the activity starts increasing again, which explains the maximum of $\Delta m^-(t)$ followed by a drop [our data for low activity downhill runs in Fig. 5.5(c) show this trend clearly]. We have presented additional supporting data in Sec. 5.3

In Fig. 5.6 we also show data for $n = 200$ where the pattern of variation is almost similar for both $\Delta m^+(t)$ and $\Delta m^-(t)$, except at very large times when $\Delta m^-(t)$ shows a flattening tendency. The similarity between the uphill and downhill runs shows that the methylation dynamics is insensitive to the ligand density. In this range of n values, the adaptation module wins over the sensing module of the signaling network because of large activity fluctuations. Irrespective of whether the cell is headed uphill or downhill along the ligand concentration profile, the activity of the receptors remains low in the run state resulting in overall methylation. The late time flattening tendency of $\Delta m^-(t)$ is nothing but a remnant of the behavior seen at $n = 100$ where very large drop in ligand density during very long downhill runs finally tends to increase the activity.

5.3 Methylation dynamics for very long runs

The time evolution of methylation level during particularly long runs provides an independent verification of the explanation we have provided for the behavior of $\Delta m^-(t)$ in Fig. 5.6. To this end we perform the following measurement. Let $\mathcal{M}^-(t, \tau)$ be the methylation level of a receptor cluster at time t during a downhill run which persists for at least time τ. In Fig. 5.7 we present data for average change in methylation (average calculated over $N^-(\tau)$ runs) as a function of time t for $\tau = 5s$ which is much longer than average run duration. These data are for the strong gradient case. For $n = 10$ a long run starts with low activity and hence for short times there is methylation. But decreasing $c(x)$ along with increasing methylation level finally raise the activity and demethylation starts at large times. Our data in Fig. 5.6b show that for large t when long runs dominate, the magnitude of $\Delta m^-(t)$ decreases with time. This is consistent with our data in Fig. 5.7b where because of initial methylation and subsequent demethylation, the net change in methylation level becomes small. Fig. 5.7b shows data for $n = 30$ where a monotonic decrease is observed. Because of stronger receptor cooperativity in this case, the input signal coming from $c(x)$ is significantly amplified and dominates the free energy. So even if the long runs started with low activity, under the influence of rapidly decreasing $c(x)$, activity increases and as a result demethylation happens. This is consistent with our data for $n = 30$ in Fig. 5.6. For $n = 100$ the long runs show even more interesting behavior. Adaptation plays important role here and the free energy is not controlled by ligand density alone, methylation starts playing a more important role. As we see from Fig. 5.7c, after initial demethylation, the activity drops significantly and methylation starts. In this time regime methylation dominates over ligand free energy. But at late times, when the downhill run has gone on for quite long, the drop in $c(x)$ becomes so large that activity is now controlled by ligand density and demethylation happens again. This behavior mirrors what we had seen for $\Delta m^-(t)$ in Fig. 5.6 for $n = 100$. Fig. 5.7d shows the data for $n = 200$ where adaptation wins over sensing at all times, and even through $c(x)$ is decreasing along the cell trajectory, that is not enough to raise the activity. We find activity remains low and methylation happens at all

times during the long runs.

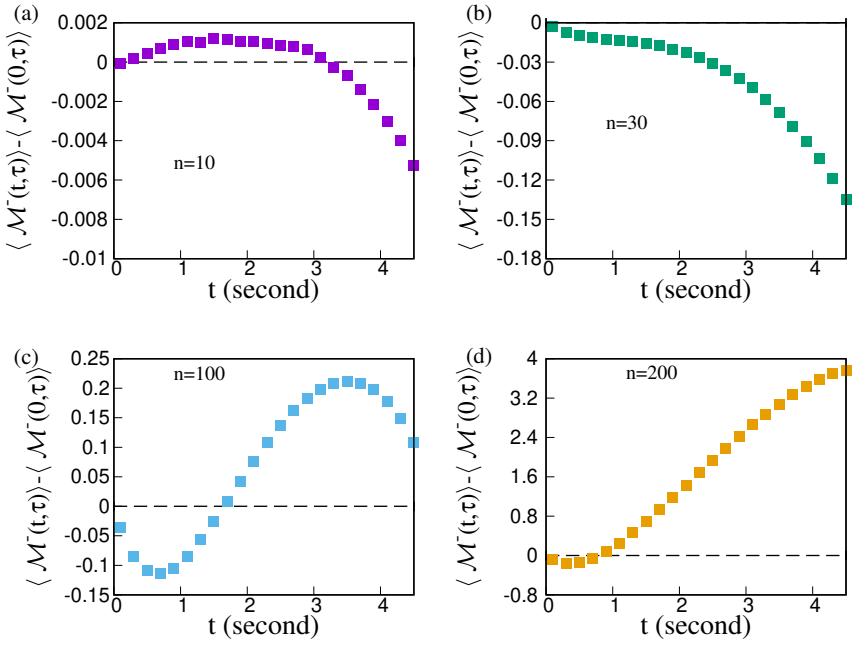

Figure 5.7: Average change in methylation for long downhill runs with duration longer than $5s$. Here, strong gradient of $c(x)$ is used. For different values of n these data correctly reflect the long time behavior of $\Delta m^{-}(t)$ shown in Fig. 5.6. These data have been averaged over at least 10^6 histories. Other simulation parameters are as in Fig. 5.6.

5.4 Variation of $\delta m^{\pm}(t)$ in strong gradient

In Fig. 5.8 we present data for $\delta m^{\pm}(t)$. As seen in the case of weak gradient, here also we find qualitatively different trend from $\Delta m^{\pm}(t)$ (see Fig. 5.6). For small n, when the variation of $\Delta m^{\pm}(t)$ is relatively milder, due to systematic dropping out of high methylation states from $N^{\pm}(t)$ populations, we find $\delta m^{\pm}(t)$ decrease monotonically. For $n = 30$, we have already shown from our data in Fig. 5.6 that $\Delta m^{-}(t)$ shows monotonic decrease with t. With dropping out of high methylation states with time, the decrease is now (quantitatively) stronger for $\delta m^{-}(t)$. For the uphill runs, $\delta m^{+}(t)$ remains negative but shows a minimum. The strong positive growth of methylation level of individual trajectories, as captured by $\Delta m^{+}(t)$, together with termination of high methylation runs with time, lowers the magnitude of $\delta m^{+}(t)$ at large times. Similar explanation can be used to interpret the data for $\delta m^{+}(t)$ for $n = 100, 200$ as well. However, $\delta m^{-}(t)$ for $n = 200$ shows a different behavior. After an initial minimum it shows a shallow maximum followed by a steep drop. While the explanation for the initial minimum remains same as in $\delta m^{+}(t)$ case, the late time steep drop can be traced back to the slower growth of $\Delta m^{-}(t)$ at late times in Fig. 5.6(h). This slower growth combined with high drop out rate of high m runs from $N^{-}(t)$ population causes the sharp decline in $\delta m^{-}(t)$ at large times.

The red lines in Fig. 5.8 left panels show data for the zero gradient case. Since the attractant concentration does not change with time in this case, one would expect less pronounced demethylation than an uphill run in strong gradient where the attractant concentration increases with time. However, our data in Fig. 5.8(a) show that the zero gradient data lie above the strong

gradient uphill data. The explanation of this effect can be found in the distribution of initial activity a_0 in Figs. 4.1 and Figs. 5.1 where the difference between mean a_0 and the adapted activity is larger for the case of strong gradient, which gives rise to stronger demethylation. From Fig. 5.1 it also follows that for larger n values the difference between mean a_0 and adapted activity is comparable for the zero gradient and strong gradient case. Moreover, the increase in ligand free energy with time along an uphill run is significantly higher for large n and strong gradient. This is why the zero gradient data fall below $\delta m^+(t)$ for large n and large t.

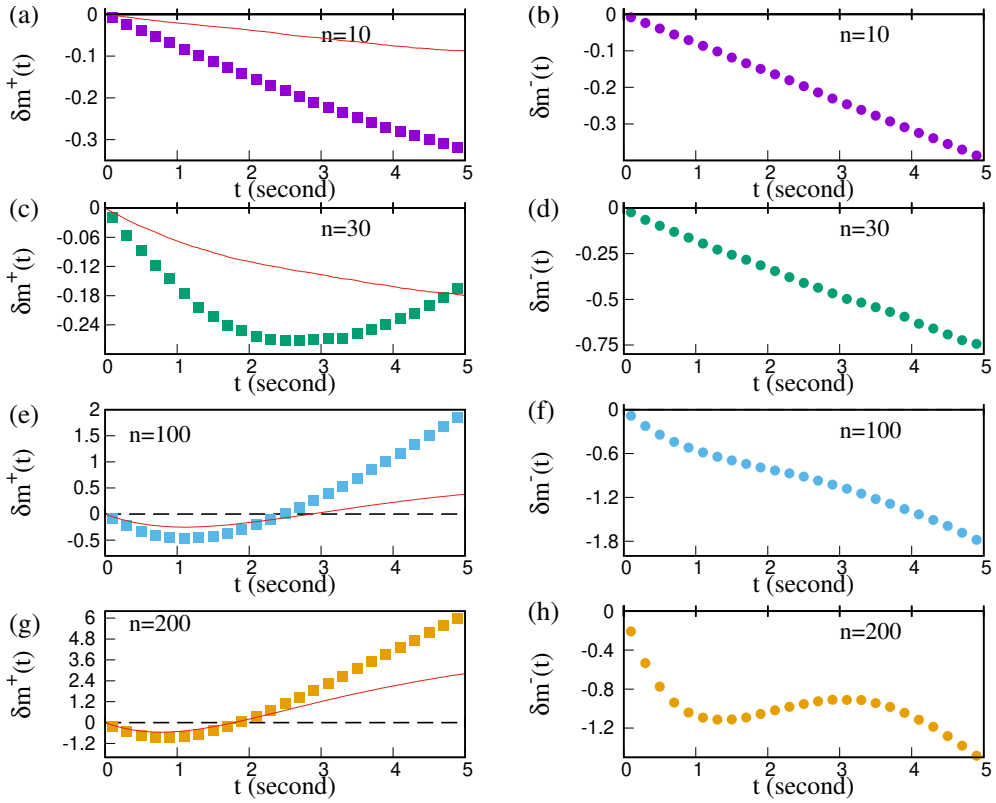

Figure 5.8: Temporal variation of $\delta m^{\pm}(t)$ for different n and strong gradient: left (right) panel with discrete square(circular) points shows data for uphill (downhill) runs. Red solid line in left panel(not shown in right panel since it is identical for both)shows data for runs along either direction in homogeneous concentration profile. While for small n both uphill and downhill runs show decreasing level of average methylation with time, there is a trend reversal for uphill runs at late times for larger values of n. This is caused by strong positive growth of $\Delta m^+(t)$ which overcompensates for dropping out of large methylation states from $N^+(t)$ population. These data have been averaged over at least 10^6 histories. Other simulation parameters are as in Fig. 5.6.

5.5 Distribution of methylation level at time t during a run

Let m_t be the methylation level of a receptor cluster (rescaled by the size of the cluster) at time t during a run. At $t = 0$ we have m_0 that denotes the initial methylation level at the start of a run. In Fig. 5.9 left and middle panels we show the distribution of m_t for $t = 0, 2, 5s$ seconds for the strong gradient case. The left panel shows the data for the uphill runs and the middle panel corresponds to downhill runs. The right panel in this figure shows data for a flat

attractant profile. In this case for $n = 10$ and 30 the methylation distribution shows a distinct second peak. We have not been able to explain this effect. However, the time-dependence of these curves are exactly as one would expect from $\delta m^{\pm}(t)$ variation shown in Fig. 5.8. In those cases when $\delta m^{\pm}(t)$ decreases monotonically with t, we find the distribution $P(m_t)$ also shifts leftward towards smaller m_t values as t increases. However, in Figs. 5.8e or 5.8g, where $\delta m^{+}(t)$ shows distinct non-monotonicity along with zero-crossing and change of sign, corresponding $P(m_t)$ also shows analogous behavior.

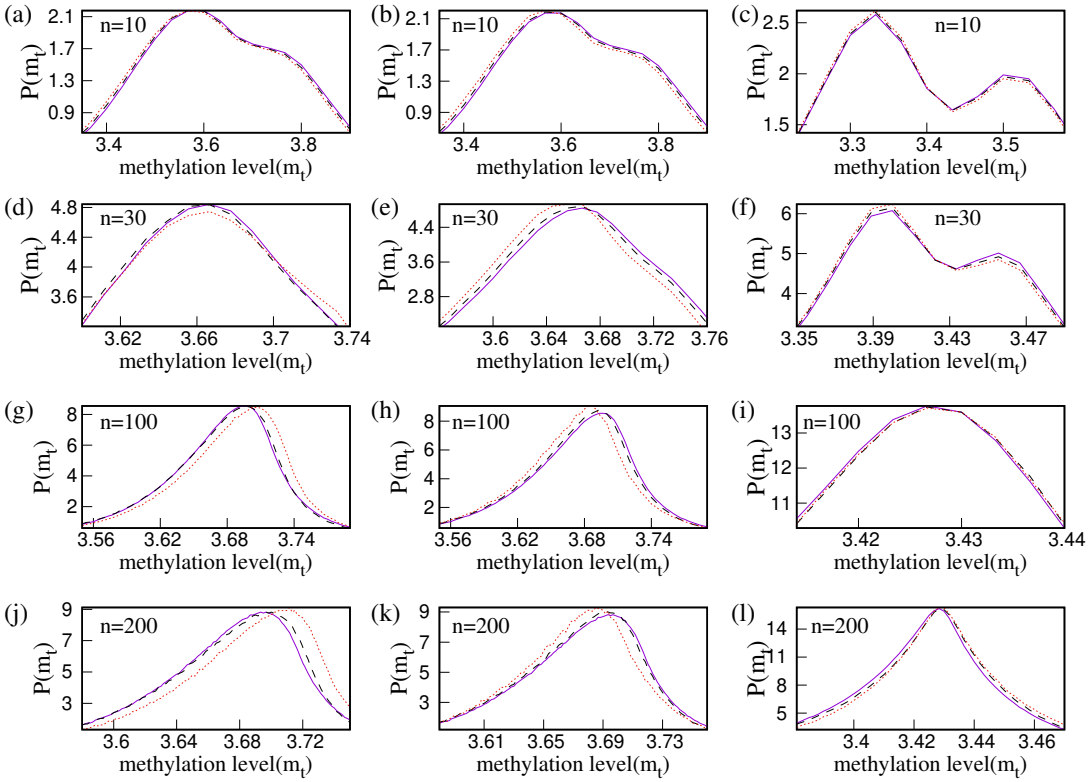

Figure 5.9: Distribution of methylation level at $t = 0$ (solid purple line), $t = 2\ s$ (dashed black line) and $t = 5\ s$ (dotted orange line). Left and middle panels show data for uphill and downhill runs for strong gradient. The right panels show data for the zero gradient case. To clearly show the shift of the peak position with time, here we have presented the zoomed data near the peak region. Each data point has been averaged over at least 10^6 histories. Other simulation parameters are as in Fig. 5.6

5.6 Data for two dimensions

We have also performed the simulations for two spatial dimensions. We see some quantitative difference from the $1D$ data here, although qualitative nature is same and our conclusions are remain valid here as well. Data for $\Delta m^{\pm}(t)$ and $\delta m^{\pm}(t)$ variation in strong gradient have been presented in Fig. 5.10 and 5.11 respectively.

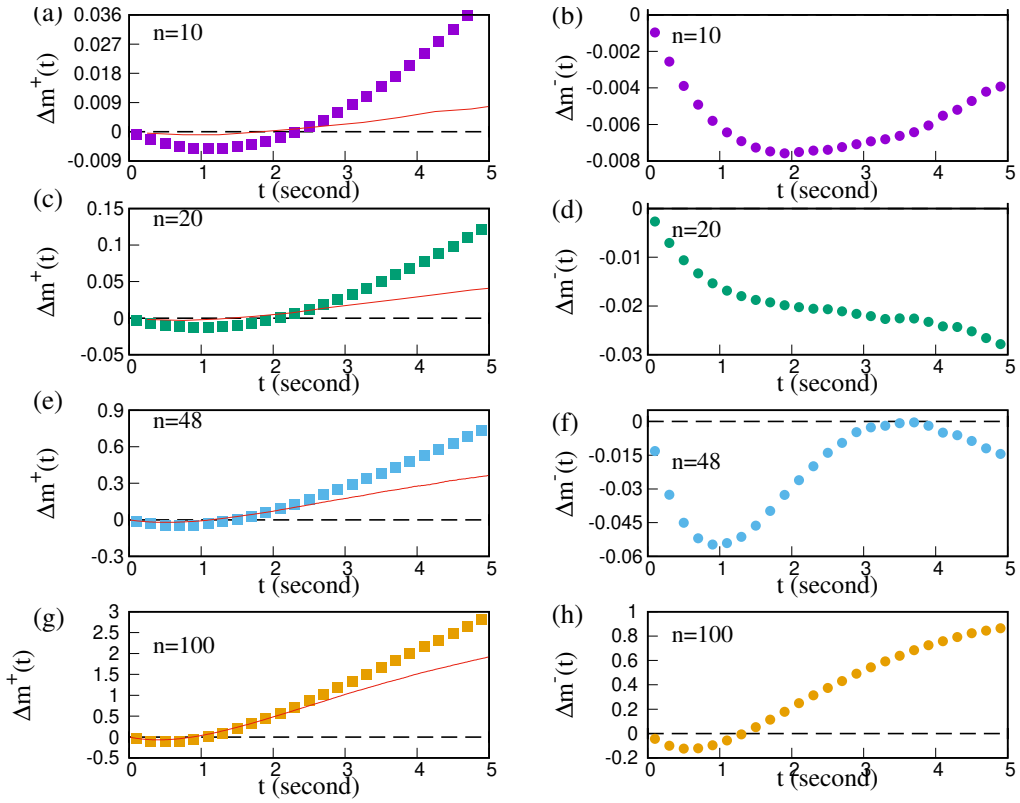

Figure 5.10: Temporal variation of $\Delta m^{\pm}(t)$ for different n and strong gradient case in two dimensions: left (right) column corresponds to uphill (downhill) runs by curves with discrete square (circular) points. Red solid line in left panel(not shown in right panel since it is identical for both) shows $\Delta m(t)$ for runs along either direction in homogeneous concentration profile. The qualitative nature of variation is similar to our data for one dimension in Fig. 5.6. These data have been averaged over at least 10^5 histories. Other simulation parameters are specified in Sec. 2.4.

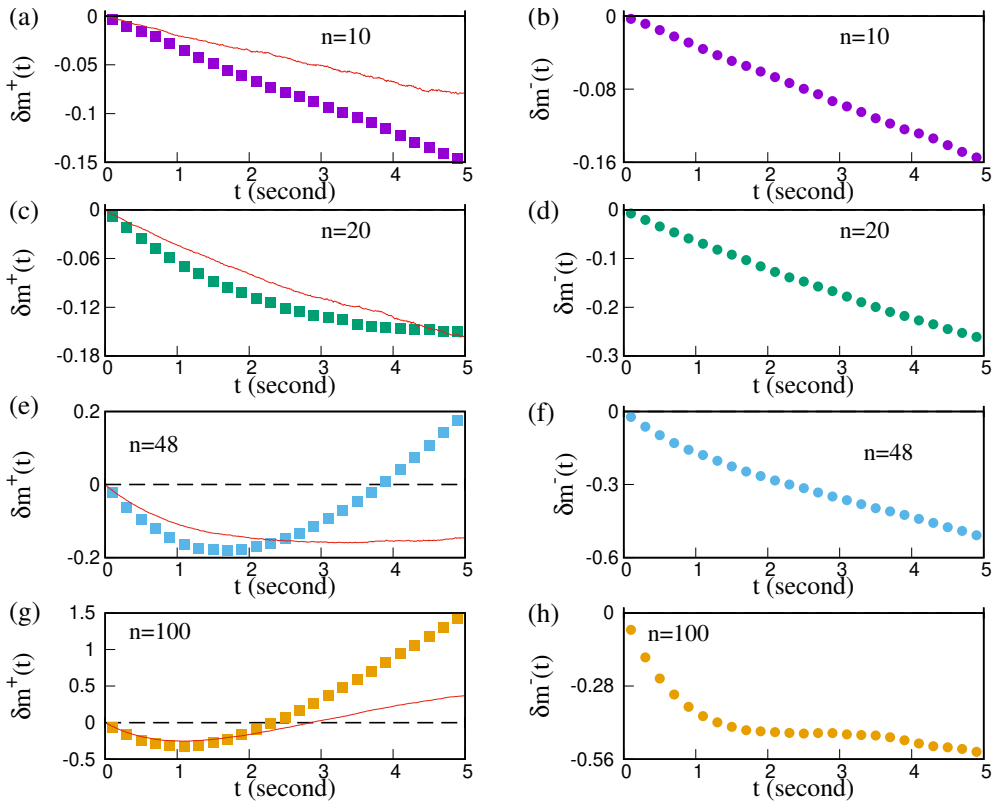

Figure 5.11: Temporal variation of $\delta m^{\pm}(t)$ for different n and strong gradient in two dimensions: left (right) column shows data for uphill (downhill) runs with discrete square(circular) points. Red solid line in left panel(not shown in right panel since it is identical for both)shows data for runs along either direction in homogeneous concentration profile. The qualitative behavior is not too different from Fig. 5.8 for the one dimensional case. These data are averaged over at least 7×10^5 histories. Other simulation parameters are same as Fig. 5.10.

5.7 Discussion

In this chapter we study the methylation dynamics of chemoreceptors of an E.coli cell while the cell navigates through a spatially varying ligand environment. Here we have performed this analysis for strong gradient of attractant profile. Our numerical simulations show that the receptor cooperativity strongly affects the methylation dynamics and gives rise to dramatic variation in the case of strong gradient of the attractant.

For strong gradient methylation dynamics in uphill runs shows similar qualitative variation as observed in weak gradient case in chapter 4. Demethylation happens just after initiation of the run due to large number of short runs with high activity and in intermediate and large time methylation happens for surviving long runs with low initial activity. But in downhill runs qualitatively different and highly non-trivial dependence of methylation dynamics on receptor cooperativity is observed. For small cluster size, long runs starting with low activity undergo methylation immediately. This methylation combined with huge drop of ligand free energy in long downhill runs raise the receptor activity to higher value. So demethylation happens at large time. As cluster size increases, cooperativity also increases and this helps the cell to sense more amplified input signal coming from ligand profile. Hence, in downhill run activity is increased to more higher value even for those long runs which start with very low initial activity and demethylation happens continuously causing methylation value to decrease monotonically. For more higher cluster size adaptation is likely to dominate over sensing and cell becomes less sensitive to change in ligand concentration now. Only those runs which has persisted for really long time experience enough drop in ligand concentration and show the domination of ligand concentration over adaptation. For even larger clusters, adaptation wins over sensing completely and methylation level changes almost similar way for uphill and downhill run.

To the best of our knowledge, such a systematic, quantitative investigation of methylation dynamics has never been performed before, even though E. coli chemotaxis is a widely studied system. Our study provides probing insights into how the amplification of input signal and a negative feedback mechanism come together to control the time-evolution of various dynamical variables which characterize the signaling network. We find highly interesting and nontrivial methylation dynamics as a result of this interplay. It is possible to experimentally verify our result. We have studied the methylation dynamics for a swimming cell. But our results can be tested for a tethered cell as well. Receptor activity has been already measured in experiment by using FRET [8]. Time-varying ligand concentration was applied to a tethered cell such that FRET output remains constant in time and from here adaptation dynamics was determined. Motivated by this we also propose an experimental protocol for a tethered cell, where counter-clockwise (clockwise) rotation of flagellar motors can be considered as run (tumble) mode and ramping up (down) the attractant concentration at particular rate at the fixed position of the cell will be analogous to uphill (downhill) run of the cell. The ramping rate can be chosen to be exactly same as the rate at which a cell running with speed v experiences change in attractant levels along its path. Of course for weak and strong gradient, this rate is going to be different. Every time the flagellar motors switch to a clockwise rotation, the attractant level should be held fixed as this corresponds to a tumble mode with zero displacement. After each tumble, when the motors switch back to counter clockwise rotation, the sign of the ramp rate can be chosen at random. Finally, when the attractant level matches the boundary values, the ramp rate should simply be reversed, which corresponds to the cell hitting a boundary wall and getting reflected back and continuing its run in the opposite direction. This way by tuning the ramp rate in sync with the rotational bias of the flagellar motors, we can create the same conditions of a swimming cell for a tethered one. By tracking the methylation level of the receptor clusters for

this tethered cell during the ramped up and ramped down attractant level, one can directly measure the quantities like $\Delta m^{\pm}(t)$ or $\delta m^{\pm}(t)$ and test our conclusions. Alternatively, the activity level of the cell can be tracked and the methylation variation can be determined from there by using the knowledge of input variation of ligand concentration.

Although we have not considered the hexagonal orientation of receptor dimers inside the cluster[9, 10] and energy cost due to membrane curvature[11, 12, 13], these will not hamper our general conclusions. Inclusion of those things in our model may bring quantitative change in the result but it won't affect our results qualitatively. The understanding of the methylation dynamics that our study provides, is much more general and simply relies on the coupling between ligand concentration, activity and methylation, and does not depend on the details of the model. It will be interesting to see whether our understanding can be applied to other kind of sensory systems also.

Bibliography

[1] Shobhan Dev Mandal and Sakuntala Chatterjee. Effect of receptor cooperativity on methylation dynamics in bacterial chemotaxis with weak and strong gradient. *Physical Review E*, 105(1):014411, 2022.

[2] Yann S Dufour, Xiongfei Fu, Luis Hernandez-Nunez, and Thierry Emonet. Limits of feedback control in bacterial chemotaxis. *PLoS Comput Biol*, 10(6):e1003694, 2014.

[3] Junjiajia Long, Steven W Zucker, and Thierry Emonet. Feedback between motion and sensation provides nonlinear boost in run-and-tumble navigation. *PLoS computational biology*, 13(3):e1005429, 2017.

[4] Chuan Xue and Xige Yang. Moment-flux models for bacterial chemotaxis in large signal gradients. *Journal of mathematical biology*, 73(4):977–1000, 2016.

[5] Weiran Sun and Min Tang. Macroscopic limits of pathway-based kinetic models for *E. coli* chemotaxis in large gradient environments. *Multiscale Modeling & Simulation*, 15(2):797–826, 2017.

[6] Gabriele Micali, Rémy Colin, Victor Sourjik, and Robert G Endres. Drift and behavior of *E. coli* cells. *Biophysical journal*, 113(11):2321–2325, 2017.

[7] Shobhan Dev Mandal and Sakuntala Chatterjee. Effect of receptor clustering on chemotactic performance of *E. coli*: Sensing versus adaptation. *Phys. Rev. E Letter*, 103:L030401, Mar 2021.

[8] Thomas S Shimizu, Yuhai Tu, and Howard C Berg. A modular gradient-sensing network for chemotaxis in *Escherichia coli* revealed by responses to time-varying stimuli. *Molecular systems biology*, 6(1):382, 2010.

[9] Ariane Briegel, Xiaoxiao Li, Alexandrine M Bilwes, Kelly T Hughes, Grant J Jensen, and Brian R Crane. Bacterial chemoreceptor arrays are hexagonally packed trimers of receptor dimers networked by rings of kinase and coupling proteins. *Proceedings of the National Academy of Sciences*, 109(10):3766–3771, 2012.

[10] Jun Liu, Bo Hu, Dustin R Morado, Sneha Jani, Michael D Manson, and William Margolin. Molecular architecture of chemoreceptor arrays revealed by cryoelectron tomography of *Escherichia coli* minicells. *Proceedings of National Academy of Sciences*, 109(23):E1481–E1488, 2012.

[11] Robert G Endres. Polar chemoreceptor clustering by coupled trimers of dimers. *Biophysical journal*, 96(2):453–463, 2009.

[12] Christoph A Haselwandter and Ned S Wingreen. The role of membrane-mediated interactions in the assembly and architecture of chemoreceptor lattices. *PLoS computational biology*, 10(12):e1003932, 2014.

[13] Will Draper and Jan Liphardt. Origins of chemoreceptor curvature sorting in *Escherichia coli*. *Nature communications*, 8(1):1–9, 2017.

Chapter 6

Effect of switching time scale of receptor activity on chemotactic performance

In this chapter, we study how different choices of the activity switching time-scale affect the chemotactic performance of E.coli. We quantify the chemotactic performance by drift velocity of the cell here. Our numerical simulations show that the chemotactic drift velocity increases and then saturates as the switching of activity becomes faster.

As value of switching rate increases, faster transition takes place between active and inactive states of a receptor cluster. This results in faster change in activity and hence faster transition between run and tumble mode. So it is expected that mean run duration should decreases with switching rate. But we see that the duration of downhill run decreases at much faster rate than the duration of uphill ones, which actually causes the enhancement of drift velocity. We explain this observation by detailed analysis of temporal variation of activity along the cell trajectory.

In chapter 2 we have described our model in details. Here we present our simulation. These results have been published in [1].

6.1 Homogeneous attractant environment

To explicitly show the effect of activity switching rate (w_a) on the temporal fluctuations of activity, we show in Fig. 6.1 the time-series of the activity state of one particular cluster. As expected, the time interval between two successive switching events drops with increasing w_a. For large w_a when the activity switching happens very frequently, the total number of active clusters fluctuates rapidly with time. The total activity that determines the tumbling bias of the cell, can go from high to low value in a short span of time. This means the residence time of the cell in run mode (or in tumble mode) decreases as w_a increases. In Fig. 6.2 we verify this for mean duration of a run. Note that while w_a affects the temporal fluctuations of activity, the range of fluctuations does not show much dependence on w_a. This range is mainly set by the value of n, the signaling team size [2, 3]. Since the number of receptors in the cell is fixed, as the team size becomes large, there are fewer teams present. The total activity of the cell is then averaged over a fewer number of teams which increases the activity fluctuations. We have explicitly verified (data not shown here) that the activity distribution does not show any significant dependence on w_a. These results are in line with [3] where w_a was varied in simulation and it was found that the temporal fluctuation of activity increases with w_a but the amplitude of fluctuation remains unchanged.

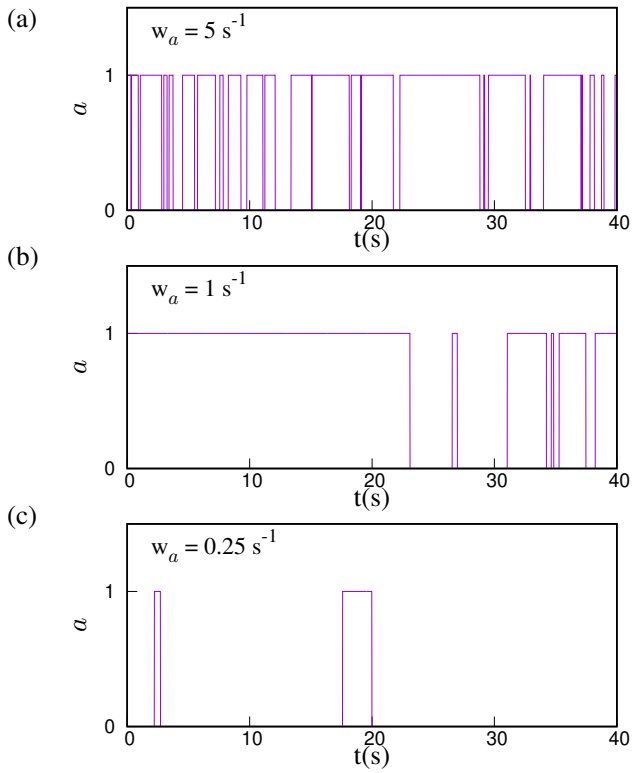

Figure 6.1: Typical time series of activity of a single cluster recorded over a time-window (40 s) along the run-tumble trajectory of swimming cell in homogeneous attractant environment. As the switching rate (w_a) increases, the switching between two activity states 0 and 1 happens more frequently.

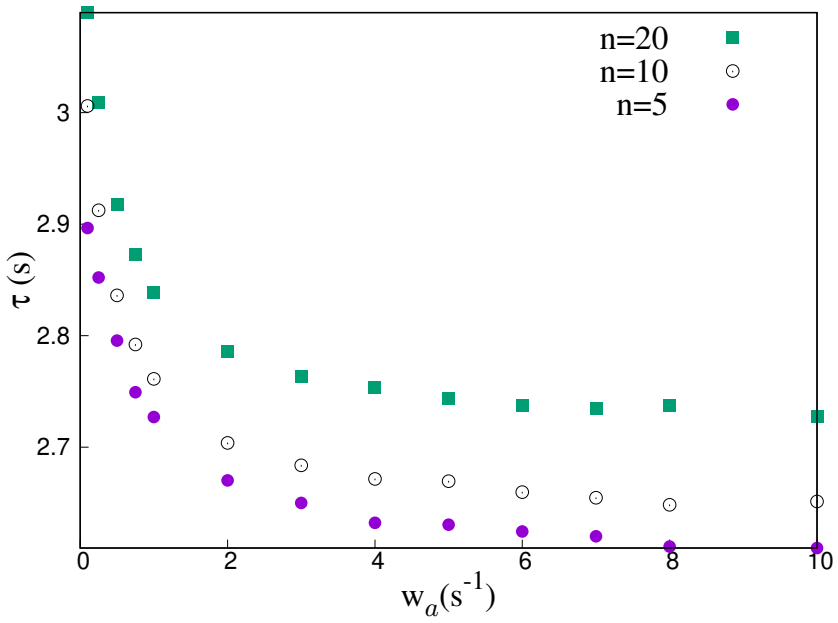

Figure 6.2: Mean run duration (τ) of the chemotactic cell in homogeneous attractant environment as a function of switching rate (w_a) for three different values of the cluster size n. The mean run duration decreases with w_a. Each data point has been averaged over at least 10^6 histories. All simulation parameters are specified in Sec. 2.4.

6.2 Chemotactic performance gets better for fast activity switching

We quantify chemotactic performance by the drift velocity V which measures how fast the cell climbs up the attractant gradient [2, 4, 5]. We define the drift velocity as $V = \frac{\Delta}{\tau}$, where Δ denotes the net displacement of the cell during a run and τ denotes average run duration. While a particular run can be directed both uphill and downhill, the form of the free energy gap between the two activity states of the cluster is such that downhill (uphill) runs are associated with an increase (decrease) in activity, and therefore, an increase (decrease) in the tumbling bias. This means the uphill runs tend to get extended and downhill runs tend to get shortened, which results in a drift motion up the gradient. A large value of V indicates faster motion of the cell up the gradient, which reflects a better chemotactic performance [2, 4, 5]. To measure how reliably the cell is able to climb up the attractant gradient, we also calculate the ratio between the net directed displacement Δ and its standard deviation σ. A large value of this ratio would also imply a strong chemotactic performance. We are interested to find out how the chemotactic performance depends on the activity switching time-scale. In Fig. 6.3a and 6.3b we present our simulation results for V and $\frac{\Delta}{\sigma}$ for different values of w_a and three different choices for the signaling team size n. We find that both these quantities increase with w_a and then saturates. To explain this variation, consider the limit $w_a = 0$ which means activity of the receptors do not flip. This will naturally impair the chemotactic ability of the cell and V will be zero. It is expected therefore for small w_a, we should observe V increasing with w_a. However, when w_a is very large, the average run duration becomes small and then it is not obvious how V is affected. To probe it further, we separately measure average duration of a rightward (uphill)

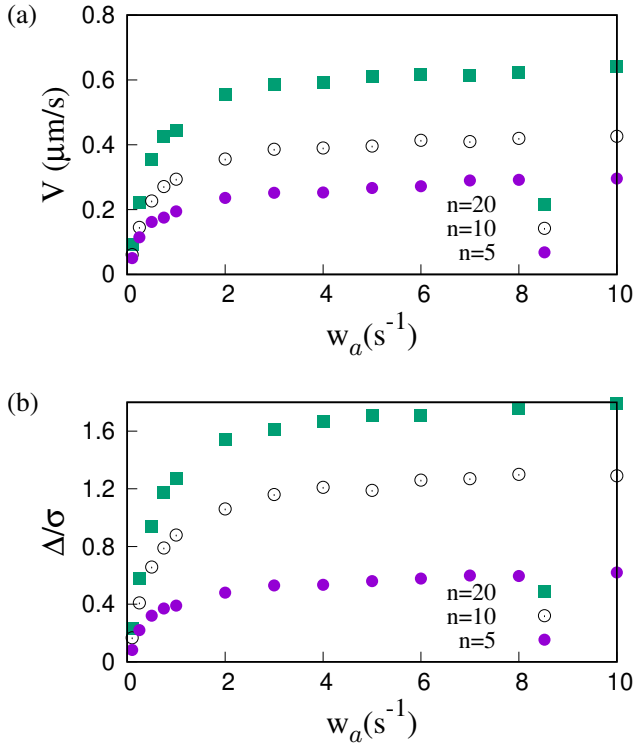

Figure 6.3: Chemotactic efficiency of the cell as a function of switching rate w_a. (a) Drift velocity (V) as function of switching w_a. Data for three different cluster size has been presented. V increases with w_a and then saturates at large values of w_a. (b) Ratio of net average displacement in a run (Δ) and fluctuation of this displacement (σ) as a function of switching rate w_a. The ratio increases with w_a and then saturates at large values of w_a. All simulation parameters are same as Fig. 6.2. These data points are averaged over at least 3×10^7 histories.

run and a leftward (downhill) run as a function of w_a. Our data in Fig. 6.4 left panel show that both runs become shorter for large w_a as expected, but mean duration τ_L of leftward runs shows a faster drop with w_a than τ_R for rightward runs. This means the difference $\tau_R - \tau_L$ increases with w_a (see Fig. 6.4 right panel). In other words, net displacement during a run increases, and mean run duration decreases with w_a, as a consequence of which V increases. In the next subsection, we present detailed explanation of this counter-intuitive behavior.

6.3 Explanation behind better performance at large w_a

Large value of activity increases the tumbling bias of the cell. Therefore, when the cell enters the tumble mode, the number of active receptor clusters tends to be high. In the tumble mode the cell position does not change, which means ligand part of the free energy remains fixed. The active receptors get demethylated and the free energy difference F between active and inactive states increases, which increases the probability of transition to inactive state. When w_a is high, more clusters flip from active to inactive state and the total activity drops quickly. Therefore, when the cell comes out of the tumble mode and starts a new run, its activity has a low value when w_a is large. Let $a_{t\to r}$ denotes the activity when the tumble to run switch takes place. In Fig. 6.5 we plot the average of this quantity $\langle a_{t\to r}\rangle$ as a function of w_a and show that

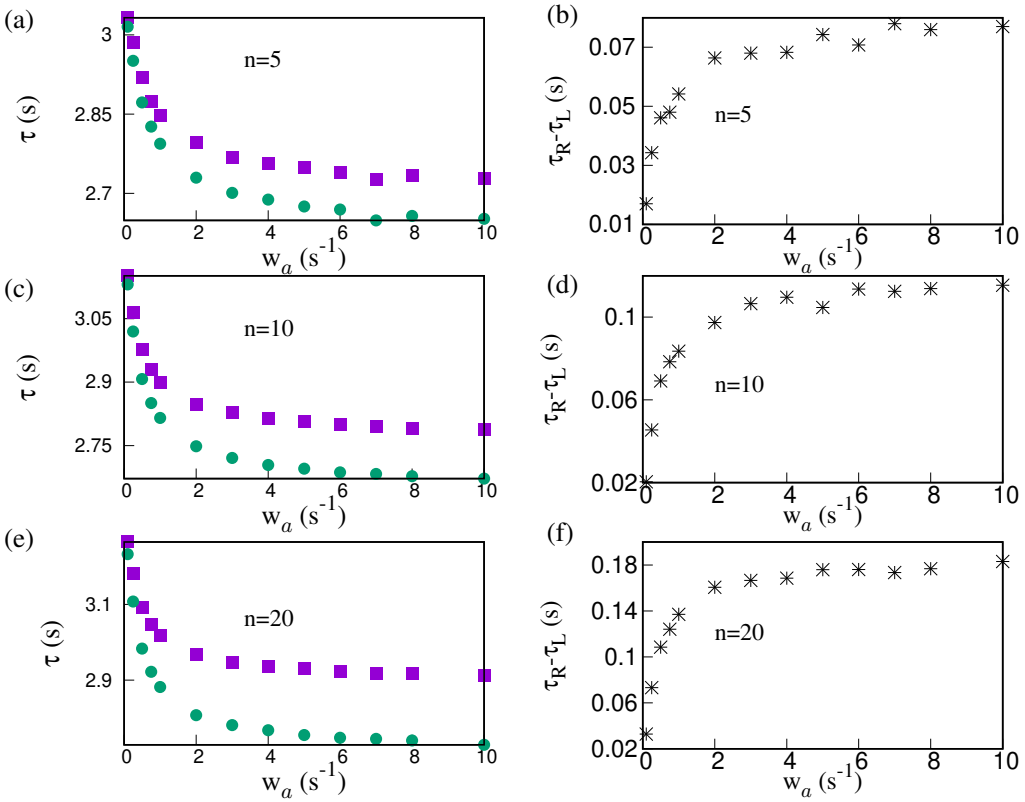

Figure 6.4: Mean duration of an uphill run (τ_R) and a downhill run (τ_L) and their difference vs w_a. Data for three different values of cluster sizes have been shown. The left panel shows that both τ_R (blue square) and τ_L (green circle) decrease with w_a but τ_L falls at faster rate than τ_R. The right panel shows the difference between τ_R and τ_L goes up with w_a and reaches a saturation. All simulation parameters are same as Fig. 6.2. These data points are averaged over at least 3×10^7 histories.

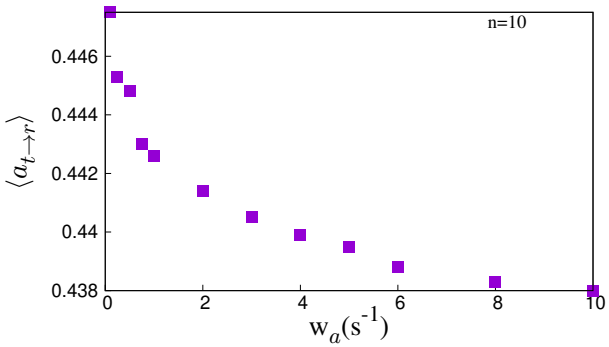

Figure 6.5: Average of the activity $a_{t\to r}$ at the instant of a tumble to run switch as a function of w_a. As w_a increases value of $\langle a_{t\to r} \rangle$ drops monotonically. Error bars of the data have magnitude of the order of 10^{-5} and hence they are actually smaller than the symbol size in the plot. All simulation parameters are same as Fig. 6.2. These data points are averaged over at least 5×10^5 histories.

it decreases with w_a.

The fact that new runs start with lower activity values as w_a increases, has an interesting implication for the activity variation during uphill and downhill runs, as shown below. Let $N^R(t)$ and $N^L(t)$ denote, respectively, the number of rightward (uphill) and leftward (downhill) runs whose duration is larger than t. Clearly, both these quantities decrease with t. Let $a_i^R(t)$ and $a_i^L(t)$ be the total activity of the cell at time t during i-th uphill and downhill run, respectively. Now we can define the following quantities:

$$\Delta a^R(t) = \sum_{i=1}^{N^R(t)} \frac{a_i^R(t) - a_i^R(0)}{N^R(t)} \tag{6.1}$$

and

$$\Delta a^L(t) = \sum_{i=1}^{N^L(t)} \frac{a_i^L(t) - a_i^L(0)}{N^L(t)}. \tag{6.2}$$

In Fig. 6.6 we plot these quantities as a function of time for two different values of w_a. Top panel (Fig. 6.6a) shows the variation of $\Delta a^L(t)$. For smaller w_a values (purple squares) when the runs start with relatively high value of activity, due to ongoing demethylation, activity drops at small t. Moreover, higher activity values make these runs prone to tumble and thus these trajectories drop out of $N^L(t)$ population quickly, which brings down the average activity. As a result, $\Delta a^L(t)$ takes negative values for small t. As t increases, however, drop in ligand concentration along the downhill run tends to increase the activity again. Due to these two opposing effects, $\Delta a^L(t)$ after reaching a minimum starts slowly increasing again. Our data show that till moderate or large t, $\Delta a^L(t)$ remains negative with its magnitude decreasing with t *i.e.* activity still decreases on an average during the run, but the magnitude of the change becomes less. At very large t change in activity becomes positive but still has a small magnitude. The situation is quite different for large w_a (green circles). Here, initial activity at $t = 0$ is low which prompts methylation and decreases the free energy difference F between active and inactive states. Also, decreasing ligand concentration along the trajectory causes F to decrease. Large w_a ensures that activity responds quickly to this free energy change and more and more clusters flip from inactive to active state. $\Delta a^L(t)$ is positive in this case and grows rapidly with time. The behavior of $\Delta a^L(t)$ is thus completely different for small and large w_a. From Fig. 6.6a it

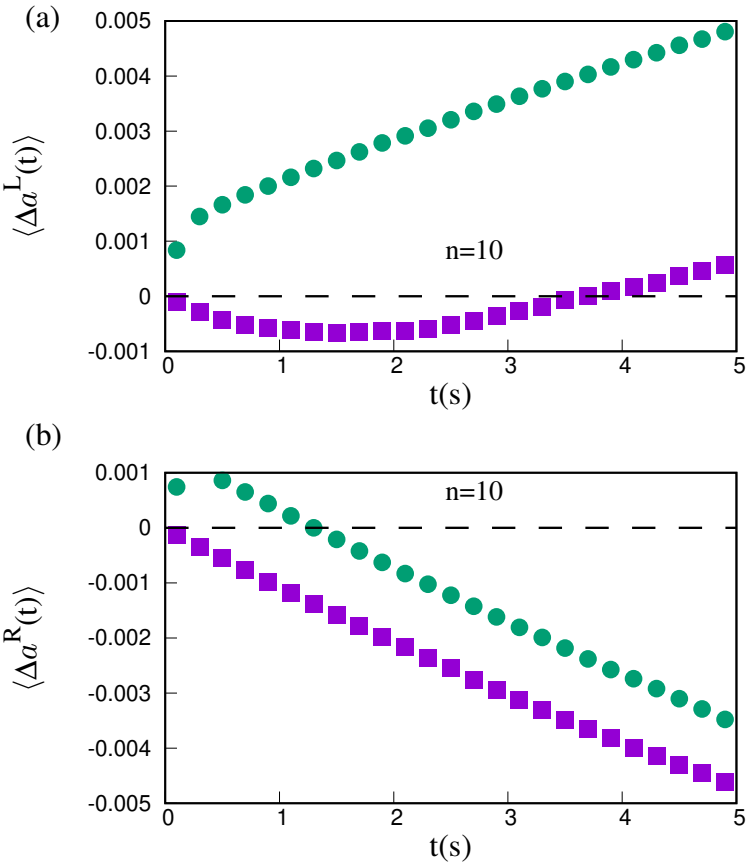

Figure 6.6: Temporal variation of activity for $w_a = 0.75\ s^{-1}$ (purple squares) and $w_a = 10\ s^{-1}$ (green circles). (a) shows data for downhill runs For and (b) shows data for uphill runs. For downhill runs qualitative nature of variation is very different for the two w_a values, while for uphill runs the variation is qualitatively similar. All simulation parameters are same as Fig. 6.2. These data points are averaged over at least 4×10^6 histories.

is clear that the values of $\Delta a^L(t)$ for small and large w_a are widely apart for the range of time we have observed.

On the other hand, Fig. 6.6b shows that the qualitative behavior of $\Delta a^R(t)$ is quite similar for large and small w_a. For small w_a (purple squares) runs start with larger activity and subsequent demethylation together with increasing ligand concentration along the trajectory cause the activity to decrease making $\Delta a^R(t)$ negative with its magnitude increasing steadily with time. For large w_a (green circles) initial activity being small, receptors tend to methylate which causes activity to increase sharply for small t. But for moderate or large times, $c(x)$ variation takes over and causes activity to decrease with time. Thus for both small and large w_a we find $\Delta a^R(t)$ shows similar temporal variation, except for very small times. For the entire time-range we have observed, the values of $\Delta a^R(t)$ for small and large w_a are relatively closer compared to Fig. 6.6a. In other words, average change in activity for small and large w_a are very different along a downhill run, but the difference is significantly less along an uphill run. This explains why τ_L decreases more strongly with w_a compared to τ_R (Fig. 6.4).

6.4 Conclusions

In this chapter we have investigated the effect of activity switching timescale on the chemotactic performance of a single *E.coli* cell. We find that the performance improves as the activity switches faster. We quantify performance by (a) the chemotactic drift velocity that measures how rapidly the cell manages to climb up the chemical concentration gradient, and (b) by the coefficient of variation of its net uphill drift. In both cases we find better performance for faster activity switches. More specifically, the average duration of a downhill run decreases rapidly with the activity switching rate w_a, but that of an uphill run decreases comparatively slowly. This asymmetry enhances the chemotactic drift. To explain this observation we monitor temporal variation of activity during uphill and downhill runs. Our detailed measurements show that during downhill runs, nature of activity variation shows widely different behavior for small and large values of w_a, while the behavior is not so different during uphill runs. This results in stronger dependence on w_a of downhill run duration which explains the above effect.

It should be possible to experimentally verify some of our main results. Direct measurement of receptor activity has already been possible using FRET based experiments [6, 7, 3]. Although most experiments focus on tethered cells, and our studies consider a swimming cell, it is possible to verify our conclusions even for a tethered cell by appropriately engineered attractant environment. By identifying the counter clockwise rotation of the flagellar motors as the run mode and the clockwise rotation as the tumble mode, one can ramp up (down) the attractant concentration to mimic an uphill (downhill) run and hold the attractant level steady for a tumble. Using this set-up the activity variation of the cell can be measured with time and our results on $\Delta a^R(t)$ and $\Delta a^L(t)$ can be verified. The switching of a receptor between active and inactive states is a result of a conformational change of the receptor molecule [8]. An experimental control over this conformational change timescale may provide some insights into its effect on the chemotactic performance of the cell. Moreover, our study can be used to estimate the activity switching rate for wild-type *E.coli*, which has not been measured so far to the best of our knowledge. The range of values of drift velocity measured in our simulations agree with experimental data for V recorded under similar attractant environment [9, 10]. A comparison between the experiments and our simulations yields w_a ranging between $0.5s^{-1}$ and $1s^{-1}$. A direct experimental measurement of w_a can help to verify this prediction.

Bibliography

[1] Shobhan Dev Mandal and Sakuntala Chatterjee. Effect of switching time scale of receptor activity on chemotactic performance of escherichia coli. *Indian Journal of Physics, Special Issue: Physical Views of Cellular processes*, 96:2619–2627, 2022.

[2] Shobhan Dev Mandal and Sakuntala Chatterjee. Effect of receptor clustering on chemotactic performance of *E. coli*: Sensing versus adaptation. *Phys. Rev. E Letter*, 103:L030401, Mar 2021.

[3] Remy Colin, Christelle Rosazza, Ady Vaknin, and Victor Sourjik. Multiple sources of slow activity fluctuations in a bacterial chemosensory network. *Elife*, 6:e26796, 2017.

[4] Subrata Dev and Sakuntala Chatterjee. Optimal methylation noise for best chemotactic performance of *E. coli*. *Physical Review E*, 97(3):032420, 2018.

[5] Sakuntala Chatterjee, Rava Azeredo da Silveira, and Yariv Kafri. Chemotaxis when bacteria remember: drift versus diffusion. *PLoS computational biology*, 7(12), 2011.

[6] Victor Sourjik and Howard C Berg. Receptor sensitivity in bacterial chemotaxis. *Proceedings of the National Academy of Sciences*, 99(1):123–127, 2002.

[7] Victor Sourjik and Howard C Berg. Functional interactions between receptors in bacterial chemotaxis. *Nature*, 428(6981):437–441, 2004.

[8] John S Parkinson, Gerald L Hazelbauer, and Joseph J Falke. Signaling and sensory adaptation in escherichia coli chemoreceptors: 2015 update. *Trends in microbiology*, 23(5):257–266, 2015.

[9] Tanvir Ahmed and Roman Stocker. Experimental verification of the behavioral foundation of bacterial transport parameters using microfluidics. *Biophysical journal*, 95(9):4481–4493, 2008.

[10] Gabriele Micali, Rémy Colin, Victor Sourjik, and Robert G Endres. Drift and behavior of *E. coli* cells. *Biophysical journal*, 113(11):2321–2325, 2017.

Chapter 7

Bacterial chemotaxis in spatio-temporally varying attractant environment

In this chapter, we study the single cell chemotactic behaviour of E.coli for a travelling wave attractant profile. In an earlier work Li et al. [1] had experimentally generated a traveling wave attractant concentration using a microfluidic device and studied the cell behavior. They tracked the position of the cell stroboscopically and calculated drift velocity from there. It was observed that for small propagation velocity of the traveling wave, the cell is able to track the wave. But when propagation velocity is large, the cell lags behind and its drift velocity even changes sign to become negative, which means the cell now moves in the opposite direction to the traveling wave.

In this chapter, we have considered a traveling wave attractant profile $c(x,t) = c_0 + Asin\frac{2\pi}{\lambda}(v_w t - x)$ and measure the chemotactic drift velocity as a function of propagation speed v_w. Unlike the stroboscopic measurement performed in [1] we calculate the drift velocity by averaging over cell position at all times and we find a qualitatively different behavior. We observe that for static wave drift velocity is also zero, as expected. As v_w increases, drift velocity becomes negative, reaches a negative minimum and then starts increasing again to reach a positive maximum from which it decreases again to become zero for very large v_w values. We explain this behavior from the relative velocity of right-moving and left-moving cell with respect to the propagating wave. As wave speed increases from zero, relative velocity of right-moving and left-moving cell starts to decrease and increase respectively because the propagating wave moves along rightward (along positive x-axis) direction. In particular when the run speed matches with the speed of the traveling wave, the cell is able to 'ride' the wave when it is moving in rightward direction, but experiences a fast oscillating profile while moving in the leftward direction. We explain the variation in drift velocity from this effect. We consider an one dimensional periodic lattice on which the cell moves. We find the cell behavior is quite different for small and large wavelength of the attractant concentration. Below we present our results for these two cases separately. We are preparing the manuscript to publish these results soon [2].

7.1 Chemotactic response for small wavelength

In this section, we present our results for $\lambda = 100\ \mu m$. We measure chemotactic drift velocity V, which is defined as the net displacement of the cell during a run. We find extremely rich behavior of V as v_w is varied. We present our data in Fig. 7.1. As expected, $V = 0$ for $v_w = 0$ and for very large v_w when the wave moves too fast, the cell is unable to sense the spatio-

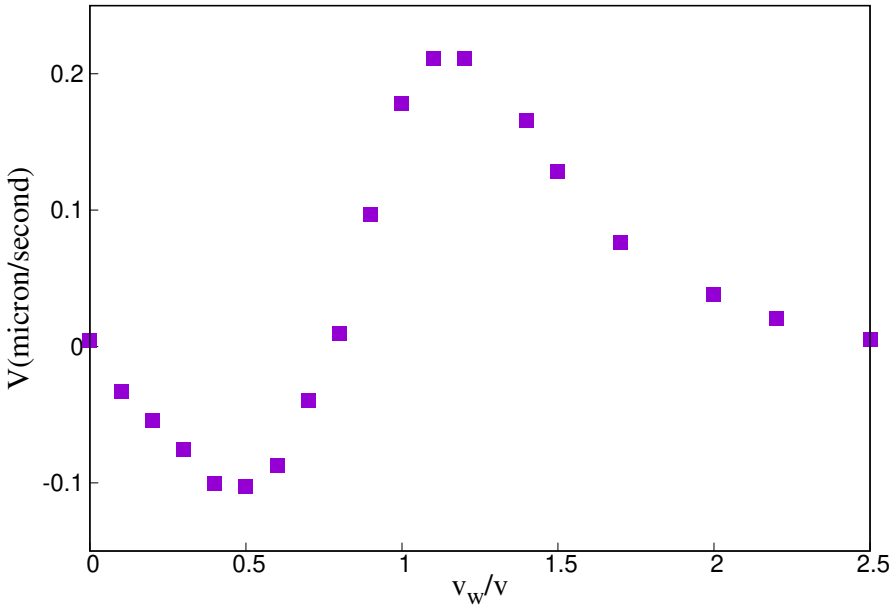

Figure 7.1: Chemotactic drift velocity V as a function of wave speed v_w rescaled by run speed v for $\lambda = 100\ \mu m$. All simulation parameters are given in Sec. 2.4. Each data point has been averaged over at least 2×10^7 histories.

temporal variation and V vanishes in this limit too. For finite v_w, however, very interesting variation in V is observed. Starting from zero, as v_w increases, V first becomes negative, reaches a minimum, then increases again, becomes positive, reaches a peak and finally vanishes for very large v_w. Therefore, by tuning v_w one can have the net drift of the cell in the same direction, or even in the opposite direction of attractant propagation.

7.1.1 Behavior of average rightward and leftward run duration

Since V is defined as the net displacement in a run, we also separately look at the mean run duration in the same direction and opposite direction of wave propagation, denoted as τ_R (rightward) and τ_L (leftward), respectively. Clearly, V is closely related to the difference $(\tau_R - \tau_L)$. In Fig. 7.2 we show the variation of τ_R and τ_L with v_w. Our data show that for very small or very large v_w both these run durations are equal. For $v_w = 0$, when the environment is static, an uphill or a downhill run along the attractant concentration profile can result from both leftward and rightward movement of the cell. There is no net displacement of the cell towards left or right in the long term. On the other hand, when v_w is very large, the cell can hardly sense the attractant gradient, rather it experiences an average attractant concentration c_0 at all times and can not therefore distinguish between a leftward and rightward run. So we have $\tau_R = \tau_L$ in both these limits which is consistent with our observation of $V = 0$ in Fig. 7.1. For intermediate v_w values, τ_R and τ_L show exactly opposite trends but it is clear from Fig. 7.2 that $(\tau_R - \tau_L)$ indeed captures the V variation in Fig. 7.1 perfectly well. In the following subsection we focus on explaining the variation of τ_R and τ_L with v_w in details. A crucial observation here is that, although the run speed of the cell is v, the effective velocity of a rightward run with respect to the moving wave is $(v - v_w)$ and that of a leftward run is $-(v + v_w)$. This means as v_w increases from zero, rightward runs become slower and slower and finally when v_w becomes equal to the run-speed, the cell simply rides the wave and experiences no change in attractant level during a

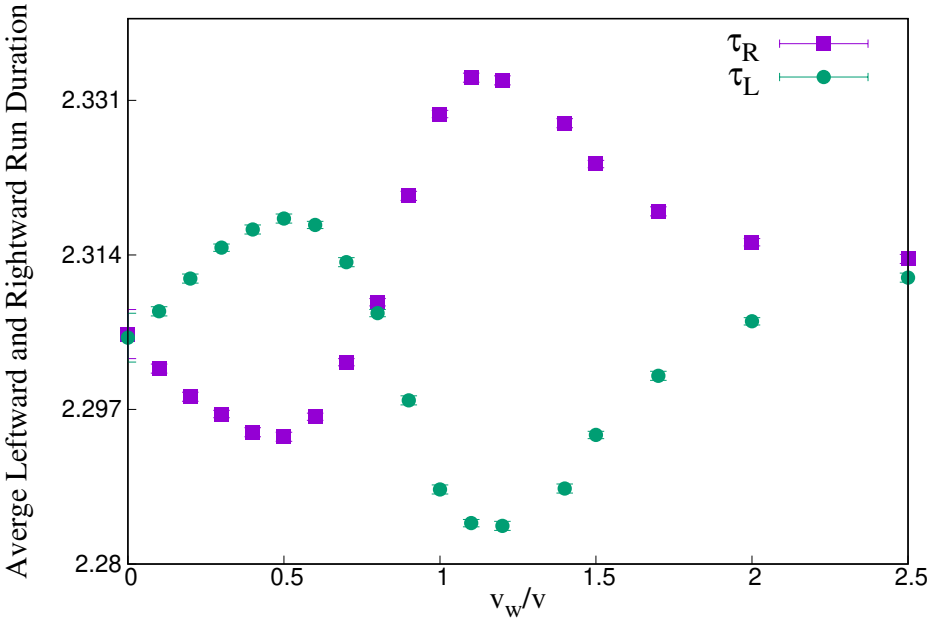

Figure 7.2: Rightward run duration τ_R (purple square points) and leftward run duration τ_L (green circular points) as function of wave speed v_w rescaled by run speed v for wavelength $\lambda = 100\ \mu m$. All simulation parameters are same as Fig. 7.1. Each data point has been averaged over at least 2×10^7 histories.

rightward run. When v_w exceeds v, the wave overtakes the right-movers, i.e. the cell effectively moves backward during a rightward run. For the left-movers, on the other hand, the effective velocity remains negative for all v_w and its magnitude increases with v_w. The different attractant environment experienced by right-movers and left-movers plays an extremely important role in determining the variation of τ_R and τ_L with v_w, as illustrated in the next subsection.

7.1.2 Runs originating from low and high attractant concentrations

We start by dividing all the runs into two groups: runs starting from regions with attractant concentration higher and lower than the average value c_0. Clearly, τ_R (τ_L) is the average duration of all those rightward (leftward) runs, some of which have originated from high concentration region, and the rest from low concentration region. Runs which originate from a region with ligand concentration lower (higher) than c_0 can be both uphill or downhill, but majority of them will be uphill (downhill), i.e. the final concentration at the end of the run will be larger (smaller) than the initial concentration at its origin. This holds everywhere, except for the special case of rightward runs with $v_w = v$. We denote by τ_R^{low} and τ_R^{high} the mean duration of rightward runs starting from low and high concentration regions, respectively. Similarly, τ_L^{low} and τ_L^{high} can be defined. We investigate how these quantities depend on v_w.

Let us specifically consider the rightward runs which originate from low concentration region. As v_w increases from zero, the effective velocity $(v - v_w)$ of these runs decreases, i.e. the cell spends longer time in the low concentration region, which in turn raises its activity and makes it tumble quicker. Therefore τ_R^{low} should decrease with v_w, and reach a minimum at $v_w = v$, when attractant level remains unchanged during a run. For $v_w > v$ magnitude of effective velocity of a rightward run increases again, which makes it possible for many rightward runs to get out of the low concentration zone and enter the high concentration zone. This lowers

the activity and increases the run duration. Our data (Fig. 7.3A, purple squares) indeed show that τ_R^{low} decreases as v_w increases, reaches a minimum at $v_w = v$ and then increases again. The behavior of τ_R^{high} is just the opposite (Fig. 7.3B, purple squares). For $0 < v_w < v$ the relative velocity of the right-movers keeps decreasing with v_w, which makes the cell spend longer time in the high concentration region and hence τ_R^{high} increases with v_w, reaching a maximum when $v_w = v$ and then decreases again.

Final τ_R is calculated after averaging over all runs, starting from low and high concentration zones. Since more tumbles occur in the low concentration region, more runs originate from here. The behavior of τ_R is therefore initially controlled by τ_R^{low} and τ_R decreases with v_w (Fig. 7.2, purple squares). But when τ_R^{low} falls much below τ_R^{high}, its contribution to τ_R becomes less significant and τ_R^{high} takes over. Therefore, τ_R increases again, reaches a peak and finally for very large v_w merges with τ_L.

For leftward runs, effective velocity keeps increasing with v_w. This means when a cell is moving leftward, the effective concentration gradient experienced by the cell keeps increasing with v_w. A steeper gradient elongates the uphill runs and shortens the downhill runs. Since τ_L^{low} (τ_L^{high}) is obtained by averaging over majority uphill (downhill) runs, τ_L^{low} (τ_L^{high}) shows increasing (decreasing) trends with v_w. Our data in Fig. 7.3 (green circles) are consistent with this, except for $v_w \sim v$, where these trends are slightly disrupted. This effect can be explained in the following way. τ_R^{low} is particularly small, when v_w is very close to v. These rightward runs are therefore associated with high activity. When these rightward runs tumble, half of them turn leftward and contribute towards τ_L^{low}. Such leftward runs therefore start with high activity and are more likely to tumble quickly. This brings down the average τ_L^{low} near $v_w = v$ point. In a similar way mild increasing tendency of τ_L^{high} for $v_w \sim v$ can also be explained.

τ_L is weighted average of τ_L^{high} and τ_L^{low}. Due to higher tumbling rate in the low concentration region, more runs tend to originate from there. So τ_L behavior is mainly guided by τ_L^{low}: it increases for small and large v_w and decreases when v_w is close to v. Although τ_L^{high} does contribute to the variation of τ_L, it never takes over from τ_L^{low} because the difference between high and low concentration run durations for left-movers is much less compared to that for right-movers.

7.2 Chemotactic response for large wavelength

The qualitative variation of V with v_w remains similar even for large λ (Fig. 7.4) although variation in V occurs over a much smaller range in this case. Our data for τ_R and τ_L in Fig. 7.5 show that qualitative dependence of mean run durations on v_w remains similar too, although the positions of maxima and minima get shifted. However, when we separately measure runs originating from high and low concentration of attractant, we find different behaviors. Although τ_R^{low} (τ_R^{high}) shows qualitatively similar behavior with v_w, as in lower λ case, the minimum (maximum) is reached at a $v_w > v$. More importantly, the qualitative trends of τ_L^{low} and τ_L^{high} are quite different. τ_L^{low} shows a minimum with v_w and τ_L^{high} shows a maximum.

7.2.1 Explanation for the shifting of minima in τ_R^{low}

To explain this observation, we note that for very large λ, the spatial variation of ligand concentration is so slow, that even when v_w is not equal to v, the change in ligand level experienced by the cell during a rightward run is negligible. Therefore, the dramatic effect observed for $v_w = v$ when λ was small (Fig. 7.3) is much subdued here. The low concentration zone which

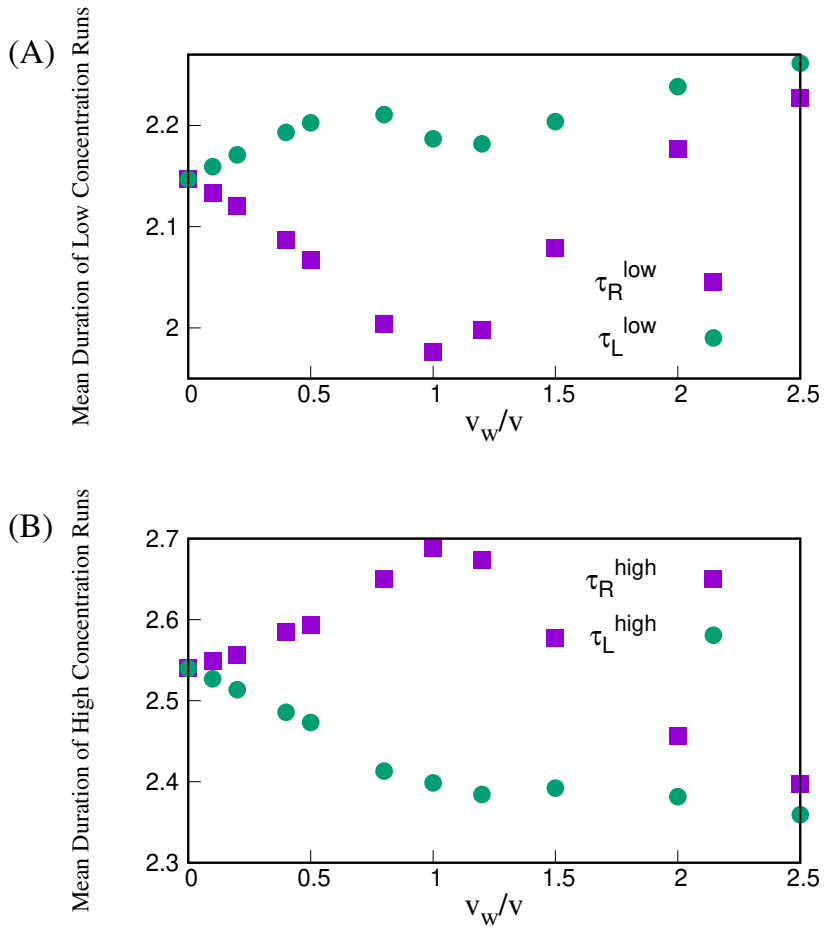

Figure 7.3: (A) Shows mean duration of runs starting from the low concentration region as a function of v_w rescaled by run speed v. Rightward run duration τ_R^{low} (purple squares) decreases with v_w, shows a minima and then increases again whereas leftward run duration τ_L^{low} increases with v_w. (B) Shows mean duration of runs starting from the high concentration region as a function of v_w rescaled by run speed v. Rightward run duration τ_R^{high} (purple squares) increases with v_w, shows a maxima and then decreases again whereas leftward run duration τ_L^{high} decreases with v_w. Data for $\lambda = 100\ \mu m$ have been presented here. All simulation parameters are same as Fig. 7.1. Each data point has been averaged over at least 3×10^7 histories.

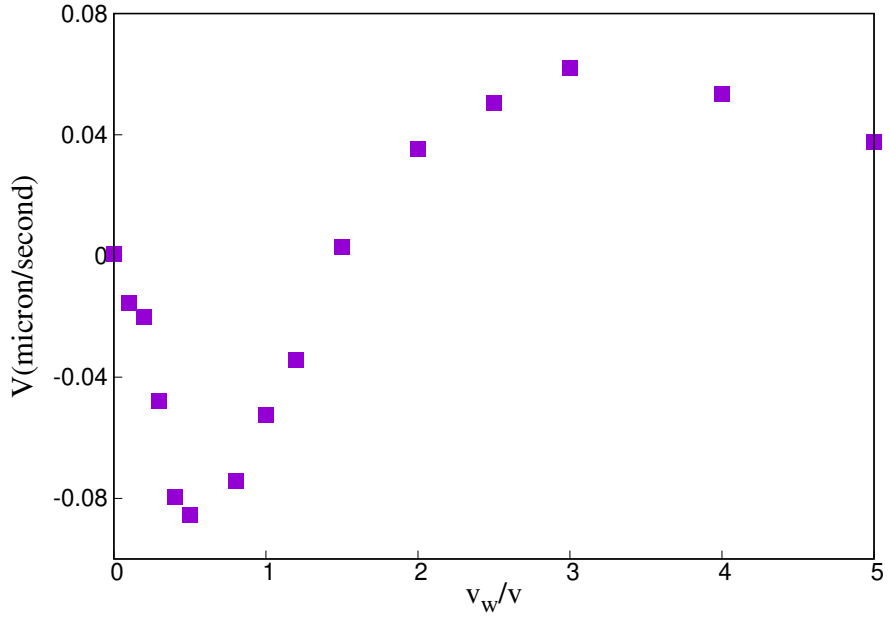

Figure 7.4: Chemotactic drift velocity V as a function wave speed v_w rescaled by run speed v for $\lambda = 500\mu m$. All simulation parameters are same as Fig. 7.1. Each data point has been averaged over at least 3×10^7 histories.

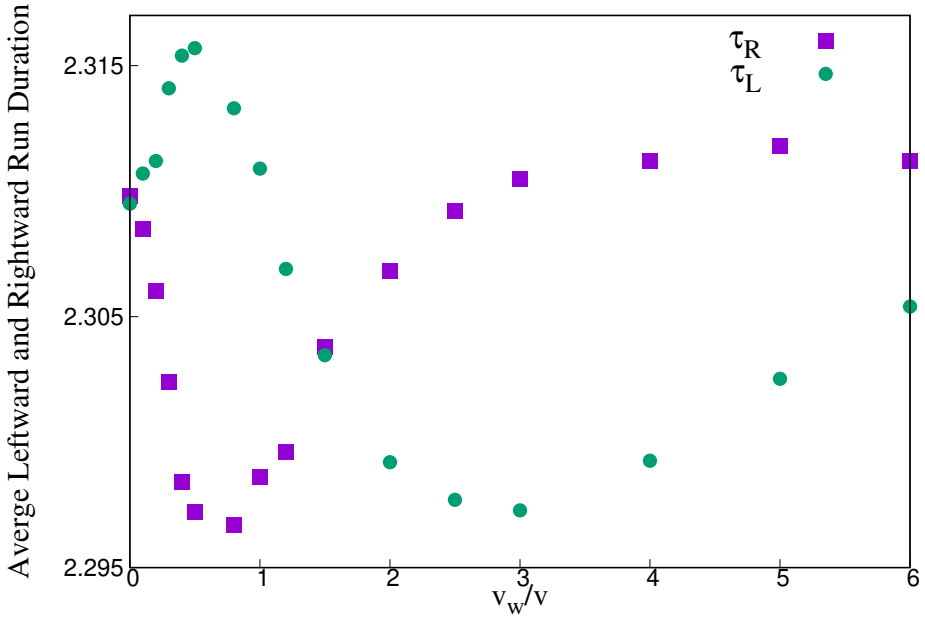

Figure 7.5: Rightward run duration τ_R (purple square points) and leftward run duration τ_L (green circular points) as function of wave speed v_w rescaled by run speed v for wavelength $\lambda = 500\mu m$. All simulation parameters are same as Fig. 7.1. Each data point has been averaged over at least 3×10^7 histories.

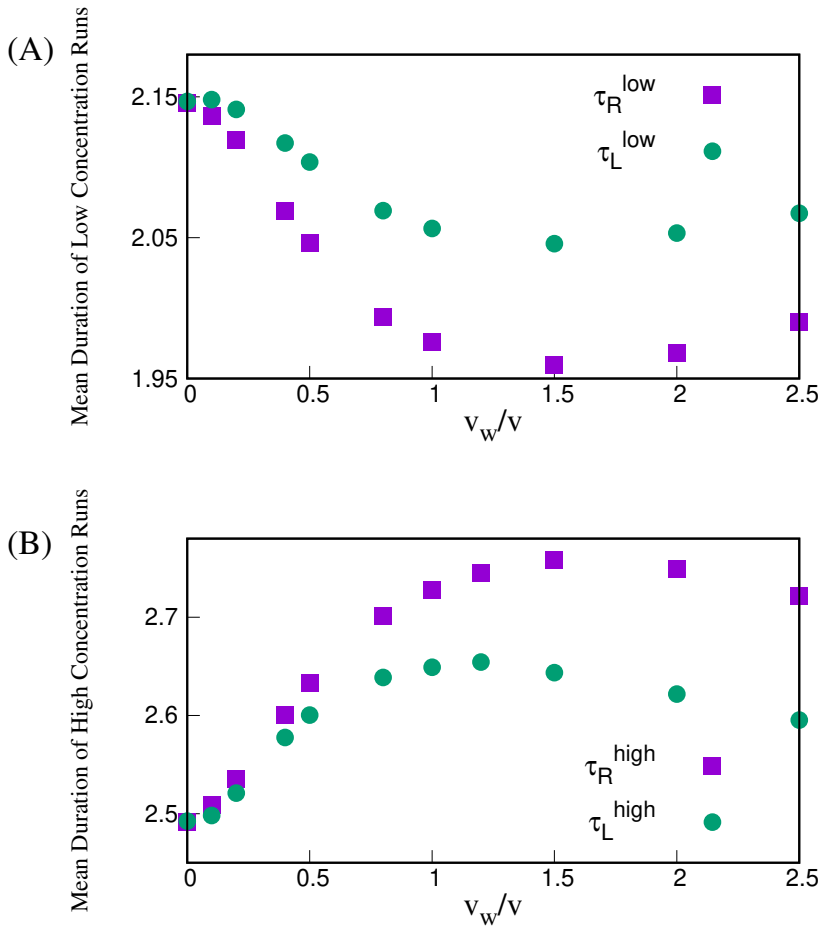

Figure 7.6: (A) Shows mean duration of runs starting from the low concentration region as a function of v_w rescaled by run speed v. Rightward run duration τ_R^{low} (purple squares) decreases with v_w, shows a minima and then increases again whereas leftward run duration τ_L^{low} increases with v_w. (B) Shows mean duration of runs starting from the high concentration region as a function of v_w rescaled run speed v. Rightward run duration τ_R^{high} (purple squares) increases with v_w, shows a maxima and then decreases again whereas leftward run duration τ_L^{high} decreases with v_w. Data for $\lambda = 500\ \mu m$ have been presented here. All simulation parameters are same as Fig. 7.1. Each data point has been averaged over at least 2×10^7 histories.

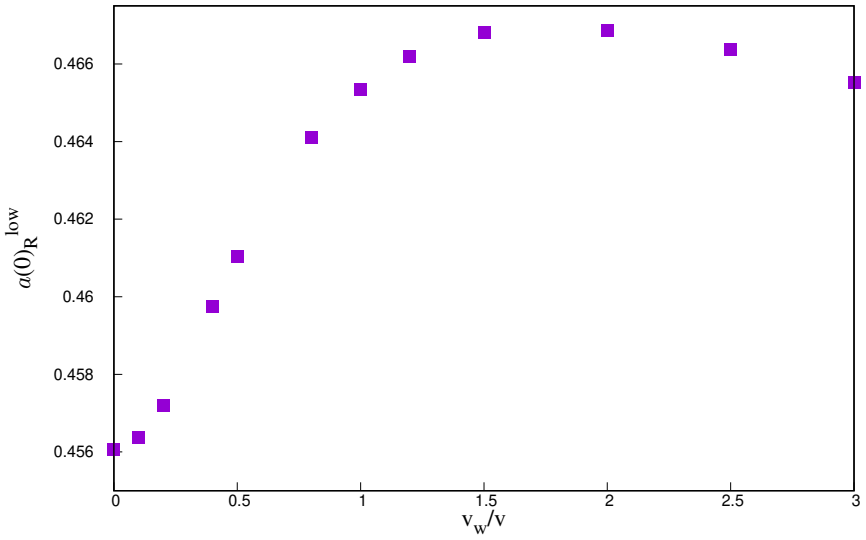

Figure 7.7: Initial activity of rightward runs starting from low concentration region $[a(0)_R^{low}]$ as a function of v_w rescaled by run speed v. We see $a(0)_R^{low}$ shows a maxima at a same value of v_w where τ_R^{low} shows minima in Fig. 7.6A. All simulation parameters are same as Fig. 7.1. Each data point has been averaged over at least 10^6 histories.

spans over half a wavelength, is so large in this case, that many of our arguments for smaller λ do not remain valid here. For example, our explanation behind τ_L^{low} variation presented in Fig. 7.3A hinged on the fact that majority of the leftward runs originating from low concentration regions are uphill, and these runs control the average. But when the low concentration region is spanned over a very large spatial range, then the number of downhill runs originating from this region is comparable and is expected to affect the behavior of τ_L^{low}.

For large λ, the change in ligand level and hence change in activity is so small during a typical run, that the duration of a run is effectively determined by the initial activity of the cell at the beginning of that run. In Fig. 7.7 we plot the average initial activity of rightward runs starting from low concentration regions. We denote this quantity by a_R^{low}. We find that a_R^{low} indeed shows a peak at the same value of v_w/v where τ_R^{low} is minimum. Since direction of a run is randomized after each tumble, same behavior is expected even for a_L^{low}. This is why τ_R^{low} and τ_L^{low} show same qualitative trend in this case. In a similar way, data in Fig. 7.6B can also be explained. However, we do not have complete understanding of why a_R^{low} in Fig. 7.7 shows a peak with v_w and why that peak occurs at $v_w > v$. More research is needed to understand these details.

7.3 Discussion

In this chapter we have studied the chemotactic response of an E.coli cell in a travelling wave attractant environment. Here we quantify the chemotactic performance by the net drift velocity of the cell. We find a non-monotonic variation of the drift velocity as a function of the speed of the travelling sin wave. For static wave and extremely fast moving wave we see that the chemotactic drift takes zero value. In between this two values drift velocity first shows a neg-

ative minimum and then a positive maximum as a function of propagating speed. We explain this intriguing effect by separately monitoring runs originating from high and low attractant concentration regions, whose behavior in turn depends crucially on the fact that the effective concentration gradient experienced by the cell during leftward and rightward runs are quite different.

Our results show that in presence of a time-periodic attractant environment, highly non-trivial time-averaged effects can be found in the cell behavior, which remain undiscovered if only stroboscopic measurements are performed [1]. In contrast to a complex traveling wave pattern generated in the experiment by Li et al. [1] we study here the simplest possible traveling wave profile, viz a monochromatic traveling wave, varying in space and time sinusoidally. It will be interesting to consider superposition of various different sine waves (Fourier modes) and study time-averaged cell response for a more complex attractant environment.

Bibliography

[1] Zhaojun Li, Qiuxian Cai, Xuanqi Zhang, Guangwei Si, Qi Ouyang, Chunxiong Luo, and Yuhai Tu. Barrier crossing in escherichia coli chemotaxis. *Physical review letters*, 118(9):098101, 2017.

[2] Shobhan Dev Mandal and Sakuntala Chatterjee. Bacterial chemtaxis in spatio-temporally varying attractant profile. Manuscript in Preparation.

Chapter 8

Conclusions

The cooperative interaction among chemoreceptors in densely organized clusters or signalling arrays has been recently found to be a significant source of fluctuation in E.coli chemotaxis. In this thesis, we have studied how this newly found source of noise affects the chemotactic behaviour of the cell.

In chapter 3 we study how the chemotactic performance of an E.coli cell depends on the cooperative interaction strength or size of the receptor cluster. We quantify the performance by localization and chemotactic drift velocity of the cell. Localization is the ability of the cell to reach that region where attractant concentration is high. Drift velocity measures how fast cell climbs up the attractant gradient. We see that there is an optimum value of interaction strength or cluster size at which chemotactic performance is maximum. By investigating further we find that increased cooperativity amplifies the input signal coming from environment and hence improves the performance. But as interaction strength increases fluctuation in the activity also gets amplified and adaptation now responds strongly to maintain the mean level of activity. So overall dynamics is controlled by the change in methylation level of chemoreceptors and cell becomes less sensitive to its ligand environment. As a result performance is deteriorated at very large cluster size and a performance peak is observed due to the sensing versus adaptation interplay. These results are published in [1].

We also study how methylation dynamics of chemoreceptors is affected by the receptor cooperativity as the cell navigates through spatially varying ligand environment. We measure the temporal variation of methylation level of chemoreceptors as cell swims up and down the gradient. In chapter 4 we present the data for weak strength of attractant gradient. For weak gradient we see methylation variation is qualitatively similar in uphill and downhill runs. For small time methylation level decreases because of a large number of runs with high initial activity undergo demethylation and again those runs with high methylation level quickly drop out from the population. But in moderate and large time we see methylation level increases. This happens because after initial dropping out of high activity runs only those runs survive which start with very low activity and hence methylation is triggered in those runs. These results are published in [2].

In chapter 5 we present the results for methylation dynamics for strong attractant gradient. For strong gradient uphill runs show similar qualitative behaviour like weak gradient case while the downhill runs show qualitatively different and highly non-trivial methylation variation. When cluster size is small downhill runs in strong gradient show sustained demethylation throughout the time-window of our observation. Because of strong gradient initial demethylation in high activity runs is also strong and surviving long runs with low activity experience huge drop in ligand concentration, which raises their activity to high value soon. Therefore,

demethylation happens even in those long runs. As cluster size increases initial demethylation becomes more strong which reduces the activity to very low value. So methylation is triggered now due to adaptation and methylation level starts increasing in moderate time. But in large time only those runs survive which undergo huge drop in ligand concentration and show demethylation due to high activity. So sensing-adaptation interplay gives rise to an oscillatory nature of methylation variation. For very large cluster size it is the adaptation that fully controls the dynamics and hence downhill runs show similar methylation variation as observed in uphill runs. These results are published in [2].

In chapter 6 we study the effect of switching time-scale of receptor activity on chemotactic efficiency of the cell at different strength of receptor cooperativity. We measure the chemotactic drift velocity as switching rate has been varied from small to large value systematically. What we observe is that the drift velocity increases with switching rate and reaches a saturation value when switching rate becomes very high. For higher cooperativity this saturation value increases due to cooperative signal amplification. In probing further we see average duration of downhill run decreases with activity switching rate at a faster rate than the same for uphill run, which enhances the chemotatic drift with switching rate. Our data show that during uphill run effect of adaptation is opposed by the effect of ligand sensing and this doesn't allow activity to increase much as switching rate increases. But in case of downhill run effect of adaptation goes in the favour of effect of ligand binding and this increases the activity to much higher value as switching rate increases. This larger increase of activity with switching rate makes downhill run duration to fall faster and enhance the drift velocity. These results are published in [3].

In chapter 7 we observe the chemotactic response of a cell in a spatio-temporally varying ligand environment at a fixed strength of receptor cooperativity. We apply a travelling wave of attractant profile and measure the chemotactic drift velocity as a function of speed of the propagating wave. Our result shows that drift velocity is zero for a static wave. As wave starts moving drift velocity decreases from zero and reaches a negative minima. As wave moves faster the drift velocity starts increasing and shows a positive maxima. For extremely large value wave speed drift velocity approaches zero. Near the minima of drift velocity we see average duration of rightward and leftward runs show a minima and maxima respectively. We explain this behaviour from the relative velocity of right-moving and left-moving cell with respect to the wave propagating in rightward direction. Relative velocity of right-moving cell decreases with speed of the wave and hence rate of change of ligand concentration as experienced by the right-moving cell becomes slower. When run speed of the cell matches with speed of the wave, right-moving cell is able to ride the wave and experiences a ligand concentration that never changes with time at all. On the other hand relative velocity of left-moving cell increases with speed of the wave and hence left-moving cell always encounters faster change in ligand concentration as wave speed increases to higher value. This opposite effect of rightward and leftward motion explains the variation of rightward and leftward run duration and as well as the drift velocity with speed of the wave. We are preparing the manuscript to publish these results soon [4].

Bibliography

[1] Shobhan Dev Mandal and Sakuntala Chatterjee. Effect of receptor clustering on chemotactic performance of *E. coli*: Sensing versus adaptation. *Phys. Rev. E Letter*, 103:L030401, Mar 2021.

[2] Shobhan Dev Mandal and Sakuntala Chatterjee. Effect of receptor cooperativity on methylation dynamics in bacterial chemotaxis with weak and strong gradient. *Physical Review E*, 105(1):014411, 2022.

[3] Shobhan Dev Mandal and Sakuntala Chatterjee. Effect of switching time scale of receptor activity on chemotactic performance of escherichia coli. *Indian Journal of Physics, Special Issue: Physical Views of Cellular processes*, 96:2619–2627, 2022.

[4] Shobhan Dev Mandal and Sakuntala Chatterjee. Bacterial chemtaxis in spatio-temporally varying attractant profile. Manuscript in Preparation.